TU Delft

Development of an in vitro model for the evaluation of a surgical insufflator

design, manufacturing and validation of a respiratory-abdominal simulation prototype

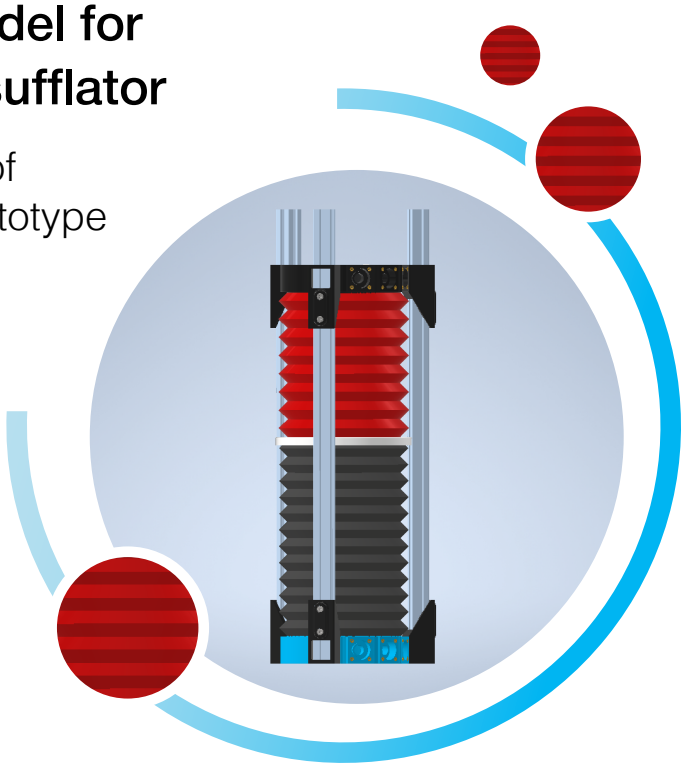

Stergios Georgantas

Delft, May 2021

Development of an in vitro model for the evaluation of a surgical insufflator

Design, manufacturing and validation of a respiratory-abdominal simulation prototype

By

Stergios Georgantas

In partial fulfillment of the requirements for the degree of

Master of Science
in Biomedical Engineering

at the Delft University of Technology,
to be defended on Thursday, May 20, 2021

Student number: 4898419

Thesis committee:			
	Prof. Dr. Ir. Jenny Dankelman	TU Delft	(Supervisor)
	Ir. Frank Sterke	TU Delft	(Daily Supervisor)
	Willem van Weteringen, M.D.	Erasmus MC	(Daily Supervisor)
	Dr. Angeliki Laskari	TU Delft	

This thesis is confidential and cannot be made public until May 20, 2026

TU Delft

ABSTRACT

Background – Abdominal insufflation is one of the most significant aspects of laparoscopic surgery, as it creates the necessary space for the manipulation of the surgical instruments. However, it is associated with several side-effects for the patient, such as disruption of the normal respiratory function. A novel surgical insufflator, capable of performing individualized pressure adjustments has been recently developed at the Erasmus MC - Sophia Children's Hospital. The performance, safety and the effect of the insufflator on pulmonary mechanics was evaluated by means of animal experiments. However, animal trials display certain disadvantages, such as limited repetitiveness, protocols that had to respect physiological limitations and ethical considerations. An in vitro approach for the assessment of the insufflator would benefit the reliability of the evaluation and contribute to a broader understanding of the effect of insufflation on the respiratory system.

Goal – The goal of this thesis is to design, develop and validate an in vitro model that simulates the interaction between the respiratory system and the abdominal cavity during surgical insufflation.

Methods – For the development of the model, a preliminary analysis was first conducted on the experimental data from one of the animal trials, to examine the respiratory and abdominal mechanical properties as a function of the intra-abdominal pressure during insufflation. The design requirements were then formulated and the design of the model was created. Finally, the model was manufactured and assembled.

Validation – Validation of the function of the simulator was performed by comparing the results from the preliminary analysis to the results obtained from the model. This was achieved by recreating the experimental conditions, implementing the developed model in place of the animal, and recording the mechanical and functional parameters that were acquired in the in vivo trial. These parameters were subsequently compared to the corresponding parameters from the in vivo trial.

Results – The airway resistance was maintained virtually stable after displaying a slight increase at the lowest levels of insufflation pressure, both in vivo and in vitro. On the other hand, the respiratory system elastance displayed a continuous increase alongside the rise in intra-abdominal pressure. The abdominal resistance was maintained constant in both the model and the animal. The abdominal compliance of the model exhibited a continuous decrease, which was more prominent in the in vivo setting. There were no fluctuations in the tidal volume for the entire range of insufflation pressures, while the volume of air flowing out of the abdomen increased at the lowest pressures, before being stabilized. The time difference between the occurrence of the tidal and abdominal volumes exhibited a more noticeable drop in the animal compared to the in vitro simulator. Finally, a continuous rise was observed in the peak inspiratory pressure and the driving pressure in both settings.

Conclusions – In vitro simulation of the respiratory-abdominal interaction during surgical insufflation is feasible, and the developed model is a good proof-of-concept. Despite some deviations in the simulated mechanical properties, the prototype gave satisfactory results in terms of the theoretical mechanical interaction between the two systems. The model offers broader knowledge of the effect of abdominal insufflation onto the respiratory mechanics and can be used as an evaluation platform for the performance of any surgical insufflator. Further improvements are expected to increase its reliability and reduce the reliance on animal experiments.

ACKNOWLEDGEMENTS

First of all, I would like to thank my supervisor, Jenny Dankelman, for her continuous help, encouragement and support throughout the last year of my studies. Her door was always open and her guidance and feedback were extremely valuable. Her work and ideas on minimally invasive surgery have contributed to great improvements in the field and are a true inspiration for biomedical engineering students.

This thesis would not have been possible without the invaluable help of Frank Sterke and Willem van Weteringen, of the department of Pediatric Surgery of the Erasmus MC - Sophia Children's Hospital. I am grateful to both for offering me the opportunity to be involved with the project. Their work on the development of the novel surgical insufflator is truly fascinating, and its potential for research as well as for improving the level of healthcare is exciting. A huge thank you to Frank, for his daily guidance since my first day, his patience as well as for sharing his ideas and expertise, from the preliminary analysis, manufacturing, troubleshooting and debugging the data acquisition codes, to the vitally important help and advice in MATLAB, LabVIEW and presentation strategies. He is a truly intelligent and remarkable engineer and researcher, always willing to help with anything and at any time. I am truly grateful for his involvement and our collaboration the last 6 months, during which I gained a lot of experience and insights into the engineering way of thinking and doing. Again, thank you Frank for your patience and dedication in helping me from the beginning of the project. Additionally, thank you to Willem, first of all for the time he invested in helping me, soldering wires for the data acquisition board, for his valuable input and insights from a clinical standpoint, the great amount of interest he showed in the progress of the project, his crucial feedback on the end goals of the preliminary analysis, the advice in writing the report and the vital solutions he offered regarding the 3D printing of the model components. I truly appreciate his guidance and encouragement and I admire his enthusiasm and passion for research and technology.

To Fatima and Lis, thank you for exchanging ideas, suggestions and talking through our projects at the lab of the department of Pediatric Surgery. I truly appreciate the help during my first attempt to use the 3D printer.

I am grateful for everyone at the Sophia Children's Hospital of Erasmus MC for making me feel welcome since the first day there, and for the people at the technical department for offering me the space to perform some initial calibration experiments and the equipment to perform soldering when it was necessary.

To my partner, Ioanna, a huge thank you for your patience, the emotional support and encouragement throughout my studies, for talking through ideas with me as well as for creating the cover page of my thesis report. Finally, I am very thankful and grateful to my parents for their unwavering support and encouragement throughout this degree.

CONTENTS

LIST OF TABLES v
LIST OF FIGURES vi
LIST OF ABBREVIATIONS ix
INTRODUCTION 1
1. Relevance of the Study 1
2. Problem Statement & Goal 2
2.1 Problem Statement 2
2.2 Goal 3
3. Report Structure 3
BACKGROUND 5
4. Respiratory Mechanics & Mechanical Ventilation 5
4.1 Overview of the Respiratory System 5
4.2 Mechanics of Breathing 6
4.3 Mechanical Ventilation 7
4.4 Respiratory Mechanics During Mechanical Ventilation 8
5. Respiratory-Abdominal Interaction 14
6. Abdominal Mechanical Properties 16
6.1 Forced Oscillation Technique (FOT) 16
6.2 Mathematical Modelling 17
METHODS 19
7. Preliminary Analysis 19
7.1 Experimental Data & Measurement Protocol 19
7.2 Respiratory Analysis 20
7.3 Abdominal Analysis 28
8. Development of the Model 33
8.1 Design Requirements 33
8.2 End-Goal 34
8.3 Individual Components 35
8.4 Design of the Model 41
8.5 Manufacturing of the Model 43
VALIDATION 45

9. Validation Methodology 45
9.1 Goal 45
9.2 Validation setup 45
9.3 Validation Protocol 48
9.4 Validation Results 49
EVALUATION 59
10. Discussion 59
11. Recommendations 62
11.1 Compliance of the Individual Components 62
11.2 Addition of Physical Interaction 63
11.3 Bicompartment Mathematical Model 63
12. Conclusions 64
REFERENCES 65
APPENDICES 72
Appendix A 72
A.1 Respiratory Analysis – MATLAB Code 72
A.2 Abdominal Analysis – MATLAB Code 80
Appendix B 83
B.1 Paper 83

LIST OF TABLES

Table 1. *The individual objectives that were defined for the achievement of the ultimate goal of the thesis 3*

Table 2. *The structure of the present report. 4*

Table 3. *The major effects of the rise in IAP on respiratory mechanics. 15*

Table 4. *The ventilation parameters that were fixed during the volume-controlled IPPV of the animal experiment. 20*

Table 5*. Measurement protocol of the in vivo experimental trial. 20*

Table 6. *The mean ± standard deviation of the respiratory resistance (R) and elastance (E) and mean squared error (MSE) as estimated by the mathematical model for every IAP in the preliminary respiratory analysis. 26*

Table 7. *The obtained parameters R, I, C and the respective error in their estimation for the abdominal wall of the examined animal at every IAP. 32*

Table 8. *Design requirements of the model. 34*

Table 9. *The desired mechanical behavior of the mechanical ventilation (respiratory) and surgical insufflation (abdominal) components of the model, as a function the increasing insufflation pressure. The data were acquired from the preliminary analysis (Table 6 and Table 7). 35*

Table 10. *The individual design requirements for the respiratory component of the model. 36*

Table 11. *The measured vs targeted mechanical properties for the respiratory component of the model. 38*

Table 12. *The individual design requirements for the abdominal part of the model. 39*

Table 13. *The measured vs targeted mechanical properties for the abdominal component of the model. 40*

Table 14. *The experimental protocol applied during the in vitro validation of the model. 48*

Table 15. *The investigated parameters of the model validation. 49*

Table 16. *The resistance, elastance and mean squared error (mean ± SD) of the respiratory bellow of the model (top) and the respiratory system of the animal (bottom) at every examined IAP. 50*

Table 17. *The resistance, elastance, inertia and the corresponding error in their estimation by the utilized mathematical model for the abdominal bellow of the in vitro model and abdomen of the animal at every examined IAP. 53*

Table 18. *The tidal and corresponding abdominal volume, and the time difference between their occurrence (mean ± SD), measured for the model (top) and during the animal experiment (bottom) at every examined IAP. 55*

Table 19. *The difference between the peak inspiratory pressure and PEEP, and the driving pressure (mean ± SD), calculated for the respiratory side of the model (top) and respiratory system of the animal (bottom) at every examined IAP. 57*

LIST OF FIGURES

Figure 1. *Illustration of the abdominal cavity before (top) and after insufflation with CO_2 (bottom) [2]. 1*

Figure 2*. The major components of the respiratory system [26]. 6*

Figure 3. *In invasive positive pressure ventilation, an endotracheal tube connected to the ventilator is inserted into the trachea of the patient and applies a positive pressure in the respiratory airway [40]. 8*

Figure 4. *Schematic representation of the pneumotachometer configuration. The air flows through the resistive mesh, which creates a pressure drop detected by the pressure transducer. The heating element prevents the accumulation of moisture and secretions [56]. 10*

Figure 5. *The esophageal balloon-tipped catheter used in adults. The distal end of the catheter is placed within the balloon, while the proximal end is connected to the measurement and recording equipment [62]. 11*

Figure 6. *Computed tomography of the chest, showing that the esophagus is adjacent to the pleural space in the mid thorax [58]. 12*

Figure 7. *Schematic representation of the cranial shift of the diaphragm and the change in its movement during abdominal insufflation [77]. 15*

Figure 8. *The abdomen can be represented as a container with 2 rigid (pelvic bone, dorsal spine) and 2 partially flexible (abdominal wall, diaphragm) borders [80]. 16*

Figure 9. *Schematic representation of the R-I-C model used for the estimation of the abdominal mechanical properties. 17*

Figure 10. *Time signals of the airway pressure and flow, trocar pressure and flow, and the esophageal pressure obtained at IAP=20 hPa. The segment of the signal marked by the black rectangular corresponds to normal, quite breathing of the animal and was selected for the respiratory analysis. The red rectangular contains the breaths that were selected for the analysis. 21*

Figure 11. *The breath selection algorithm detected the minima in the V_t waveform. The marked minima on the V_t waveform indicate the initiation of each breath (IAP=20 hPa). 22*

Figure 12. *A systematic shift was observed at the V_t signal due to the flow sensor drift error (IAP=20 hPa). 23*

Figure 13. *The post-processed waveforms of Paw, Vaw and Vt, that were used for the respiratory analysis (IAP=20 hPa). 24*

Figure 14. *The waveform of the airway pressure predicted by the mathematical model, superimposed over the measured pressure signal (IAP=20 hPa). 26*

Figure 15. *Graph of the airway resistance R (top) and respiratory elastance E (bottom) versus the IAP, as estimated by the mathematical model utilized in the preliminary analysis. The two parameters define the respiratory function and mechanical properties of the animal that was used in the experiment. 27*

Figure 16. *The data section that corresponds to the application of the FOT was selected for the abdominal analysis (marked by the red rectangular (IAP=20 hPa). 28*

Figure 17. *The pressure signal applied on the abdominal wall during the FOT and the resulting flow (IAP=20 hPa) 29*

Figure 18. *The real and imaginary part of the mechanical impedance (resistance and reactance) and the coherence estimated and marked at each frequency (IAP=20 hPa). 30*

Figure 19. *The measured R and X values and the resulting predictions by the algorithm for IAP=20 hPa. 32*

Figure 20. *The curves mechanical parameters of the abdominal wall (resistance and compliance), obtained by the RIC model after the application of the FOT. 33*

Figure 21. *Graphical representation of the functional end-goal of the device. That is, the mechanical behavior of the ventilation (left) and insufflation (right) component of the model. 35*

Figure 22. *The cross-sectional feature of the respiratory bellow, created in Autodesk Inventor. 37*

Figure 23. *Left: The respiratory bellow in the Ultimaker S5, once 3D printing was completed. Right: The respiratory bellow after removal from the 3D printer. 37*

Figure 24. *The airway pressure, flow and volume waveforms obtained for the respiratory bellow, when connected to the mechanical ventilator. 38*

Figure 25. *The latex bellow used as the abdominal component in the model. 39*

Figure 26. *The resistance and reactance curve estimated for the latex abdominal bellow with the use of the mathematical model described in 7.3 ..... 40*

Figure 27. *The 3D design of the model, created in Autodesk Inventor. 42*

Figure 28. *The configuration between the frame connector (black), the extrusion profile and the bellow connector (blue). The frame connector is initially mounted to the bellow connector. The extrusion profile is inserted and mounted to the frame connector, fixing the system in place. 42*

Figure 29. *The respiratory bellow connector was 3D printed at Erasmus MC. 43*

Figure 30. *The 3D printed respiratory bellow connector with the 3 mounted frame connectors. The tube socket that are not in used are sealed with the seal connectors, 3D printed with white TPU 95A. 44*

Figure 31. *The physical respiratory-abdominal model developed in the context of this thesis. 44*

Figure 32. *The setup used for the validation of the developed model. 46*

Figure 33. *Measurements were made by two pneumotachometers: one placed between the output of the ventilator and the respiratory bellow (left) and another one placed between the insufflator and the abdominal component of the model (right). 47*

Figure 34. *An additional pressure sensor was utilized to verify that the pressure set by the insufflator could be maintained within the abdominal bellow of the model. 47*

Figure 35. *The time signals of the airway pressure, flow and tidal volume for the respiratory compartment of the in vitro model, at the maximum insufflation pressure of 20 hPa. 49*

Figure 36. *Graphical representation of R (top) and E (bottom) for the respiratory component of the model and the respiratory system of the animal, as a function of the IAP. 51*

Figure 37. *Graph the compliance C of the respiratory component of the model and the respiratory system of the animal as a function of the IAP. 52*

Figure 38. *Graphical representation of R (top) and C (bottom) for the abdominal component of the model and the abdomen of the animal, as a function of the IAP. 54*

Figure 39. *Graphs of V_t and V_{ab} for the in vitro model and the animal used in the clinical trial as a function of the IAP. 55*

Figure 40. *Graph of the effect of IAP on the time difference Δt between the occurrence of V_t and V_{ab} for the model and the animal used in the clinical trial. 56*

Figure 41. *Graph of PIP-PEEP for the in vitro model and the animal used in the clinical trial as a function of the IAP. 58*

Figure 42. *Graph of the driving pressure ΔP for the respiratory side of the in vitro model (top) and the respiratory system of the animal used in the clinical trial (bottom) as a function of the IAP. 58*

LIST OF ABBREVIATIONS

IAV	Intra-Abdominal Volume
IAP	Intra-Abdominal Pressure
C_{ab}	Abdominal Compliance
P	Pressure
V	Volume
PPV	Positive Pressure Ventilation
ETT	Endo-Tracheal Tube
VCV	Volume-Controlled Ventilation
PCV	Pressure-Controlled Ventilation
A/C	Assist-Controlled
P_{aw}	Airway Pressure
V_t	Tidal Volume
PEEP	Positive End-Expiratory Pressure
$PEEP_i$	Intrinsic Positive End-Expiratory Pressure
P_{vent}	Ventilation Pressure
P_{mus}	Inspiratory Muscle Pressure
E_{RS}	Respiratory System Elastance
R_{AW}	Airway Resistance
$\dot{V}_I$	Inspiratory Flow
I	Inertia
$\ddot{V}_I$	Instantaneous Variation of the Inspiratory Flow
C_{RS}	Respiratory System Compliance
LSF	Least Squares Fitting
P_{es}	Esophageal Pressure
C_{CW}	Chest Wall Compliance
C_L	Lung Compliance

ARDS	Acute Respiratory Distress Syndrome
P_{alv}	Alveolar Pressure
ΔP	Driving Pressure
P_L	Transpulmonary Pressure
VILI	Ventilator-Induced Lung Injury
FRC	Functional Residual Capacity
$\dot{V}_{aw}$	Airway flow
P_{tr}	Trocar pressure
$\dot{V}_{tr}$	Trocar flow
FOT	Forced Oscillation Technique
Z	Mechanical Impedance
R	Resistance
X	Reactance
FiO_2	Fraction of Inspired Oxygen
$ETCO_2$	End-Tidal CO_2
RLS	Recursive Least Squares
γ^2	Coherence
TPU	Thermoplastic Polyurethane
R_{tr}	Trocar Resistance
V_{ab}	Abdominal Volume
PIP	Peak-Inspiratory Pressure

INTRODUCTION

1. Relevance of the Study

The first step in laparoscopic surgery is the creation and establishment of the pneumoperitoneum. The term refers to the presence of gas within the peritoneal cavity, and it is achieved with pressurized insufflation of CO_2 gas prior to the laparoscopic procedure. Intra-abdominal insufflation is performed with the use of a surgical insufflator, a gas pump, the function of which is to deliver the CO_2 and maintain a stable pressure in the abdomen of the patient.

The goal of the pneumoperitoneum is to increase the intra-abdominal volume (IAV) and create sufficient space for visualizing the organs and manipulating the instruments [1]. As the gas is delivered into the peritoneal cavity, the intra-abdominal pressure (IAP) increases, distending the abdomen and increasing the IAV, generating the internal workspace that is necessary for performing the surgery. A graphical illustration of the insufflated abdomen is displayed in Figure 1.

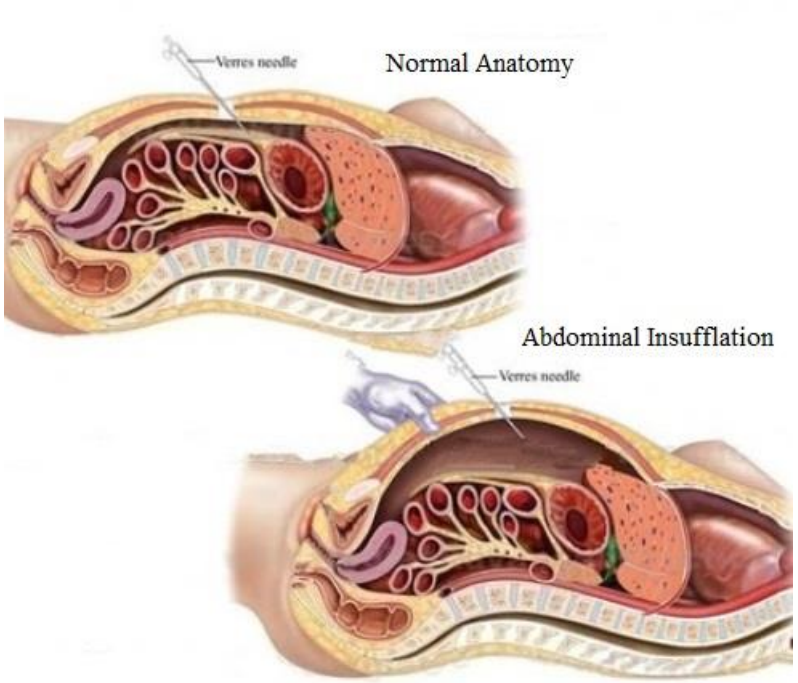

Figure 1. *Illustration of the abdominal cavity before (top) and after insufflation with CO_2 (bottom)* [2].

Maintaining a stable insufflation pressure is one of the greatest challenges in laparoscopy. During the procedure, gas inevitably escapes through the trocar, which opens to accommodate the surgical instruments, leading to a loss of pressure [3,4]. A considerable decrease in the pneumoperitoneum volume is also observed during several intraoperative situations, such as when surgical suctioning is performed, usually to remove blood or the smoke created with electrocautery [4]. Conventional surgical insufflators respond to gas leakage and pressure loss by adjusting the volume of the delivered

CO_2 [5]. However, such insufflation systems usually have a delay in their response [6,7]. An abrupt decrease in the insufflation pressure leads to a reduction in the created abdominal workspace. This, in turn, prolongs the surgical and anesthesia times and increases the risk of complications for the patient [3,4].

Typically, compensation of the insufflator for pressure loss results in an increase in IAP, often leading to considerable pressure spikes [3,7]. High pneumoperitoneum pressures are associated with organ damage, due to decreased blood perfusion [7], arrhythmias as well as increased risk of thrombosis [3,7,8]. Additionally, the function of the respiratory system is severely impacted, while the overstretching of the abdominal wall and the diaphragmatic muscle fibers result in post-operative abdominal pain [7,9].

Furthermore, it should be noted that the stretching capacity of the abdomen is patient-dependent, which means that there is no universal pressure that can be utilized for the establishment of an optimal pneumoperitoneum for every patient [1]. The insufflation pressure is set by the surgeon and is seldom adjusted. Due to the lack of any quantitative assessment or feedback, the selection of the insufflation pressure is solely based on the surgeon's experience [1]. Nevertheless, accurate individualized adjustment and maintenance of the pneumoperitoneum is of paramount importance for ensuring the efficacy of laparoscopic procedures as well as patient safety [3,4,6,10].

To resolve these challenges faced by the conventional devices, a novel surgical insufflator has been developed at the department of Pediatric Surgery of Erasmus MC - Sophia Children's Hospital. This new device offers several enhancements over conventional devices, and has the ability to maintain a stable pneumoperitoneum at an optimal, individualized pressure. The newly-developed insufflator is capable of accurately measuring the tension at the abdominal wall. Based on this measurement, it can real-time adjust the intra-abdominal pressure, setting it at the optimal level for each patient and keeping it constant throughout the course of the surgery. This minimizes the negative effects of insufflation, while increasing patient safety and the efficacy of the laparoscopic procedure.

2. Problem Statement & Goal

2.1 Problem Statement

Evaluation of the performance and the effect of the insufflator on the respiratory function of the patient is an important aspect of its development. Recently, the performance of the novel insufflator has been assessed with animal experiments. Nevertheless, experimenting on animals is a difficult, time-consuming and expensive procedure due to the strict legislation and protocols as well as the ethical considerations that need to be addressed. Besides, there are limitations in the number of tests and the different settings that can be examined, while the lack of repeatability in the results is an additional disadvantage.

Instead, the insufflator could be evaluated with an in vitro simulator. Such models allow for a significantly faster and inexpensive testing procedure. Moreover, they offer higher flexibility, as different intra-operative situations can be simulated and various settings of the insufflator can be examined within each trial. In addition, practical considerations suggest that it is more meaningful for the performance of a device to be assessed in vitro before proceeding to animal trials. In this manner, a first evaluation can be acquired, which allows the device to be set to the maximum of its potentiality prior to the in vivo assessment [11].

However, despite the variety of existing simulators for the respiratory system [12–18], there is currently no report in the literature of an in vitro model that combines and simulates the interaction between the respiratory system and the insufflated abdomen. Such a model would enable further testing of the new insufflator, allowing the investigation of the mechanical effects on respiratory

function during several intraoperative settings. This, in turn, means that more of its technical and operational characteristics can be examined. Furthermore, it would allow an initial assessment of the insufflator before proceeding to in vivo trials, complementing the overall assessment procedure and increasing its efficiency. Thus, a broader understanding of the insufflator's performance could be obtained.

Finally, although this study focuses on the surgical insufflator developed at Erasmus MC, the abovementioned statements are applicable for the evaluation of every surgical insufflator. A great amount of research is being performed on the development of new types of insufflators to encounter the challenges faced by the conventional devices. Consequently, the problems of this study can be expanded to the entire field of surgical insufflator manufacturing.

2.2 Goal

The goal of this thesis is to develop an in vitro model that simulates the interaction between the respiratory system and the abdominal cavity during surgical insufflation. The model is intended for providing an evaluation platform for the performance of the newly developed surgical insufflator and obtaining broader knowledge of the effect of abdominal insufflation onto the respiratory mechanics. Additionally, the in vitro model could be potentially used for head-to-head comparison between different surgical insufflators.

The goal of the project was divided into smaller objectives that needed to be delivered, which are presented in Table 1. First, a preliminary analysis was conducted on data obtained from animal experiments. This analysis was performed to define the mechanical parameters of the respiratory system and abdominal cavity, as a function of the abdominal pressure during insufflation. The design requirements were then formulated and the design of the model was created. Finally, the model was manufactured and assembled. Validation of its performance was achieved by comparing the results from the preliminary analysis to the results obtained from the model.

Table 1. *The individual objectives that were defined for the achievement of the ultimate goal of the thesis*

1. Preliminary analysis – Respiratory system
2. Preliminary analysis – Insufflated abdomen
3. Determine the individual model components
4. Design and assembly
5. Validation

3. Report Structure

The present report is divided into 4 main sections: Background, Methods, Validation and Discussion. The chapters and contents of each section are presented and described in Table 2.

Table 2. *The structure of the present report.*

Section	Chapters	Content Description
Background	4. Respiratory Mechanics & Mechanical Ventilation 5. Respiratory-Abdominal Interaction 6. Abdominal Mechanical Properties	These chapters provide background information on the methods utilized for carrying out this thesis. Chapter 4 focuses on the major functional mechanical parameters of the respiratory system. Chapter 5 discusses the interaction between the respiratory system and the abdomen during insufflation, while Chapter 6 is related to the mechanical properties of the abdomen during insufflation, and the approaches that are used for estimating them.
Methods	7. Preliminary Analysis 8. Development of the Model	This section refers to the methods and steps used for the accomplishment of this thesis. Chapter 7 presents the preliminary analyses that were conducted for the respiratory system and the abdomen of the animals. Chapter 8 reflects on the entire process of designing and manufacturing the physical model, from defining the design requirements to the delivery of the final device.
Validation	9. Validation Methodology	In Chapter 9, the goal and the protocol of the validation are discussed and the experimental setup used for the assessment of the in vitro model is described. Finally, the results of the validation are presented
Evaluation	10. Discussion 11. Recommendation 12. Conclusions	The final chapters of the thesis include the interpretation of the obtained results and discuss the clinical relevance, recommendations for future research as well as the end-points of the present work

BACKGROUND

4. Respiratory Mechanics & Mechanical Ventilation

Mechanical ventilation is necessary for providing adequate respiratory support in patients who are severely diseased or under general anesthesia [19]. In laparoscopic procedures, as the patient is anesthetized, intraoperative mechanical ventilation is mandatory in order to maintain pulmonary gas exchange.

Respiratory mechanics result from the interaction between the chest wall and the lungs and can be investigated by the measurement of pressure and flow as a means to express and assess the respiratory function [20]. Several indices and parameters can be estimated based on these measurements during mechanical ventilation [21]. Knowledge of the physiology of the respiratory system and the basic breathing mechanics is of great importance for interpreting the interaction between the ventilator and the patient [22]. For this reason, a basic overview of the respiratory system and the mechanics of pulmonary ventilation are given, followed by a description of the major respiratory parameters during mechanical ventilation.

4.1 Overview of the Respiratory System

The respiratory system, of which the major structures of which are shown in Figure 2, starts at the nose and mouth and continues through the airways to the lungs. Its main function is to provide oxygen to the body while eliminating carbon dioxide that is produced in the tissues. To achieve this, the respiratory system enables the movement of air into the lungs (pulmonary ventilation) and the diffusion of oxygen from the lungs to the blood with simultaneous diffusion of CO_2 from the blood to the lungs (internal respiration) [23].

Functionally, the respiratory system consists of a conducting and a respiratory zone. The conducting zone includes the nose and mouth, pharynx, larynx, trachea, bronchi and bronchioles, which form a rigid conduit for the air to flow into and out of the lungs [23]. The respiratory zone is the actual site of gas exchange, located deep within the lungs. It consists of the respiratory bronchioles, alveolar ducts and alveoli, tiny thin-walled sacs which allow the diffusion of inhaled O_2 to into the blood in exchange for CO_2 [23]. As the process of pulmonary ventilation is the major point of focus, internal respiration is beyond the scope of this thesis. Thus, the gross anatomy and physiology of the lungs as well as the conducting passageways, are examined, with emphasis on the mechanics that create the flow of air. The functional anatomy of the structures that contribute to gas exchange in the microscopic level are not included.

The lungs are a pair of air-filled organs, located on either side of the thoracic cavity [24]. They contain the bronchial tree consisting of bifurcating airways, which branch off into tubes of decreasing diameters. The bronchial tree eventually leads to the pulmonary alveoli, which are the site of gas exchange [23]. From a mechanical standpoint, three main parts can be distinguished: the air in the conducting airways, the lungs as the structures that contain the gas, and the thoracic cavity that encloses the lungs [25].

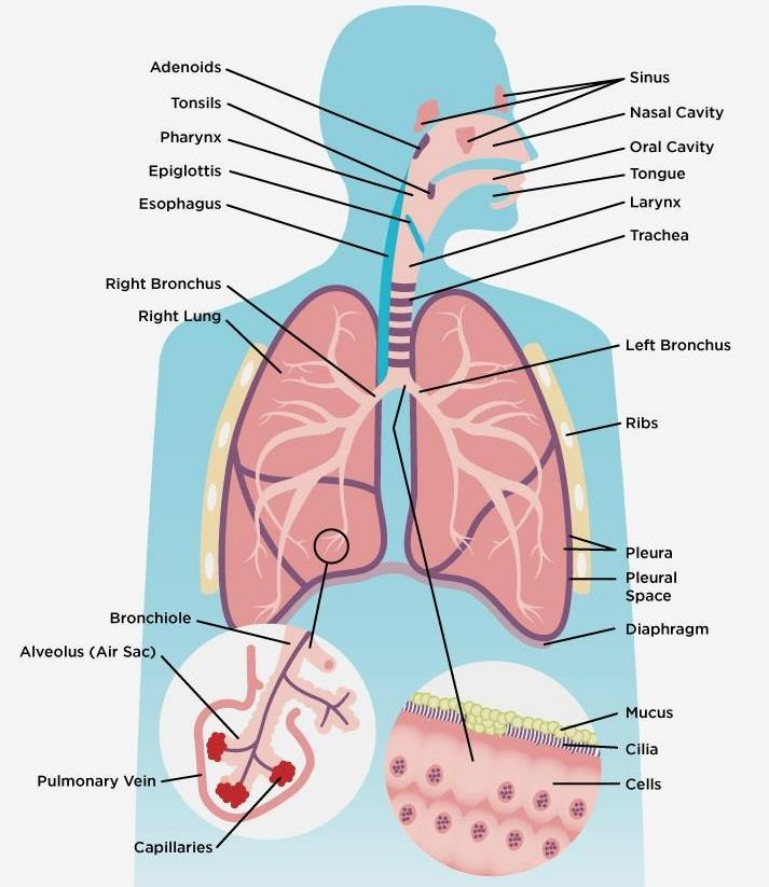

***Figure 2**. The major components of the respiratory system* [26].

Each lung is covered by a double-layered membrane, called the pleura. The parietal pleura is the external layer that covers the thoracic wall and the superior surface of the diaphragm, while the visceral pleura covers the external lung surface [23]. The pleura cavity, the space between the parietal and visceral pleura, is filled with the pleural fluid. The pleural fluid is a viscous secretion that acts as a lubricant, cushioning the lungs and reducing the friction generated as they glide across the rib cage and thoracic wall during breathing [27]. In addition, the surface tension of the pleural fluid prevents separation of the pleural layers. Therefore, the lungs cling tightly to the thoracic wall, expanding and recoiling due to the alternate increase and decrease of the volume of the thoracic cavity during breathing [23].

4.2 Mechanics of Breathing

Pulmonary ventilation (breathing) is the mechanical process which involves the flow of air into the lungs during inspiration and out of the lungs during expiration [28]. This generated flow is due to the pressure differences between the atmosphere and the air inside the lungs, as a result of changes in the volume of the thoracic cavity. Three main pressures are involved in pulmonary ventilation: 1) the atmospheric pressure, 2) the pulmonary pressure (pressure inside the alveoli of the lungs) and 3) the pleural pressure (pressure in the pleural cavity).

The relationship between the pressure and volume of a gas is given by Boyle's Law, which states that for a specified amount of gas, maintained at a constant temperature, the pressure and volume are inversely proportional [29]. For comparing the same gas under two different sets of conditions, Boyle's Law is expressed as:

$$P_1V_1 = P_2V_2 \quad (1)$$

,where P and V are the pressure and volume of the gas, while subscripts 1 and 2 denote the initial and resulting conditions respectively. Breathing takes place according to Equation 1, which shows that an increase in volume results in a proportionate decrease in the pressure of the gas. Likewise, a decrease in the volume leads to an increase in the pressure.

Inspiration is the process which fills the lungs with air. It occurs as a result of the contractile action of the inspiratory muscles – the diaphragm and the external intercostal muscles. More specifically, during normal inspiration, the diaphragm contracts and moves inferiorly, extending the thoracic cavity [23]. At the same time, the external intercostal muscles contract as well, elevating the ribs and sternum superiorly [23]. Of note, the action of the diaphragm is more significant than the rest of the inspiratory muscles in producing volume changes during normal inspiration. The distention of the thoracic cavity stretches the lungs and increases the intrapulmonary volume [23]. As a result, according to Boyle's Law, the pulmonary pressure drops in relation to the atmospheric pressure. The created pressure gradient causes air to flow into the lungs, gradually increasing the pulmonary pressure until it becomes equal to the atmospheric, when inspiration ends.

Expiration, the process of letting air out of the lungs, is a passive process that occurs as a result of lung elasticity. After the end of inspiration, the inspiratory muscles relax to their resting length decreasing the volume of the thoracic cavity [23]. Due to their elasticity, the lungs recoil passively and the intrapulmonary volume decreases as well [23,28]. As the alveoli are compressed, the pulmonary pressure increases to above the atmospheric pressure, creating a pressure gradient that forces gases to flow out of the lungs.

4.3 Mechanical Ventilation

It is clear that, in physiological breathing, the action of the inspiratory muscles as well as the elastic properties of the chest wall and the lungs play a major role in establishing the pressure gradient that leads to the flow of air into and out of the lungs [22]. However, general anesthesia deteriorates both gas exchange in the lungs and respiratory mechanics [30,31]. The utilized anesthetic agents significantly depress the activity of the respiratory centers in the brain stem, as well as the respiratory muscles [32]. Therefore, the respiratory drive and the muscular component of breathing are greatly reduced or even completely ceased [22]. As a result, the use of a mechanical ventilator is necessary for generating a positive pressure and creating the airflow for gas exchange, independently of the action of the inspiratory muscles.

Positive-pressure ventilation (PPV) involves the delivery of air or a mixture of oxygen and other gases into the lung, by applying a positive pressure in the airway of the patient [33]. As gas flows into the lungs, the pulmonary pressure gradually rises until the ventilator breath is terminated. Expiration occurs passively as the result of the elastic recoil of the chest and lungs, which forces the gas out to the less pressurized conductive airways [33,34]. Historically, negative pressure ventilation had been widely used for respiratory treatment of patients suffering from poliomyelitis by enclosing the patient's torso inside a machine, called the iron lung, that created vacuum conditions [35]. However, the resurgence of poliomyelitis with the epidemic of Copenhagen in 1952 and the low availability of iron lungs led to the implementation of PPV into clinical practice [35,36].

Positive-pressure ventilation can be applied non-invasively by delivering the gas into the airway of the patient with the use of a face mask, or invasively by inserting an endotracheal tube (ETT) through the nose or mouth into the trachea [33], as illustrated in Figure 3. The ETT is then connected to the ventilator, which applies the positive pressure at the airway of the patient. General anesthesia and the use of an ETT is the golden standard during laparoscopic surgery, as it allows for more accurate control of the mechanical ventilation [37]. With the exception of relatively simple and short procedures

without general anesthesia, almost all patients require endotracheal intubation prior to laparoscopic surgery to prevent inadequate ventilation or other respiratory disorders resulting from the pneumoperitoneum [38,39].

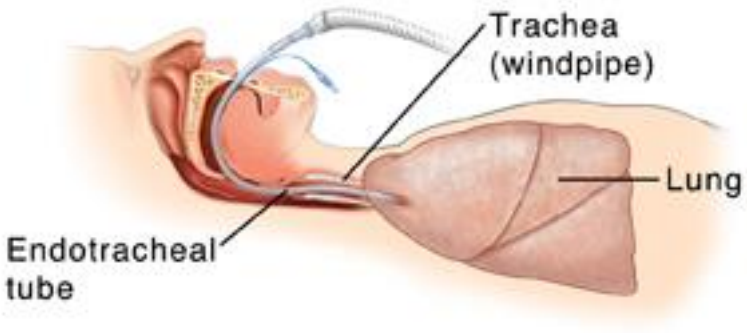

Figure 3. *In invasive positive pressure ventilation, an endotracheal tube connected to the ventilator is inserted into the trachea of the patient and applies a positive pressure in the respiratory airway [40].*

With regards to the operation modes of mechanical ventilation, positive-pressure ventilation can either be volume-cycled, pressure-cycled or a combination of the two. In volume-cycled ventilation, a constant volume of gas is delivered with each breath, whereas pressure-cycled ventilation administers the gas at a fixed pressure [41]. Of these, the major and most commonly used modes of mechanical ventilations during general anesthesia are volume-controlled ventilation (VCV) and pressure-controlled ventilation (PCV) [42]. Both of these ventilation modes enable the maintenance of a minimum respiratory rate independently of the ability of the patient to breath spontaneously, and are commonly referred to as assist-control (A/C) ventilation modes [41].

VCV is a volume-cycled mode of ventilation that delivers a fixed tidal volume (V_t). This means that the volume of air that moves in and out of the lungs with each respiratory cycle is kept constant. The resultant airway pressure (P_{aw}) is not set and varies with the mechanical properties of the respiratory system. On the contrary, during PCV, pulmonary ventilation is accomplished at a fixed inspiratory pressure. Therefore, V_t varies depending on the mechanical properties of the respiratory system.

VCV is the most commonly used mode of ventilation in the clinical setting, and is considered as the simplest and most effective solution for mechanical ventilation [41,43]. It has been shown that VCV is a safe and effective approach for patients during general anesthesia [43]. With regards to laparoscopy, VCV is the preferred ventilation mode as it ensures the delivery of a fixed tidal volume to the patient [44], despite the changes in the compliance of the chest wall and lungs, that can occur due to muscle relaxation and the increase of the IAP. For this reason, the estimation and interpretation of the mechanical parameters of the respiratory system in this thesis is based on the volume-controlled mode of mechanical ventilation.

4.4 Respiratory Mechanics During Mechanical Ventilation

As mentioned, respiratory mechanics refer to the measurement of pressure and flow as a means to assess the respiratory function. Meaningful interpretation of these measurements and their derived respiratory parameters are crucial not only for the evaluation of the physiological lung function, but also for the assessment of the impact of intraperitoneal insufflation on the respiratory system and the optimization of the mechanical ventilation strategy [21,22]. A basic overview of the respiratory physiology and the major respiratory parameters during intra-operative VCV is presented, followed by the effect of abdominal insufflation on the respiratory function.

4.4.1 Input Parameters

In VCV, a fixed amount of gas, the tidal volume, is delivered into the lungs with each breath. The amount of air entering the lungs gradually increases until the desired V_t is achieved within the specified inspiratory time, marking the end of inspiration. Once V_t is delivered, the expiratory valve of the ventilator opens and passive expiration takes place [45].

The desired V_t, respiratory rate, inspiratory to expiratory ratio (I:E) and positive end-expiratory pressure (PEEP) are set as input parameters in the ventilator during the VCV mode [22]. The respiratory rate refers to the number of breaths that take place each minute. The I:E ratio is defined as the ratio of the inspiratory time over the expiratory time, indicating what proportion of each breath cycle is assigned to the inspiratory and expiratory phase [46]. For instance, a typical I:E ratio value is 1:2, which means that, within each breath cycle, the expiratory phase takes twice the time to be completed than the inspiratory phase.

PEEP is the intrapulmonary pressure that exists at the end of expiration in mechanical ventilation [47,48]. There are two types of PEEP: the extrinsic PEEP, which is applied by the mechanical ventilator, and the intrinsic PEEP ($PEEP_i$), which occurs due to incomplete expiration. The accumulation of air in the lungs, because of incomplete exhalation before the initiation of the inspiration phase, gradually increases the intrapulmonary pressure at end-expiration, which is referred to as $PEEP_i$ [49,50]. On the other hand, extrinsic PEEP is applied by the mechanical ventilator to mitigate the collapse of the unstable alveolar units [51]. At the end of expiration, the mechanical ventilator exerts a set pressure, which opposes passive expiration and maintains the airway pressure above the atmospheric [52]. The level of extrinsic PEEP, typically between 3-5 cmH_2O, is directly set on the ventilator and is one of the first input parameters selected at the initiation of mechanical ventilation. Once all the input parameters are set and adjusted depending on the characteristics of the patient, mechanical ventilation is initiated and the measurements are obtained.

4.4.2 Measured Parameters

Airway Pressure, Flow and Tidal Volume

One of the fundamental measurements during mechanical ventilation is the airway pressure (P_{aw}). It is measured in the proximal airway, typically in the mouth, with the use of a pneumotachometer. Pneumotachometers are widely used for the measurement of both the airway pressure and flow. They consist of a tube containing a flow-resistive element, typically a fine mesh screen, and a heating element [53], as illustrated in Figure 4. As the gas flows through it, the resistive element creates a known pressure drop, which is linearly proportional to the flow. The airway pressure is measured by a pressure transducer with respect to the ambient pressure [53]. The heater prevents the accumulation of water, which occurs due to condensation of water vapor during breathing and can significantly alter both the resistive properties of the mesh screen and the flow characteristics [54].

Therefore, the placement of the pneumotachometer enables the measurement of the flow of gas in the airway as well. Since the detected pressure gradient between the two sides of the resistive mesh is linearly proportional to the flow of gas through it, the inspiratory flow can be continuously measured alongside the airway pressure [55].

Despite being a parameter that is set on the ventilator in VCV, the tidal volume is also monitored during anesthesia. V_t is not directly measured, but is calculated as the integration of the inspiratory flow indicating the amount of gas that flows in the lungs with each breath. Monitoring of the volume and evaluating its approximation to the set value is particularly useful for assessing the operation of the ventilator and detecting the presence of leaks in the mechanical ventilator-endotracheal tube configuration [21].

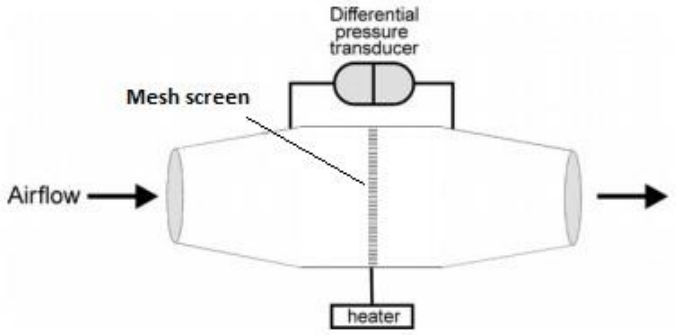

Figure 4. *Schematic representation of the pneumotachometer configuration. The air flows through the resistive mesh, which creates a pressure drop detected by the pressure transducer. The heating element prevents the accumulation of moisture and secretions* [56].

Equation of Motion

Airway pressure is plotted as a function of time and the shape of the waveform depends on the airway flow, V_t as well as the active breathing effort of the patient, if it exists [21]. Thus, the airway pressure can be predicted mathematically by the equation of motion of the respiratory system (Equation 2), which relates it to the airway flow and V_t [57]:

$$P_{vent} + P_{mus} = E_{RS} \cdot V_t(t) + R_{aw} \cdot \dot{V}_I(t) + PEEP + PEEP_i + I \cdot \ddot{V}_I(t) \quad (2)$$

where P_{vent} is the airway pressure that is applied by the mechanical ventilator, P_{mus} is the pressure created by the action of the inspiratory muscles of the patient, E_{RS} is the elastance of the respiratory system, V_t is the tidal volume, R_{aw} is the airway resistance, $PEEP$ is the extrinsic PEEP applied by the ventilator, $PEEP_i$ is the intrinsic PEEP. The last term, consisting of the inertia, I, due to acceleration of the air column and the instantaneous variation of the inspiratory flow ($\ddot{V}_I$) is the inertance component. During normal quiet breathing, its effect is assumed to be insignificant compared to the other terms of the equation and is, therefore, usually neglected [21]. In addition, when the breathing activity of the patient is completely suppressed, as is the case in laparoscopy due to general anesthesia, P_{mus} is disregarded as well.

The term $E_{RS} \cdot V_t(t)$ represents the pressure required to overcome the elastic forces of the respiratory system and depends on the tidal volume and the elastance of the respiratory system [57]. The elastance is defined as the inverse of the compliance:

$$E = \frac{1}{C} = \frac{\Delta P}{\Delta V} \quad (3)$$

Consequently, the term $E_{RS} \cdot V_t(t)$ can be alternatively written as $V_t(t)/C_{RS}$, where C_{RS} is the compliance of the respiratory system. The term $R_{aw} \cdot \dot{V}_I(t)$ denotes the pressure that is required to overcome the frictional forces that occur due to the flow of gas across the airway. It is, therefore, related to the amount of energy that is dissipated across the airway and is determined by the inspiratory flow as well as the airway resistance (R_{aw}) [57].

Overall, each breath can be expressed by the equation of motion in relation to the three measured variables (pressure, flow and volume), the extrinsic (or intrinsic) PEEP if present, and two derived parameters (E_{RS} or C_{RS} and R_{aw}) [57]. These parameters are known as the dynamic properties of the

respiratory system and can estimated with the use of a multiple linear regression analysis, called linear least-squares fitting (LSF), to fit the equation of motion to the measured variables of pressure, flow and volume ($P_{aw}, \dot{V}_I, V_t$) [21,57]. This method assumes a linear single-compartment mathematical model, which does not take into account any changes in C_{RS} and R_{aw} within each breath. Furthermore, it assumes that the breathing of the patient is entirely passive (P_{mus}=0) and neglects the effect of inertial forces [21].

One of the major advantages of the LSF approach is the fact that that it allows superimposing of the pressure waveform predicted by the mathematical model onto the measured airway pressure, enabling the assessment of the 'goodness of fit' [57]. Of note, this mathematical approach is incorporated into the operational software of several ventilators for the real-time estimation of the dynamic respiratory parameters [21].

Esophageal Pressure

Estimation of the pressure within the pleurae of the lungs, or pleural pressure (P_{pl}), is challenging during mechanical ventilation, as the direct measurement is not feasible. Therefore, the most commonly used approach to assess P_{pl} is to estimate it by measuring the esophageal pressure (P_{es}) [21,22].

Measurement of P_{es} is accomplished with the use of an esophageal balloon, placed over a thin catheter [58,59]. The catheter contains several small holes at its distal end, which is placed within the 10-cm balloon. The balloon prevents occlusion of the holes by esophageal tissue and, as it is inflated, maintains an amount of air in and around the catheter, enabling the measurement of pressure [58]. The proximal end of the catheter is connected to a pressure transducer. The catheter-balloon configuration is depicted in Figure 5.

The balloon-tipped catheter is inserted through the nose or mouth of the patient and is placed in the lower third of the esophagus. Due to the passive nature of the esophagus as a structure and its proximity to the pleural space, as shown in Figure 6, the pressure in the pleural space is transmitted to the esophageal balloon and the measurement of P_{es} is a close approximation of P_{pl} [60,61]. Accurate placement and adequate inflation of the esophageal balloon is of great significance for obtaining reliable P_{es} measurements [59]. The appearance of cardiac oscillations in the P_{es} waveform is an indication of correct placement of the catheter in the lower third of the esophagus, adjacent to the heart [21].

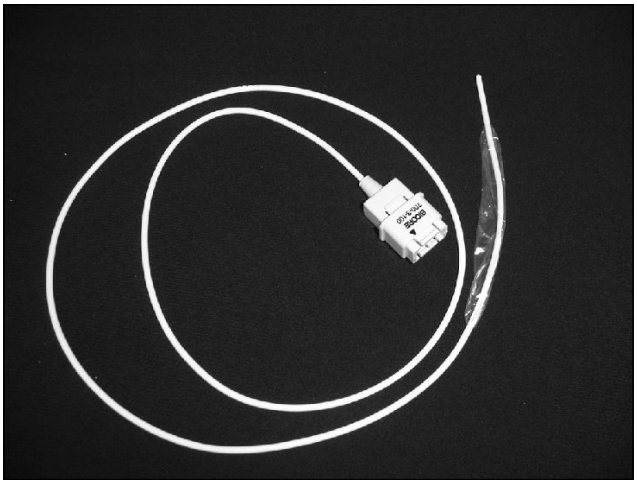

Figure 5. *The esophageal balloon-tipped catheter used in adults. The distal end of the catheter is placed within the balloon, while the proximal end is connected to the measurement and recording equipment* [62].

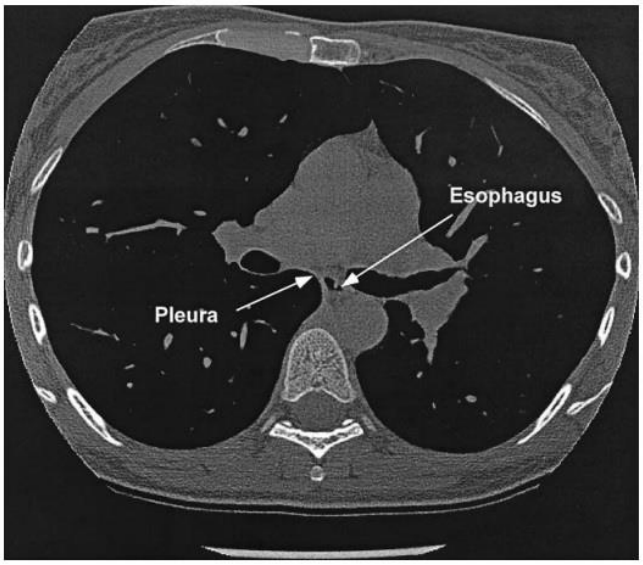

Figure 6. *Computed tomography of the chest, showing that the esophagus is adjacent to the pleural space in the mid thorax* [58].

4.4.3 Derived Parameters

Respiratory System Compliance (C_{RS})

The respiratory system compliance (C_{RS}) is a measure of the ability of the respiratory system to be distended during ventilation [22]. In each respiratory cycle, it represents the ratio between the tidal volume (V_t) and the pressure that is required to achieve its delivery:

$$C_{RS} = \frac{\Delta V}{\Delta P} = \frac{V_t}{\Delta P} \tag{4}$$

As described in 4.4.2, fitting of the equation of motion (Equation 2) to the measured variables, with a method such as LSF, leads to the estimation of the respiratory system elastance (E_{rs}) and, by extension, the respiratory system compliance (C_{RS}), since the elastance is defined as the inverse of compliance (Equation 3). C_{RS} is also expressed as the addition in parallel of the chest wall (C_{CW}) and lung compliance (C_L):

$$\frac{1}{C_{RS}} = \frac{1}{C_{CW}} + \frac{1}{C_L} \tag{5}$$

From Equation 5, it is clear that the total respiratory system compliance is determined by the compliance of the chest wall and lungs. In addition, the value of the total C_{RS} is lower than the compliance of each of the single compartments (C_{CW}, C_L) [22].

Airway Resistance (R_{aw})

R_{aw} represents the resistance that the respiratory tract opposes to airflow during ventilation. It can be calculated as the ratio of the pressure difference between the external atmosphere and the alveoli (ΔP) and the flow of the gas ($\dot{V}$):

$$R = \frac{\Delta P}{\dot{V}} \quad (6)$$

R_{aw} is one of the dynamic parameters of the respiratory system during mechanical ventilation and can be calculated, similarly to C_{RS}, by applying the LSF algorithm to the equation of motion (Equation 2). The diameter of the airway is the most significant factor that determines R_{aw}. The Hagen–Poiseuille law of fluid dynamics, which assumes a laminar, viscous and incompressible flow, dictates that the resistance of a long cylindrical tube can be expressed as:

$$R = \frac{8\eta L}{\pi r^4} \quad (7)$$

, where η is the dynamic viscosity of the fluid, while L and r are the length and radius of the tube respectively. Equation 7, despite the fact that it is not a strict representation of the respiratory airway resistance due to the assumption of laminar flow, suggests that small changes in the airway diameter result in large changes in R_{aw}, as it depends on the fourth power of the airway radius. Physiologically, R_{aw} is insignificant in the proximal part of the airway due to the large diameter in combination with the low air viscosity. As the airway diameter of the conducting zone gradually decreases towards the lungs, the number of branches gradually rises, increasing the overall cross-sectional area. Therefore, the highest R_{aw} is observed at the medium sized bronchi of the respiratory system. Although it is generally stable, respiratory diseases – such as asthma – can affect R_{aw}, which is also dependent on the diameter of the ETT during mechanical ventilation.

Alveolar Pressure (P_{alv})

Alveolar (or intrapulmonary) pressure, P_{alv}, is the pressure inside the alveoli of the lungs. In volume-controlled mechanical ventilation, P_{alv} is dependent on the tidal volume and the compliance of the respiratory system [21]:

$$P_{alv} = \frac{V_t}{C_{RS}} + PEEP \quad (8)$$

Driving Pressure (ΔP)

In the absence of active breathing effort by the patient, the driving pressure (ΔP) is defined as the pressure above the PEEP level, which is applied by the mechanical ventilator to the entire respiratory system to achieve ventilation [63]. ΔP is expressed as the ratio of the tidal volume (V_t) over the respiratory system compliance (C_{RS})[48,64]:

$$\Delta P = \frac{V_t}{C_{RS}} \quad (9)$$

C_{RS} is correlated to the lung volume that is ventilated [65]. Equation 9 shows that ΔP is the ratio of V_t normalized to the ventilated lung volume. Thus it represents the global strain in the lungs, and is an important respiratory parameter during mechanical ventilation [63,64]. Of note, ΔP consists of two components: one linked with lung distention and the other with the expansion of the chest wall [63].

There have been several reports that the intraoperative driving pressure is related to the occurrence of major post-operative complications, such as pneumonia, edema and acute respiratory distress syndrome (ARDS) [66,67].

Transpulmonary Pressure (P_L)

The transpulmonary pressure (P_L) is defined as the difference between the airway pressure (P_{aw}) and the pleural pressure (P_{pl}) [68,69].

$$P_L = P_{aw} - P_{pl} \tag{10}$$

Therefore, P_L reflects the pressure that is required to create the flow of air through the airway and the pressure necessary to overcome the elastic recoil of the lung tissue, which is frequently associated with lung injury [63,69]. P_{pl} is usually measured at 2 two critical points, under static conditions (zero flow): end-inspiration and end-expiration. At these conditions, P_L represents the pressure that distends the alveoli of the patient [21,63]. The transpulmonary pressure corresponds to the elastic component of the lungs and can be used for quantifying the stress applied to the lung tissue [70]. Transpulmonary pressure is monitored during mechanical ventilation as it is frequently related to lung injury [63,69].

For estimating the pressure in the pleurae, the esophageal pressure is utilized, which corresponds directly to P_{pl} [21,63]. Consequently, the equation for measuring the transpulmonary pressure becomes:

$$P_L = P_{aw} - P_{es} \tag{11}$$

It should be noted that, in the context of this study, P_L is measured with the use of Equation 11 at end-inspiration.

The transpulmonary pressure reflects the mechanical load that is exerted to the lungs during mechanical ventilation and, by extension, the mechanical stress applied to the lung tissue [68,69]. It is regarded as a contributing factor to the occurrence of ventilator-induced lung injury (VILI) and its estimation allows assessing the risk of injury during ventilation [69–71].

5. Respiratory-Abdominal Interaction

The interaction between the respiratory system and the abdominal cavity is an important consideration. During laparoscopy, the pressurized pneumoperitoneum exerts a direct mechanical effect on the respiratory system because of the rise in the intra-abdominal pressure (IAP). As the thoracic and abdominal compartment are linked by the diaphragm, the mechanical properties of the respiratory system and the overall respiratory function are dependent on the IAP level.

Intra-abdominal insufflation is an integral aspect of laparoscopy, as it creates the necessary intra-abdominal workspace that is necessary for performing the surgery [1]. Depending on the patient and the abdominal compliance (C_{ab}), IAP may reach levels up to 25 mmHg (from the physiological level of ≈3 mmHg) for a sufficient IAV to be generated [1,10].

The establishment and maintenance of the pneumoperitoneum greatly affects the respiratory mechanics [72]. The rise in IAP obstructs the movement of the diaphragm during breathing and forces it forces it so shift cranially, as Figure 7 shows [72,73]. The restricted movement of the diaphragm may decrease the tidal volume and functional residual capacity (FRC) [74,75]. In addition, the chest wall becomes stiffer at higher insufflation pressures [21,72]. As a result, the compliance of the respiratory system decreases due to the drop in C_{CW}, while C_L remains constant. Application of a PEEP by the mechanical ventilator ameliorates this effect by opposing the collapse of the alveoli and the reduction in V_t, maintaining the lung volume after expiration [72,76].

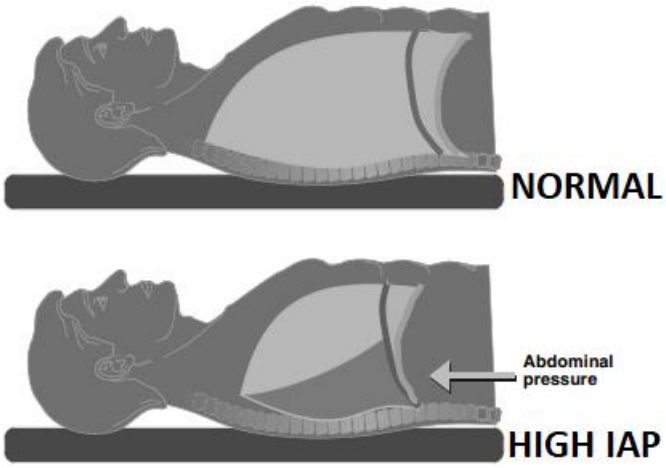

Figure 7. *Schematic representation of the cranial shift of the diaphragm and the change in its movement during abdominal insufflation* [77].

To counteract the reduction in V_t, volume-controlled ventilation (VCV) is applied to maintain adequate pulmonary gas exchange. Despite the beneficial effect of PEEP, the decrease in respiratory compliance inevitably results in a rise in the peak inspiratory pressure (PIP) as well as ΔP [71–73,78]. This is due to the fact that higher pressures are required to achieve the delivery of a constant tidal volume in the respiratory system during VCV. Consequently, this rise in the intrathoracic pressure eventually leads to an increase in the work of breathing [72,79]. The major mechanical effects of the increase in IAP on respiratory function are summarized in Table 3.

Table 3. *The major effects of the rise in IAP on respiratory mechanics.*

Respiratory Function	Effect
Functional Residual Capacity	Decrease
Peak Airway Pressure	Increase
Driving Pressure	Increase
Chest Wall Compliance	Decrease
Respiratory Compliance	Decrease
Work of Breathing	Increase

6. Abdominal Mechanical Properties

During insufflation, the abdomen of the patient can be viewed as a container, and the CO_2 gas as the means to generate the additional intra-abdominal space [1]. This container is composed of both rigid (spine and pelvis) and partially flexible (abdominal wall, diaphragm) external sides, as Figure 8 demonstrates [80]. As more gas is gradually administered, the abdominal wall expands and increases in height. As the insufflated abdomen distends across the sagittal plane and obtains a dome-like shape, the diaphragm moves cranially.

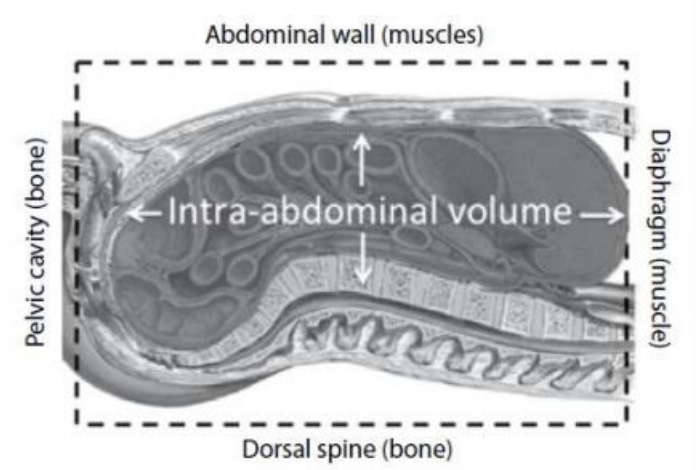

Figure 8. *The abdomen can be represented as a container with 2 rigid (pelvic bone, dorsal spine) and 2 partially flexible (abdominal wall, diaphragm) borders [80].*

The mechanical properties of the elastic boundaries of the abdominal cavity, such as the abdominal wall and diaphragm, set the limits of abdominal distention [1]. Estimation of the abdominal mechanical behavior is of particular importance, as it is patient-dependent and defines the IAV-IAP relationship during surgical insufflation.

The abdominal mechanical properties are expressed as the abdominal compliance (C_{ab}). This represents a measure of the ease of abdominal distention, and depends on the elasticity of the abdominal wall as well as the diaphragm [1,80]. By definition, the abdominal compliance is the ratio of the change in IAV over the change in IAP and is expressed in L/cmH_2O:

$$C_{ab} = \frac{\Delta(IAV)}{\Delta(IAP)} \tag{12}$$

6.1 Forced Oscillation Technique (FOT)

A minimally invasive approach for estimating C_{ab} is the application of the Forced Oscillation Technique (FOT). FOT is a simple and effective method for measuring the mechanical properties of physiological systems, and has been extensively used for the assessment of the mechanical behavior of the respiratory system [81,82].

The technique involves the application of an oscillating low-amplitude external pressure signal in a sequential oscillation frequency range, and the measurement of the generated flow [81]. The mechanical properties of the abdominal wall are derived from the relationship between the externally applied oscillatory pressure (input) and the resulting oscillatory flow (output). The basic setup for the

application of FOT includes a driver for producing the excitation pressure signal, a flow sensor for measuring the generated flow of air, and a pressure sensor for measuring the pressure at the input of the system.

Measurement of the oscillatory pressure and flow allows the quantification of their relationship. The complex ratio between the stimulating pressure (P) and the generated oscillatory flow ($\dot{V}$) as a function of the oscillatory frequency (ω) defines the mechanical impedance (Z)[82] :

$$Z = \frac{P(\omega)}{\dot{V}(\omega)} \tag{13}$$

The mechanical properties of the abdomen are specified by estimating $Z(\omega)$, which is the transfer function between the input and output signals of FOT. $Z(\omega)$ arises from the resistive, inertial and elastic contributions of the abdomen and can be expressed by separating its resistive (R) and reactive (X) components [82]:

$$Z(\omega) = R(\omega) + jX(\omega) \tag{14}$$

The resistance R is related to energy dissipation, while the reactance X is associated with energy storage.

6.2 Mathematical Modelling

Once $Z(\omega)$ is estimated, the acquired impedance data are fitted onto mathematical models that define the relationship between parameters of known physiological meaning and the impedance. [83]. With this method the mechanical properties specific to the abdomen can be quantified by identifying the parameters of the mathematical model. Accurate fitting of the data in the model is necessary, so that all the relationships between the parameters and the resulting mechanical properties are described. This ensures that the obtained parameters are physiologically meaningful [83].

A commonly utilized mathematical model is the RIC model, which represents the abdomen as a combination of resistance R, inertance I and compliance C in series, as Figure 9 demonstrates [81].

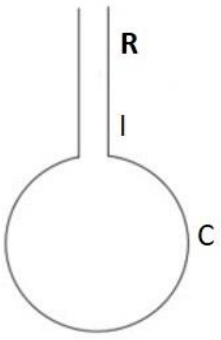

Figure 9. *Schematic representation of the R-I-C model used for the estimation of the abdominal mechanical properties.*

The resistive component of Equation 14 corresponds to the resistance R of the mathematical model, while the reactance consists of the inertial component I, which arises from the acceleration of

the gas mass in the system and the elastic component, C, representing the abdominal compliance. Thus, the RIC model expresses the mechanical impedance as[82] :

$$Z(\omega) = R + j\omega I + \frac{1}{j\omega C} \tag{15}$$

Equation 15 shows that there is a specific frequency, called the resonant frequency ω_o, at which the reactance is zero and Z(ω) depends only on the resistive component:

$$\omega_o = \sqrt{\frac{1}{C\ I}} \tag{16}$$

At the resonant frequency, the magnitude of the mechanical impedance is minimized [82]. For low frequencies, the effect of the inertial term on Z and X depends only on the compliance C of the abdomen:

$$X(\omega) = -\frac{1}{j\omega C} \tag{17}$$

Estimation of the RIC model parameters is achieved with the use of a multivariable regression analysis tool, such as the Least-Squares Method. This results in the quantification of the abdominal mechanical properties, as a value for C_{ab} is obtained.

Overall, the process of estimating of the abdominal mechanical properties begins with the application of FOT to calculate the mechanical impedance of the system, which correlates the simulating pressure to the resulting flow. Then, the obtained impedance data are fitted to a physiologically meaningful mathematical model, such as the RIC model. Finally, identification of the model parameters results in the quantification of the abdominal mechanical properties.

METHODS

The goal of this study is the development of an in vitro model capable of simulating the interaction between the respiratory system and the insufflated abdomen. To accomplish this goal, a preliminary analysis was first conducted, to examine the respiratory and abdominal mechanical properties as a function of IAP during insufflation. Once this information was acquired, the design requirements were formulated and the individual components of the model were selected. Finally, the physical model was designed, manufactured and assembled. All the steps of this process, the implemented methods and utilized materials are explained and described in this section.

7. Preliminary Analysis

The preliminary analysis aimed at investigating the mechanical properties of both the respiratory system and the abdomen during surgical intra-abdominal insufflation. Since the goal of the study is to simulate and the respiratory-abdominal interaction, obtaining knowledge on the mechanical interplay is of great importance. This way, the end-goals of the model as well as the design process can be determined, in addition to the knowledge that is obtained on the examined systems.

The preliminary analysis is divided into 1) the respiratory analysis, performed for assessing the respiratory function and mechanical properties as a function of IAP and 2) the abdominal analysis, for estimating the mechanical properties of the abdomen during surgical insufflation.

7.1 Experimental Data & Measurement Protocol

The preliminary analysis was performed on data obtained from animal experiments that were conducted at Erasmus MC in August 2019, for evaluating the performance of the novel insufflator in vivo. A 20-kg piglet underwent intra-abdominal insufflation at a range of IAP values, followed by the application of FOT, while its respiratory function was assessed. The piglet remained under general anesthesia and breathing was achieved by mechanical ventilation.

Volume-controlled mechanical ventilation was applied using the neonatal intensive care ventilator Fabian HFO (Acutronic Medical Systems AG, Hirzel, Switzerland). Volume-controlled Intermittent Positive Pressure Ventilation (IPPV) was selected as the ventilation strategy. Ventilation was applied with an air-oxygen mixture FiO_2 40% and I:E ratio 1:2, while V_t was set at 8 ml/kg (≈160 ml), PEEP at 5 cmH_2O and the end-tidal CO_2 ($ETCO_2$) within a range of 7 kPa. The parameters set at the mechanical ventilator are summarized in Table 4.

Table 4. *The ventilation parameters that were fixed during the volume-controlled IPPV of the animal experiment.*

Mechanical Ventilation Parameters	
Air-oxygen mixture FiO_2	40%
PEEP	5 cmH_2O
V_t	8 ml/kg
$ETCO_2$	3.5-7 kPa

During the trial, the abdomen of the anesthetized and ventilated animal was insufflated with CO_2. Abdominal insufflation was performed at 5, 8, 10, 12, ,14, 16, 18 and 20 hPa using the novel surgical insufflator. The gas was administered into the abdomen of the animal through a trocar that was placed at the umbilical level.

At each IAP level, the airway pressure and flow (P_{aw} and $\dot{V}_{aw}$, respectively) were continuously measured with a pneumotachometer at the endotracheal tube. Likewise, the pressure and flow of the insufflation gas (trocar pressure, P_{tr}, and trocar flow, $\dot{V}_{tr}$) were measured by a pneumotachometer placed at the trocar. In addition, the esophageal pressure was measured with the use of an esophageal balloon, that was inserted through the mouth and placed in the esophagus of the piglet.

Finally, before increasing the IAP, an FOT measurement was performed in the abdomen of the animal to estimate the abdominal mechanical properties at each IAP. An external pressure signal was applied by the insufflator to the abdominal wall at 0.5, 1, 2, 3, 5, 10, and 15 Hz. Once the FOT measurement was obtained, the IAP changed to the following value and the described process was repeated.

Of note, the described experimental protocol refers only to the methods that are relevant to the preliminary analysis in the context of this thesis, excluding any additional instrumentation, devices and measurements that were utilized in the broader project of Erasmus MC. The interface for controlling the insufflator and acquiring the measurements was developed in LabVIEW, and the obtained data were stored in a laptop. The measurement protocol of the animal trial is synopsized in Table 5.

Table 5*. Measurement protocol of the in vivo experimental trial.*

Measurement Protocol	
IAP	5, 8, 10, 12, 14, 16, 18, 20 hPa
FOT Frequencies	0.5, 1, 2, 3, 5, 10, 15 Hz
Airway pressure, Airway flow	Airway pneumotachometer
Trocar pressure, Trocar flow	Trocar pneumotachometer
Esophageal pressure	Esophageal balloon

7.2 Respiratory Analysis

The respiratory analysis was performed in MATLAB and was based on the recorded pressure and flow at the airway and esophagus of the animal. The recorded P_{aw} and $\dot{V}_{aw}$ at every examined IAP were utilized for assessing the respiratory function.

First, a specific segment of the entire experimental data set was isolated, during which normal, quite breathing took place. This was done to ensure that the obtained pressures and flows are solely due to ventilation at the fixed insufflation pressure, without any interference by the FOT. Indicatively,

the time signals acquired from the animal at IAP=20 hPa are depicted in Figure 10, alongside the segment that was isolated, which is contained in the black rectangular.

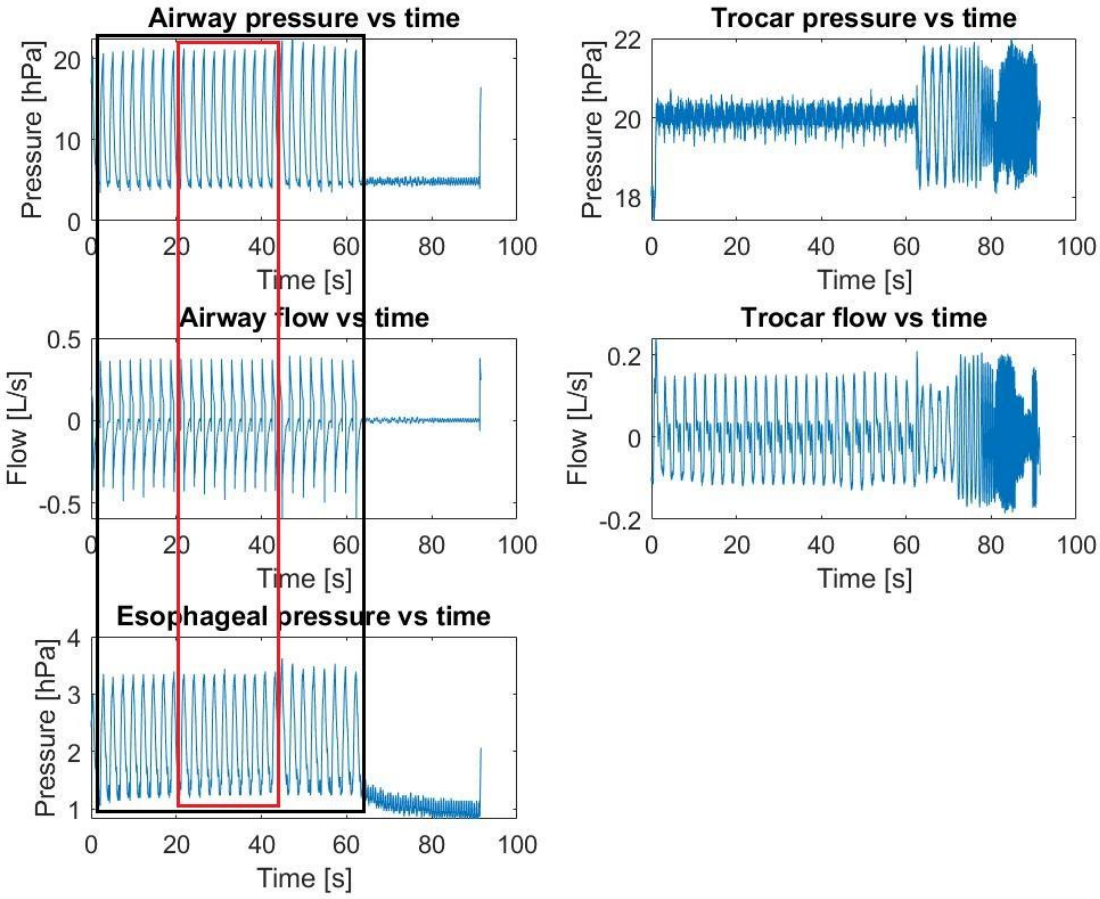

Figure 10. *Time signals of the airway pressure and flow, trocar pressure and flow, and the esophageal pressure obtained at IAP=20 hPa. The segment of the signal marked by the black rectangular corresponds to normal, quite breathing of the animal and was selected for the respiratory analysis. The red rectangular contains the breaths that were selected for the analysis.*

7.2.1 Breath Selection

Once mechanical ventilation was initiated, there was a transitional period of time, during which the ventilation parameters gradually increased towards the set values before being stabilized. The respiratory analysis was performed for a specific number of breaths within the isolated segment, during which tidal volumes and pressures of mechanical ventilation were stable. This was done to ensure reliable results, which truly reflect the respiratory mechanical properties. It was necessary for the analysis to be performed on the same number of breaths at every examined IAP to secure consistency of the results at the entire IAP range. After examination of the available data for every IAP, 10 full breaths were isolated and analyzed at each insufflation pressure level, because it was the maximum number of stabilized breaths that could be found at every IAP. Additionally, such a number was considered acceptable for providing the analysis algorithm with sufficient information in order to give reliable results. Therefore, once the signal segment that is depicted within the black rectangular of

Figure 10 was isolated, the next step was to furtherly process the data and select 10 full breaths, shown within the red rectangular.

To achieve the breath selection, the time signal of V_t was obtained first, by numerically integrating $\dot{V}_{aw}$ over time. The tidal volume was utilized as a marker of the initiation of each breath, because the inspiratory phase begins at V_t=0, since all the inspired air has been expelled out of the lungs at the end of expiration. Then, V_t gradually increases until it reaches its maximum value at end-inspiration. Then, the expiration phase is initiated and V_t drops back to zero at end-expiration, right before the next breath begins.

Thus, breath selection was achieved by creating an algorithm, which detected the minima in the V_t waveform, each one indicating the start of a breath. The minimum peak separation time was set at 1.6 s, equal to the expiration time. This way, it was ensured that the algorithm ignored any local minima during expiration and detected the smallest minimum, which truly reflected the start of each breath, as depicted in Figure 11. Using this algorithm, only 10 full breaths were isolated for every IAP and the remaining of the initially selected data segment was disregarded.

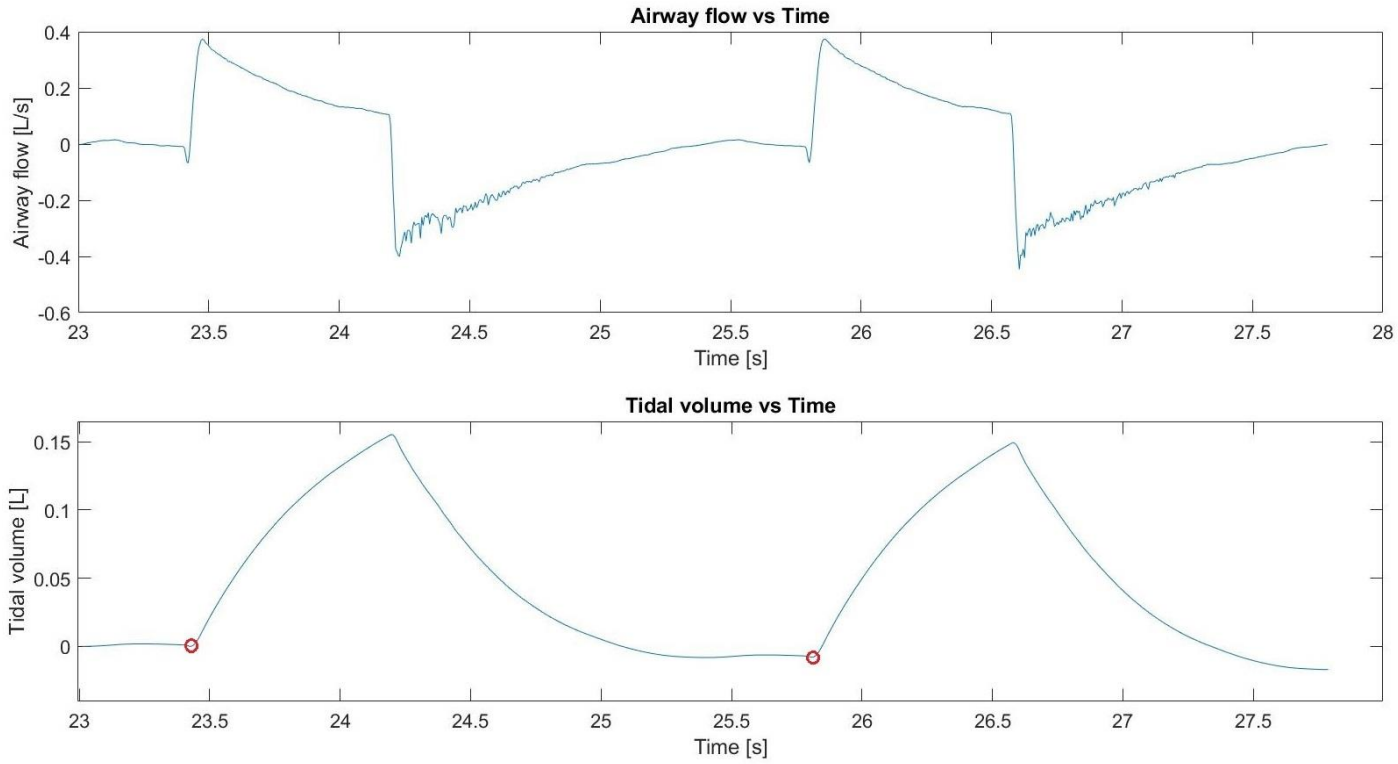

Figure 11. *The breath selection algorithm detected the minima in the V_t waveform. The marked minima on the V_t waveform indicate the initiation of each breath (IAP=20 hPa).*

7.2.2 Sensor Drift Error Correction

Once breath selection was completed, it was observed that the V_t time signal displayed a systematic decrease over time, as Figure 12 shows. This near-linear trend in the waveform is due to a phenomenon called sensor drift error, an invariably encountered problem when integrating a flow signal. It occurs due to asymmetries in the flow sensor or differences in the temperature and humidity

levels between the inspired and expired air[84]. The occurrence of small errors in the measurement of flow by the sensor results into progressively larger errors after integrating to obtain V_t [85]. Since each volume estimation is based on the previous value of the measured flow, the errors accumulate roughly proportionally to the time. This systematic error was corrected in order to obtain the actual values of the tidal volume without any distortions in the waveform.

The linear trend in the signal was removed by subtracting the mean from the tidal volume data, forcing the mean of the waveform to zero. Subsequently, the difference between the first element of the V_t waveform and 0 was calculated and the absolute value of this difference was added to the entire V_t signal. This was done to ensure that the first element of the V_t waveform, which corresponds to the beginning of the first analyzed breath, is zero. Consequently, the processing of the V_t signal led to the removal of the sensor drift error without distorting the data by shifting their mean value.

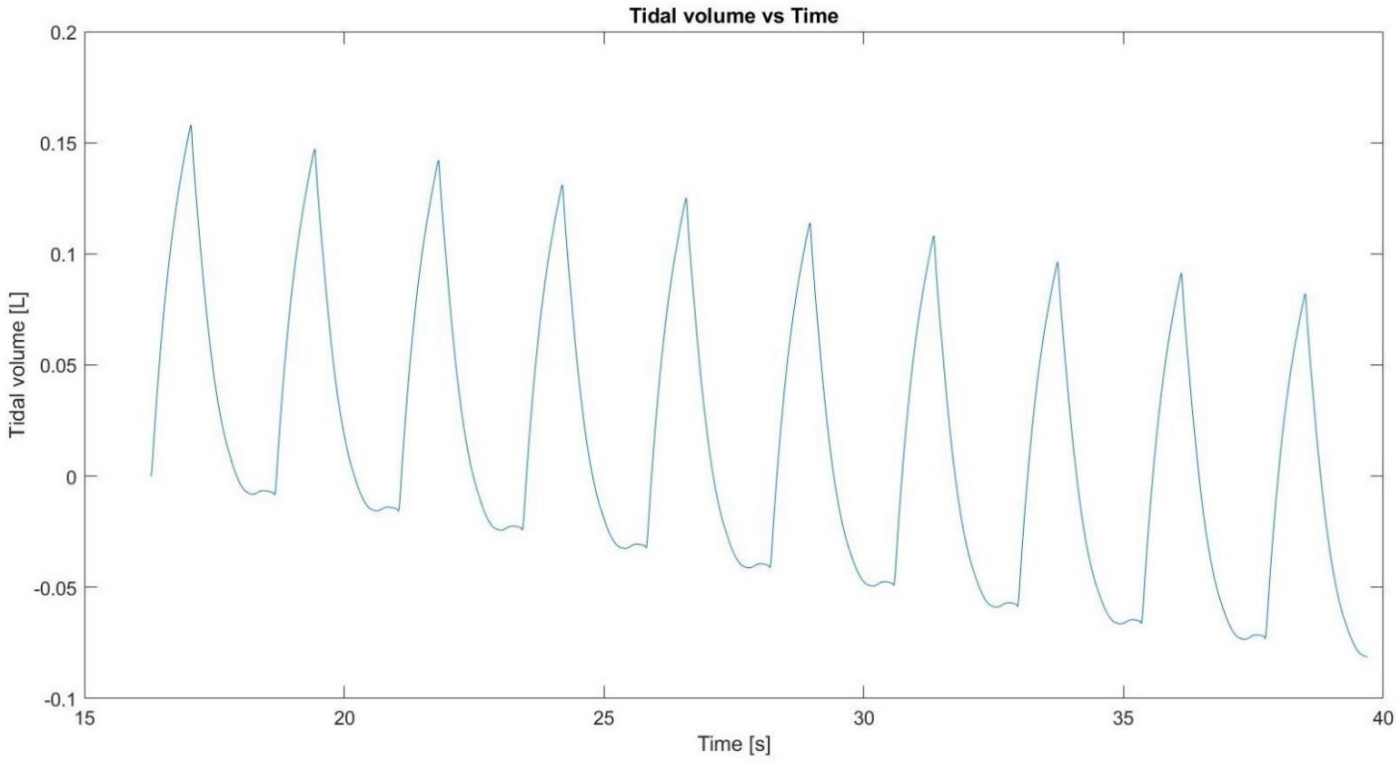

Figure 12. *A systematic shift was observed at the V_t signal due to the flow sensor drift error (IAP=20 hPa).*

Once the drift error was corrected, the time signals P_{aw}, $\dot{V}_{aw}$ and V_t, which are depicted in Figure 13 for IAP=20 hPA, were obtained for the selected 10 breaths to begin the analysis. Notably, it is shown that the removal of the linear trend in the tidal volume signal resulted in a stable waveform of the tidal volume measurements.

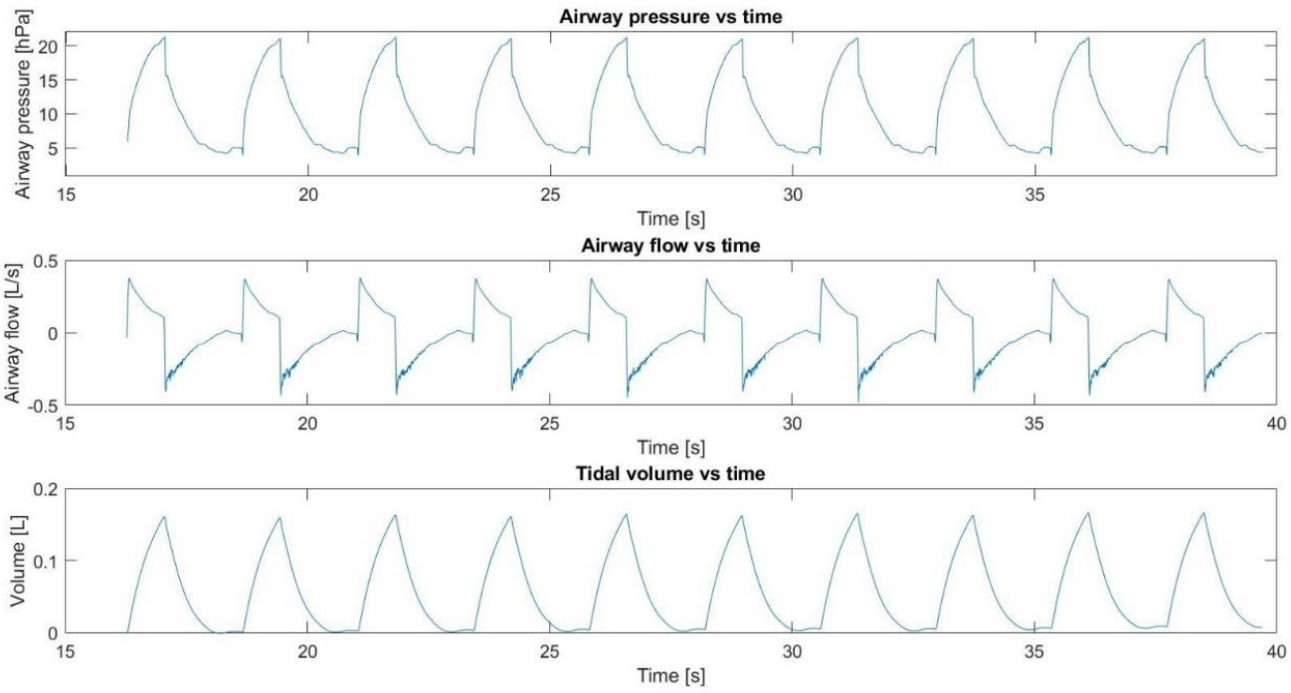

Figure 13. *The post-processed waveforms of P_{aw}, $\dot{V}_{aw}$ and V_t, that were used for the respiratory analysis (IAP=20 hPa).*

7.2.3 Mathematical Model and Regression Analysis Algorithm

For the respiratory analysis, a mathematical model was fitted to the measured respiratory parameters (P_{aw}, $\dot{V}_{aw}$ and V_t) with a linear multiple regression analysis tool. Using the regression analysis algorithm, the parameters of the mathematical model, which represented the mechanical properties of the respiratory system, were identified. The mathematical model selected for the respiratory analysis in this study was:

$$P_{aw} = R\dot{V}_{aw} + EV_t \tag{18}$$

This linear, single-compartment model was first used by Lauzon et al[84]. Equation 18 is derived directly from the equation of motion (Equation 2), which was described in 4.4. The airway pressure (P_{vent} + $PEEP$) can be estimated as a function of the airway flow and tidal volume, since there was no active breathing by the animal during ventilation ($P_{mus} = 0$) and the inertance term is negligible. Since the mathematical model is related to the equation of motion, its parameters R and E have a valuable physiological meaning, representing the airway resistance, R_{aw}, and the respiratory system elastance, E_{RS}, respectively. Therefore, by function-fitting the model to the measured P_{aw}, $\dot{V}_{aw}$, and V_t, an estimation of P_{aw} as well as an estimation of R and E- which define the respiratory mechanical properties - are obtained. The algorithm that was used for fitting the mathematical model to the measured data was the Recursive Least-Squares (RLS) algorithm.

The selection of the linear mathematical model in combination with the RLS algorithm was made because of its simplicity and its effectiveness in simulating the respiratory function in the examined intra-operative situation. The linear mathematical model assumes that the mechanical parameters R and E are constant. In addition, the RLS allows periodic re-estimation of R and E for each

breath. Therefore, the model-algorithm combination gives the breath-to-breath variation of the mechanical respiratory parameters, assuming that they are constant for each examined breath. This is considered as the physiological condition for a healthy respiratory system and is the most commonly encountered situation in laparoscopic surgery. On the other hand, within-breath variations of the mechanical properties are an indication of the presence of a respiratory disease.

The analysis, which was performed in MATLAB, began by considering the linear model first:

$$Y = XA + N \tag{19}$$

,where Y was the vector of the predicted pressure by the model ($\hat{P}_{aw}$), X was the matrix of the independent parameters (P_{aw},$\dot{V}_{aw}$ and V_t), A was the vector of parameters to be estimated (R, E) and N was the error between predicted and the modelled pressure.

The RLS algorithm calculated the parameters (A) by minimizing the sum of the squared residuals between the prediction of the pressure by the model and the actual measured P_{aw}. The least-squares estimate was given by:

$$\hat{A} = [X^T X]^{-1} X^T Y \tag{20}$$

The predicted pressure $\hat{P}_{aw}$, R and E were calculated and stored for each of the 10 analyzed breaths. The estimated pressure was also plotted over the measured pressure to obtain a visual representation of the behavior of the mathematical model. The mean squared error (MSE) between the estimated and measured pressure was computed according to Equation 21 and stored for each breath as well, giving an indication on the accuracy of the analysis:

$$MSE = \frac{1}{n}\sum_{i=1}^{n}\left(P_{aw_i} - \hat{P}_{aw_i}\right)^2 \tag{21}$$

where n is the number of the measured data points.

The analysis procedure was repeated for every examined IAP. The results from each IAP were exported to a separate common MATLAB data file and were subsequently processed, such that the mean and standard deviation of R, E and MSE were computed for the 10 breaths at every IAP. Finally, the respiratory mechanical parameters were plotted over IAP to examine the effect of the increase in the insufflation pressure on the respiratory mechanics.

Additional processing of the results from the animal data was also performed to obtain a broader understanding of the effect of the insufflator on respiratory function. Besides the mechanical parameters, the effect of IAP on V_t, V_{tr} (volume of gas in the trocar), PIP and ΔP were investigated as well.

The first aim of the preliminary analysis was the estimation of the physiological mechanical properties as a starting point for designing the physical model. The obtained mechanical parameters were used for achieving this goal. The additional investigated parameters were utilized in the validation of the developed device.

7.2.4 Respiratory Analysis Results

The predicted airway pressure, $\hat{P}_{aw}$, was the output of the mathematical model and is depicted in Figure 14. The signal of the estimated pressure is superimposed onto the measured airway

pressure so that the 'goodness of fit' can be visualized. The depicted waveform was obtained for IAP=20 hPa, for which the highest error was observed.

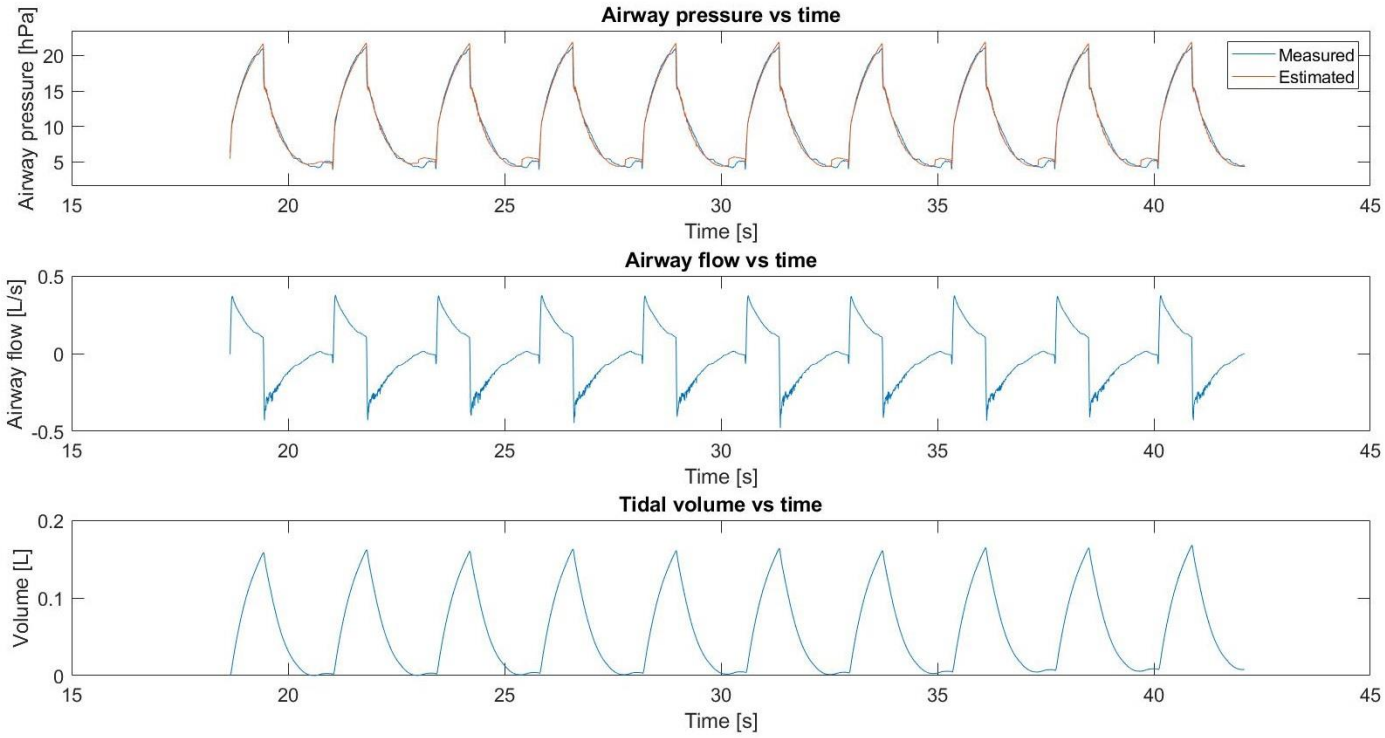

Figure 14. *The waveform of the airway pressure predicted by the mathematical model, superimposed over the measured pressure signal (IAP=20 hPa).*

The estimated parameters of the model, R and E, as well as the calculated MSE for every IAP value that was used in the animal experiment are summarized in Table 6. In addition, the relationship between the estimated mechanical properties of the respiratory system and IAP is visualized in Figure 15.

Table 6. *The mean ± standard deviation of the respiratory resistance (R) and elastance (E) and mean squared error (MSE) as estimated by the mathematical model for every IAP in the preliminary respiratory analysis.*

IAP [hPa]	R [$cmH_2O \cdot s/L$]	E [cmH_2O/L]	MSE [hPa^2]
5	9.0 ± 0.1	48.0 ± 0.1	6.8 ± 0.5
8	9.6 ± 0.2	52.5 ± 0.3	7.0 ± 0.4
10	10.1 ± 0.1	57.3 ± 0.2	7.4 ± 0.5
12	10.6 ± 0.2	63.1 ± 0.4	8.8 ± 0.5
14	10.9 ± 0.2	71.2 ± 0.5	10.7 ± 1.0
16	11.1 ± 0.2	79.7 ± 0.8	14.2 ± 2.1
18	11.2 ± 0.1	89.0 ± 0.3	22.8 ± 1.2
20	11.1 ± 0.2	97.8 ± 1.2	26.3 ± 5.6

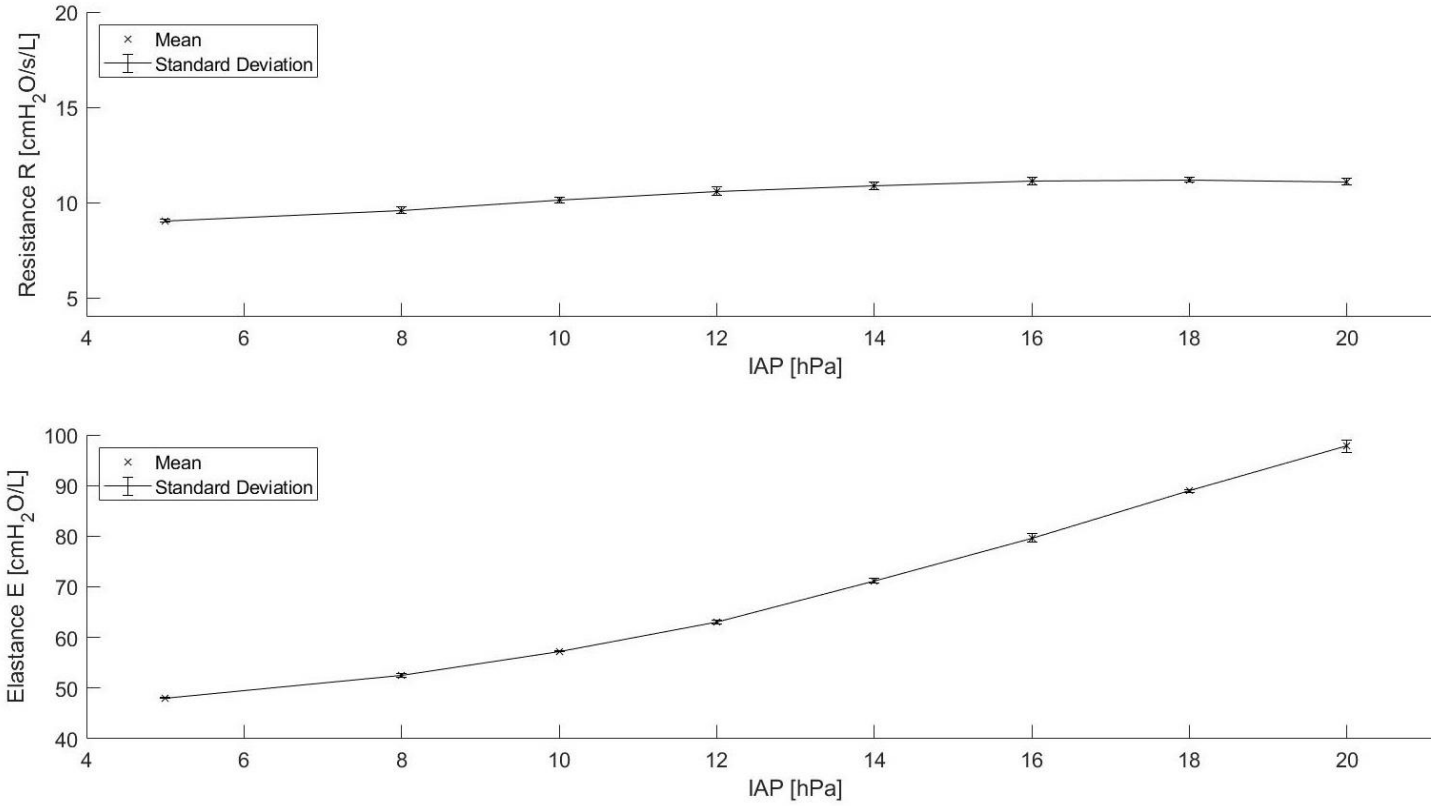

Figure 15. *Graph of the airway resistance R (top) and respiratory elastance E (bottom) versus the IAP, as estimated by the mathematical model utilized in the preliminary analysis. The two parameters define the respiratory function and mechanical properties of the animal that was used in the experiment.*

The linear model in combination with the RLS algorithm displayed good accuracy in estimating the respiratory parameters, as evidenced by both Figure 14 and Table 6. Although Table 6 shows that there is a gradual increase in the MSE alongside the rise in IAP, it is generally kept at low values, as is also confirmed by Figure 14.

With respect to the mechanical parameters, Figure 15 suggests that the airway resistance R_{aw} displays only a slight increase alongside the rise in the insufflation pressure. On the other hand, there is a strong dependence of the respiratory elastance E_{RS} on IAP. The estimated E_{RS} exhibited an increasing behavior that was consistent with the increase in IAP. Starting at 48 cmH_2O/L at 5 hPa, the elastance showed an increase of more than 100% at the highest IAP of 20 hPa. This behavior shows that the respiratory system becomes less compliant at high abdominal pressures, and that the rise in IAP is a significant factor that affects the respiratory function.

The results and insights obtained from the preliminary respiratory analysis were used as the basis for defining the design requirements and selecting the respiratory component of the physical model. Such a component should mimic the mechanical behavior of the animal's respiratory system during insufflation. That is, the trend shown in Figure 15 and the dependence of E_{RS} on IAP should be reflected in the in vitro model, so that it can be considered as an adequate representation of the physiological conditions.

7.3 Abdominal Analysis

After the completion of the respiratory analysis, a secondary analysis was performed to investigate the abdominal mechanical behavior during insufflation. The mechanical behavior of the abdomen is defined by its mechanical properties, which can be determined by estimating the mechanical impedance. Estimation of the mechanical impedance was accomplished by analyzing the results from the FOT which was applied on the abdominal wall of the animal, as described in 7.1. The abdominal analysis was performed in MATLAB.

The first step of the abdominal analysis was to manually isolate the segment of data that corresponded to the application of FOT, as shown in Figure 16. The parameters that were of interest were the pressure and flow measured in the trocar (P_{tr}, $\dot{V}_{tr}$). The trocar pressure was the externally applied signal by the insufflator on the abdominal wall, while the trocar flow was the resulting response, which depended on the mechanical properties of the abdomen. The mechanical impedance was calculated as the transfer function between these two signals.

The isolation of the marked data segment was done to ensure that the abdominal analysis focused on the FOT without any other interferences, so that the results truly reflect the abdominal mechanical behavior of the animal. The isolated data section and the FOT pressure and flow signals for IAP=20 hPa in the frequency spectrum of [0.5, 1, 2, 3, 5, 10 and 15 Hz] are shown in Figure 17.

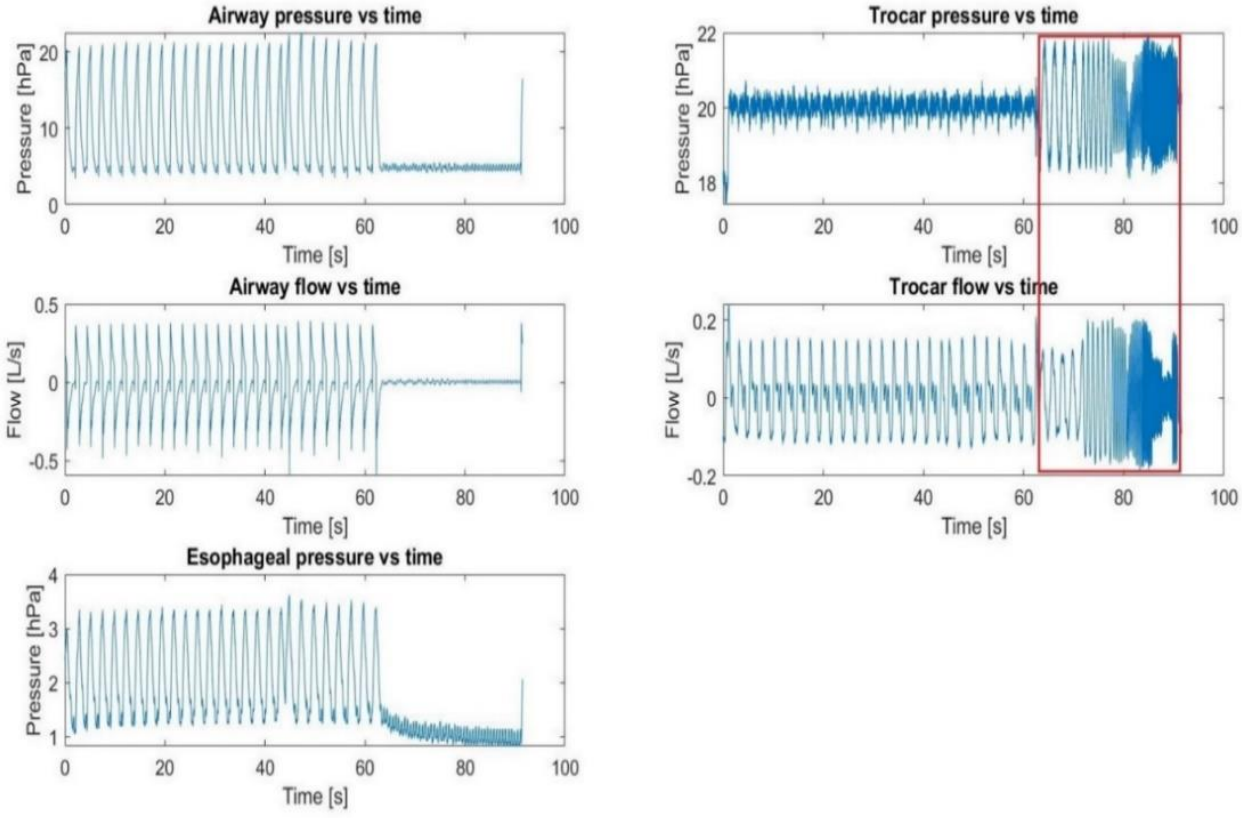

Figure 16. *The data section that corresponds to the application of the FOT was selected for the abdominal analysis (marked by the red rectangular (IAP=20 hPa).*

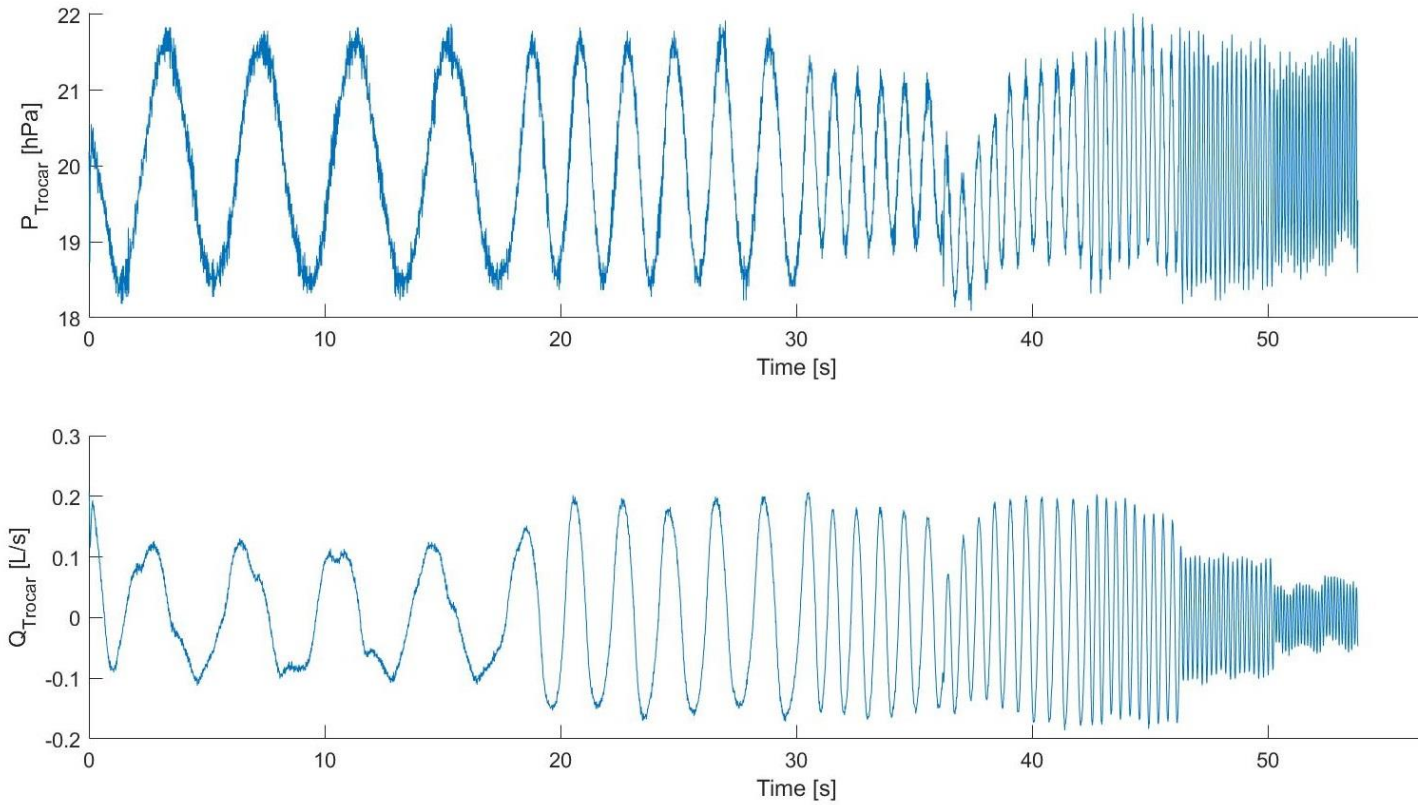

Figure 17. *The pressure signal applied on the abdominal wall during the FOT and the resulting flow (IAP=20 hPa)*

7.3.1 Mechanical Impedance Estimation

After the segment isolation, the mechanical impedance (Z) of the abdomen was calculated as a function of frequency. Since Z(ω) is defined as the ratio between the imposed insufflation pressure and the resulting trocar flow, its computation was achieved by estimating the transfer function between the two time signals in MATLAB.

$$Z = \frac{P_{trocar}}{Q_{trocar}} \tag{22}$$

Because impedance is a complex ratio, it can be separated into a real and an imaginary part:

$$Z(\omega) = R(\omega) + jX(\omega) \tag{23}$$

where $Re(Z) = R$ and $Im(Z) = X$ are the resistance and reactance of the abdomen respectively.

Although the frequency spectrum for the FOT in the animal experiment ranged up to 15 Hz, the frequencies considered for the abdominal analysis of this study were 0.5, 1, 2, 3, and 5 Hz. The decision for neglecting the frequencies 10 and 15 Hz from the analysis is explained by expressing the reactance as:

$$X = \omega I - \frac{1}{\omega C} \tag{24}$$

where I is the inertia due to gas acceleration and C is the compliance of the abdomen. In this case, C represents the elastic properties of the abdomen. Equation 24 shows that at sufficiently low frequencies, the inertial term is negligible and X depends only on the elastic properties of the abdomen. As the frequency increases, the inertial forces increase as well and directly oppose the elastic forces. As a result, the inertial term becomes important and the compliance term, $\frac{1}{\omega C}$, is gradually reduced to the point where it becomes insignificant compared to ωI. Thus, at high frequencies, only the inertial effect is reflected in the reactance. This means that at these conditions, the reactance is not affected by the mechanical properties of the system, but from the inertial properties of gas flow.

Barnas et al.[86] specified that, for the abdominal wall, the inertial term has a negligible and irrelevant contribution to the overall reactance for up to 5 Hz. Therefore, it was decided that the abdominal analysis should be extended up to 5 Hz in order for the acquired results to truly reflect the compliance of the abdomen.

After the frequency range was decided, Z(ω) was calculated as the transfer function between the pressure and flow signals in the trocar. An estimation of the transfer function was derived in MATLAB at each frequency in every examined IAP. The obtained transfer function defined the impedance spectrum, and determined the real and imaginary part of Z(ω). In addition, the coherence (γ^2) values between the input (P_{trocar}) and output (Q_{trocar}) signals was determined by obtaining the magnitude-squared coherence estimate at every examined frequency.

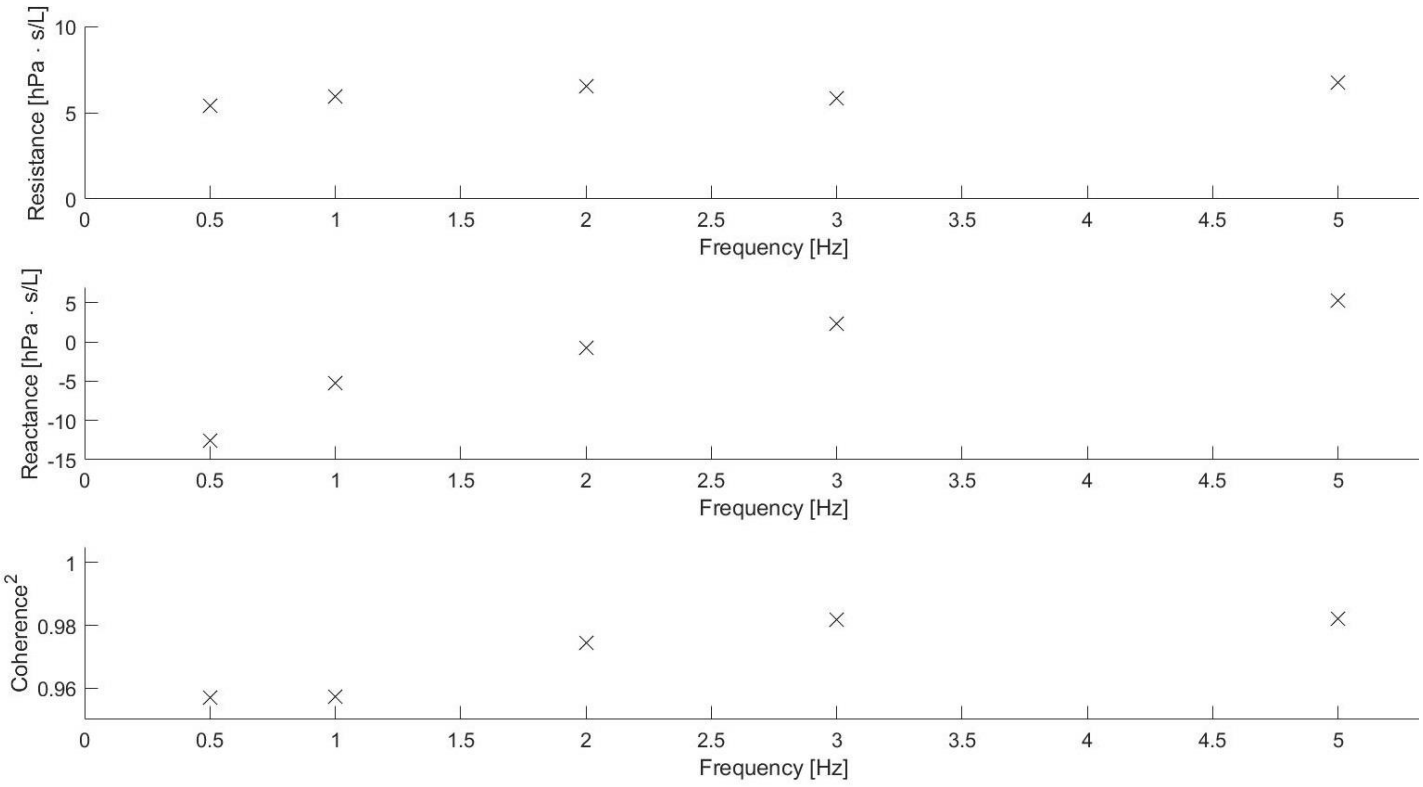

Figure 18. *The real and imaginary part of the mechanical impedance (resistance and reactance) and the coherence estimated and marked at each frequency (IAP=20 hPa).*

This method was applied for every examined IAP and yielded an estimation of the resistance and reactance at each frequency. Indicatively, the R and X estimations as well as the coherence γ^2 for IAP=20 hPa are depicted in Figure 18. It is observed that resistance is largely unaffected by the increase in the frequency, in contrast to the reactance, which exhibits a strong dependence. The coherence was maintained at a high level, above 95%, for the entire frequency range. The reactance X displays negative values at the lowest frequencies, and gradually increases, reaching positive values as the frequency rises. This behavior comes in accordance with the theory described above. The observed trend in X is due to the fact that the inertial component becomes more dominant at higher frequencies, opposing the effect of the compliance term. This gradual shift in the dominance of I and C is reflected in the shift of X from negative to positive values.

7.3.2 Estimation of Abdominal Resistance, Inertance and Compliance

Acquiring the mechanical impedance for every IAP gave an overview of the mechanical properties of the abdomen as a function of frequency. Nevertheless, the goal of the abdominal analysis was to quantify the abdominal mechanical properties and explore its mechanical behavior as a function of IAP. This was accomplished by fitting the obtained resistance and reactance estimations, for every IAP, to a mathematical model. The selected model was the RIC model, which was described in the introduction, so that the abdominal compliance C_{ab} could be estimated:

$$Z_{est}(\omega) = R + j\omega I + \frac{1}{j\omega C} \tag{25}$$

Z_{est} denotes the predicted impedance by the mathematical model. The RIC model is directly derived from the mathematical expression for the impedance and its parameters correspond to the mechanical properties of the abdomen. The resistance R is frequency-independent, as confirmed by Figure 18, I represents the inertance of the gas within the abdomen, while C is the abdominal compliance.

The real and imaginary part of each estimated impedance obtained in 7.3.1 was fitted to the RIC model, which predicted the mechanical impedance $Z_{est}(\omega)$ and gave an estimation of R, I, and C, which defined the mechanical behavior of the abdominal wall. The fitting of the measured impedance was done in MATLAB using the multivariable nonlinear algorithm of the Least-Squares Method. The function of the algorithm was to yield Z_{est} by minimizing the error for each k measurement, defined as the deviation between the measured (Z) and estimated impedance (Z_{est}):

$$\text{err} = \sum_{k=1}^{K} \sqrt{[(Re\{Z_{est}(\omega_k)\} - Re\{Z(\omega_k)\})^2 + (Im\{Z_{est}(\omega_k)\} - Im\{Z(\omega_k)\})^2]} \tag{26}$$

or simply:

$$\text{err} = \sum_{k=1}^{K} (|Z_{est}(\omega_k) - Z(\omega_k)|) \tag{27}$$

The initial values of R, I and C, that were necessary for the mathematical analysis, were obtained with using a minimization algorithm in MATLAB, which finds the minimum of an unconstrained multivariable function. The least-squares algorithm was fitted with the calculated impedance values that were estimated for every IAP, predicted Z_{est} and returned the parameters R, I and C. The real and

imaginary part of the impedance prediction by the mathematical simulation for IAP=20 hPa is shown in Figure 19. The estimated parameters R, I, and C as well as the error yielded by the algorithm for every examined IAP are summarized in Table 7.

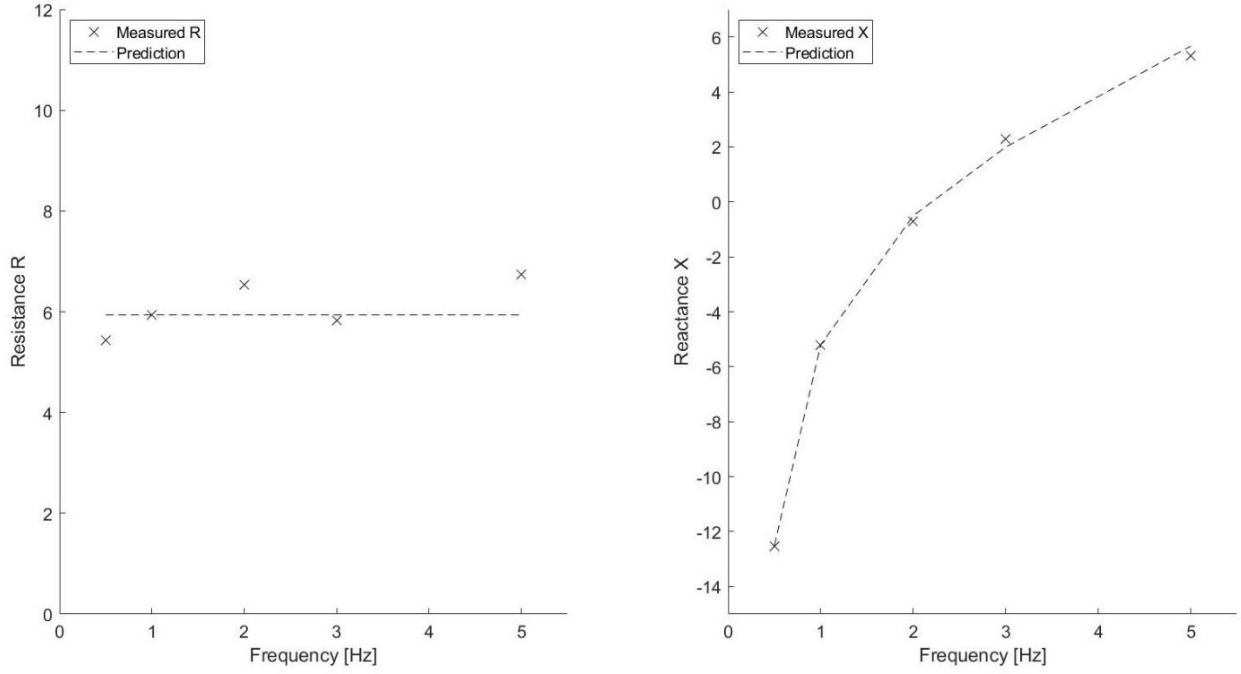

Figure 19. *The measured R and X values and the resulting predictions by the algorithm for IAP=20 hPa.*

Table 7. *The obtained parameters R, I, C and the respective error in their estimation for the abdominal wall of the examined animal at every IAP.*

IAP [hPa]	R [$cmH_2O \cdot L/s$]	I [$cmH_2O \cdot s^2/L$]	C [L/cmH_2O]	Error [$cmH_2O \cdot s/L$]
5	5.3	0.20	0.465	2.7
8	5.6	0.22	0.122	2.9
10	5.9	0.22	0.085	2.1
12	6.0	0.21	0.069	1.8
14	6.1	0.21	0.049	1.7
16	6.1	0.21	0.035	1.9
18	6.0	0.21	0.028	2.4
20	5.9	0.22	0.024	2.3

The curves of the mechanical parameters R_{tr} and C_{ab}, representing the resistance in the trocar and compliance of the abdominal wall of the animal respectively, are shown in Figure 20. It is observed that the resistance in the abdomen of the animal is generally independent of the increase in the IAP. On the contrary, the compliance of the system decreases significantly as the IAP rises, which means that the abdomen of the animal becomes stiffer at higher insufflation pressures.

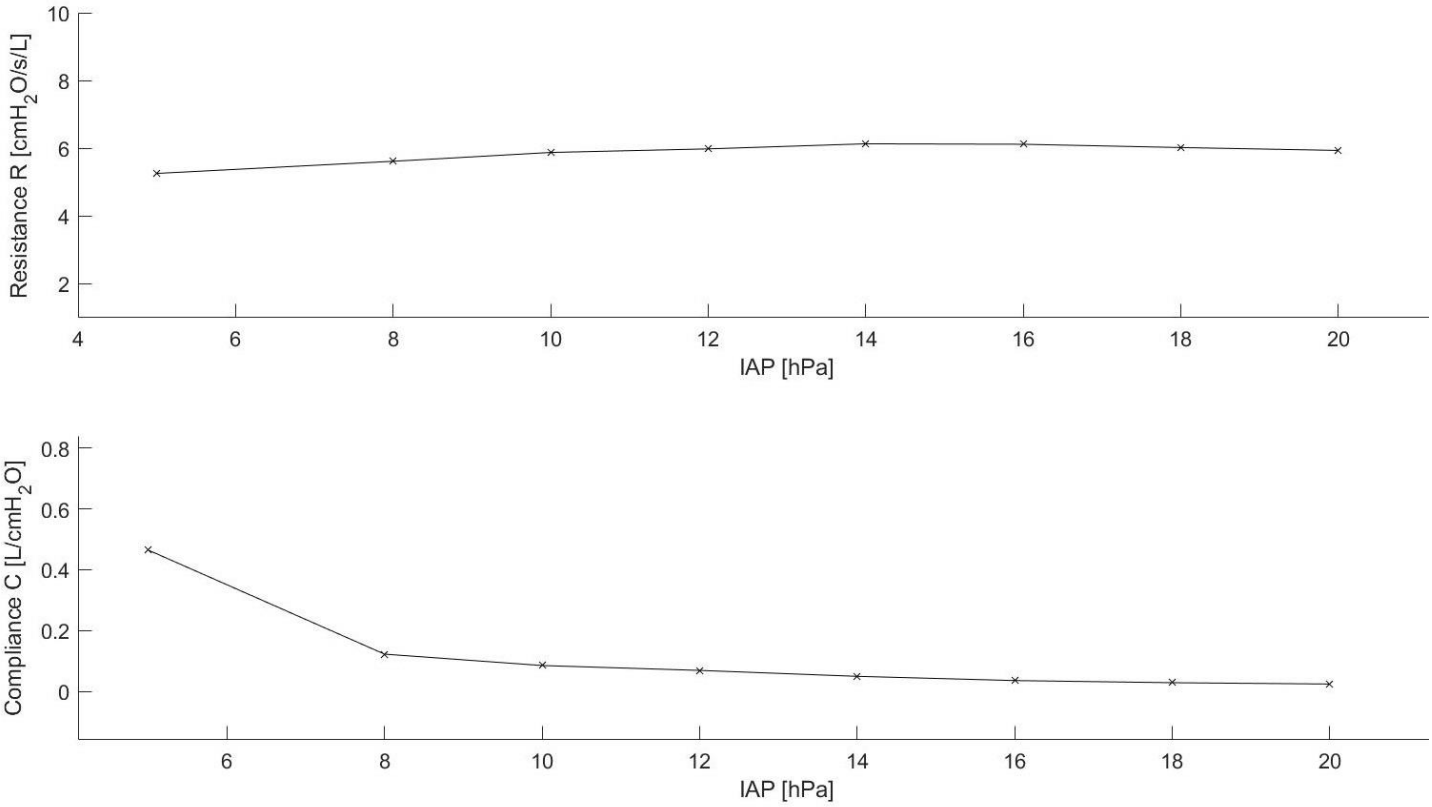

Figure 20. *The curves mechanical parameters of the abdominal wall (resistance and compliance), obtained by the RIC model after the application of the FOT.*

The abdominal analysis was performed on the same data as the respiratory analysis. Therefore, the acquired results were consistent with the respiratory analysis and the whole picture on the respiratory-abdominal interaction was viewed. Knowledge of the behavior of both the examined sides as well as their mechanical interplay laid the foundations for the development of the in vitro simulator.

The abdominal preliminary analysis defined the mechanical behavior of the abdominal wall of the animal during insufflation. In combination with the analysis in the respiratory system, a broader understanding of the interaction between the respiratory system and the abdominal was acquired, making it possible to formulate the design requirement and goals of the in vitro device, and proceed with its development.

8. Development of the Model

8.1 Design Requirements

The development phase of the physical model began with specifying the design requirements. That is, the functional attributes that allow converting the concept ideas into design features. The design requirements apply specifically to the aims and intended use of the device. Therefore, their

formulation was accomplished by breaking down the problem statement and translating it into the necessary features of the device.

Evaluation of the performance and effect of the insufflator onto respiratory mechanics can be achieved with an in vitro model, which simulates the mechanical behavior and interaction between abdominal cavity as well as the respiratory system over a range of insufflation pressures. The design requirements of the in vitro model are presented in Table 8.

Table 8. *Design requirements of the model.*

Design Requirements
1. In vitro
2. Distinct respiratory component
3. Compatibility with the mechanical ventilator
4. Distinct abdominal component
5. Compatibility with the surgical insufflator
6. Respiratory and abdominal component are in contact
7. R and E estimation during respiratory-abdominal interaction

In order to emulate the intra-operative abdominal insufflation, the developed in vitro model should simulate both the respiratory system and the abdomen of the patient . The respiratory compartment should be connected to the mechanical ventilator, while the abdominal part should be insufflated at different pressures by the surgical insufflator. Finally, placing the two components in contact and performing the measurements described in Chapter 7, enables the estimation of the mechanical properties of each component as well as their interaction, by obtaining the values for R and E.

8.2 End-Goal

Once the design requirements were defined, the next step was to determine the goals with respect to the functional behavior the device. This way, the decisions regarding the selection of the individual components of the model could be made. The functional end-goals were derived from the results of the preliminary analysis (data shown in Table 6 and Table 7), since they are related to the desired mechanical behavior.

The targeted mechanical behavior of the ventilation (respiratory) and insufflation (abdominal) compartment of the model are expressed in terms of the resistance and compliance of each component as a function of the increasing insufflation pressure, and summarized in Table 9. In addition, a graphical representation of the desired behavior of the individual compartments of physical model is depicted in Figure 21.

Table 9. *The desired mechanical behavior of the mechanical ventilation (respiratory) and surgical insufflation (abdominal) components of the model, as a function the increasing insufflation pressure. The data were acquired from the preliminary analysis (Table 6 and Table 7).*

	Mechanical Ventilation Side		Surgical Insufflation Side	
IAP [hPa]	**R [$cmH_2O \cdot L/s$]**	**C [L/cmH_2O]**	**R [$cmH_2O \cdot L/s$]**	**C [L/cmH_2O]**
5	9.0	0.021	5.3	0.465
8	9.6	0.019	5.6	0.122
10	10.1	0.017	5.9	0.085
12	10.6	0.016	6.0	0.069
14	10.9	0.014	6.1	0.049
16	11.1	0.013	6.1	0.035
18	11.2	0.011	6.0	0.029
20	11.1	0.010	5.9	0.024

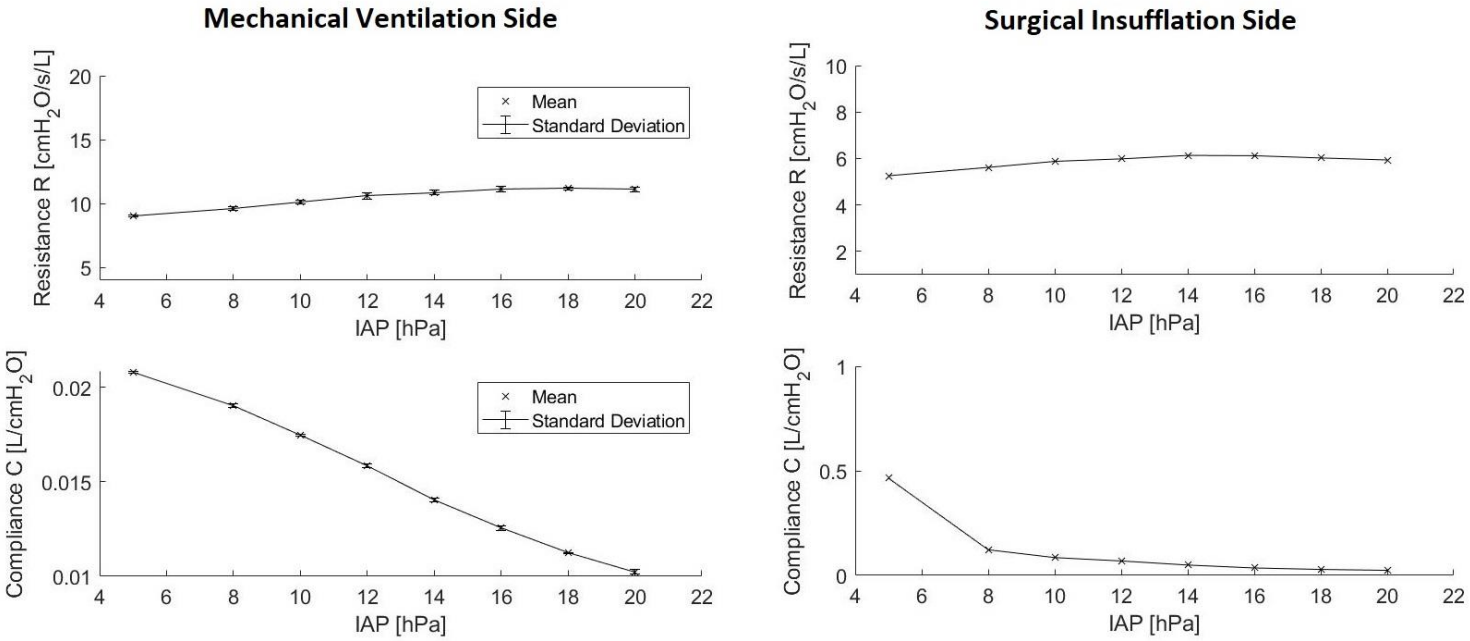

Figure 21. *Graphical representation of the functional end-goal of the device. That is, the mechanical behavior of the ventilation (left) and insufflation (right) component of the model.*

8.3 Individual Components

8.3.1 Mechanical Ventilation Side (Respiratory Component)

The respiratory compartment of the model represents the respiratory system of the patient and is connected to the mechanical ventilator. Therefore, such a compartment should be able to reproduce the alternate expansion and contraction that occurs during breathing, as the inspired air enters and leaves the lungs. Besides, the respiratory component should have a sufficient volume to

accommodate the tidal volume that was used in the animal experiments (V_t≈160ml). Air-tightness was an additional requirement in order to minimize the leakage of air coming from the mechanical ventilator. Finally, its mechanical properties should approach the mechanical properties of the respiratory system of the pig that was used in the clinical trial. The individual design requirements of the respiratory compartment are shown in Table 10.

Table 10. *The individual design requirements for the respiratory component of the model.*

Respiratory Component Requirements
1. Expandable during air inspiration
2. Accommodation of the physiological V_t (≈160ml)
3. Air-tight
4. Similar mechanical properties to the respiratory system of the pig

After specifying the functional attributes of the respiratory component, the decision on whether the entire respiratory system would be modelled as one or whether each lung would be modeled separately, needed to be made. A single-compartment respiratory model was selected, because of its simplicity and its ability to adequately simulate the healthy respiratory system [87]. Although dual-compartment models are generally selected for simulating various respiratory diseases [14,15,88], single-compartment respiratory models are capable of sufficiently reproducing the functional conditions of a healthy respiratory system, which is typically the case during a laparoscopic surgery. This feature of the single-compartment simulator, in combination with its simplicity and the fact that it comes in accordance with the linear single-compartment analysis that was used for estimating the respiratory mechanical properties of the animal in 7.2, led to its implementation in the physical model.

The respiratory compartment of the model was chosen to be represented by a passive model. Passive respiratory models are ventilated externally and allow the investigation of the mechanical properties of the model. Compliant bellows or rigid containers are typically utilized to simulate the lungs [89]. On the other hand, active models generate spontaneous breathing, usually with a cylinder-piston configuration connected to a driving mechanism, such as a motor [90]. The passive model was selected because it is a better approach to the intra-operative conditions of laparoscopy, during which the breathing of the patient is entirely achieved by the mechanical ventilator, as the activity of the respiratory muscles is completely suppressed.

Subsequently, a search in the literature was performed to obtain knowledge on the existing passive, single-compartment models of the respiratory system. The results of the search revealed that the most commonly used passive representation of the respiratory system is a compliant bellow [12,91,92], mainly due to the fact that it can expand during inspiration and restore its resting size in expiration. Moreover, bellows are capable of reproducing a non-linear pressure-volume relationship, similar to the mechanical behavior of the lung [90].

Consequently, the respiratory component of the physical model was decided to be composed of a compliant bellow. At first, a 3D design of the bellow was created with the use of Autodesk Inventor. Then, the bellow was 3D-printed using the Ultimaker S5 (Ultimaker B.V., The Netherlands) at Erasmus MC. The selected printing material was thermopliastic polyurethane (TPU 95A), one of the most compliant materials that can be used in 3D printing. Its selection was driven by the need for flexibility, so that alternate expansion and contraction can take place when connected to the mechanical ventilator. In addition, a thickness of 0.8 mm was selected to contribute to its compliance. The height of the bellow was set at 16 cm and its volume was ≈1600 ml, which was not only sufficient to

accommodate the tidal volume, but also a good approximation of the physiological lung volume in the pig [93]. A printing temperature of 230°C, a print speed of 19 mm/s and 108% material flow compensation were selected for as manufacturing settings, to ensure a consistent print of an adequate quality. The cross-sectional feature of the 2D sketch created in Autodesk Inventor is depicted in Figure 22, while the 3D printed respiratory bellow is shown in in Figure 23.

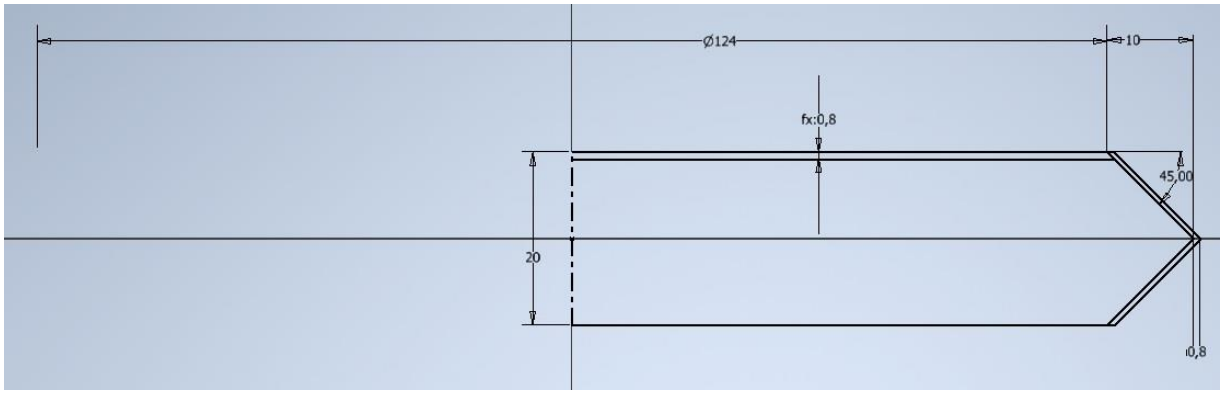

Figure 22. *The cross-sectional feature of the respiratory bellow, created in Autodesk Inventor.*

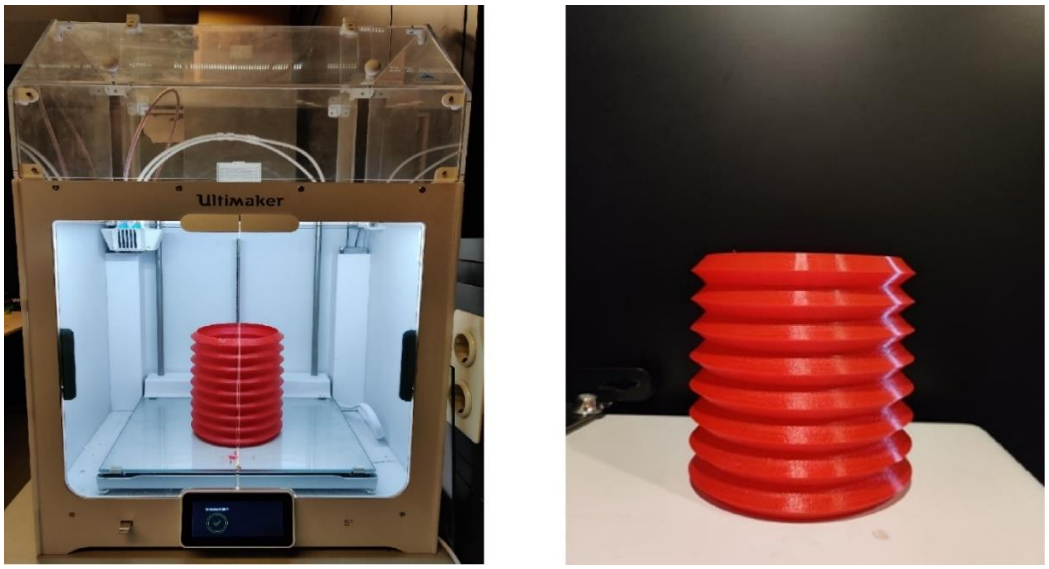

Figure 23. *Left: The respiratory bellow in the Ultimaker S5, once 3D printing was completed. Right: The respiratory bellow after removal from the 3D printer.*

Once the printing of the respiratory bellow was completed, it was connected to the mechanical ventilator to measure its mechanical properties and validate whether the requirements 3 and 4 of Table 7 are fulfilled. The compliance of the bellow corresponded directly to the compliance of the simulated respiratory system, while the resistance element was represented by a 16.5 cm long tube (d=1cm) that connected the bellow to the mechanical ventilator (simulating the ETT that was used during the animal experiments). Measurement of the mechanical properties of the bellow was achieved with the use of the analysis tool described in 7.2 for 10 full breaths delivered by the ventilator. The results of the measurements suggested that air-tightness of the bellow was sufficient, as it was capable of maintaining the volume of air that was set in the ventilator. Additionally, the results, which are demonstrated in Figure 24, indicated that the bellow is characterized by a resistance value of R = 8.1 cmH2O·L/s and an elastane of E= 65.4 cmH_2O/L. The obtained parameters were then

compared to the corresponding values obtained during the animal experiment, at IAP=5 hPa, which was the lowest pressure utilized in the animal experiment and the starting point for the comparison. This way, it was possible to examine whether the mechanical properties of the bellow were an approximation of the mechanical properties of the animal's respiratory system.

The estimated parameters alongside the error in the mathematical model are summarized in Table 11 and compared to the values acquired from the respiratory system of the animal at 5 hPa. Overall, it was concluded that the respiratory bellow represents an adequate approximation of the desired mechanical properties. The bellow exhibited good ability of simulating the physiological airway resistance, compared to the clinical trial. With respect to the elastance, it displayed a slightly less compliant mechanical behavior than the respiratory system of animal. Overall, the results are considered reliable, since the resulted error was below 10 hPa^2 (error=9.7 hPa^2) and the developed respiratory bellow was regarded as appropriate for implementation in the physical model.

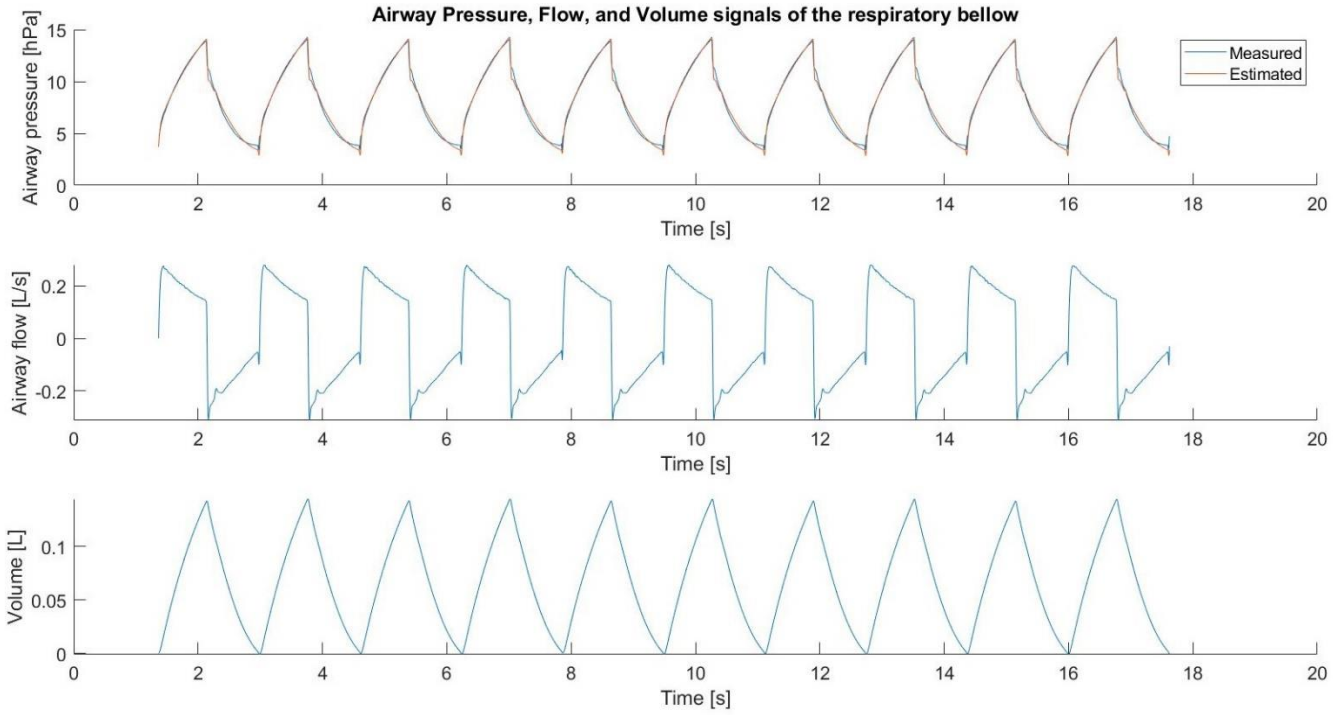

Figure 24. *The airway pressure, flow and volume waveforms obtained for the respiratory bellow, when connected to the mechanical ventilator.*

Table 11. *The measured vs targeted mechanical properties for the respiratory component of the model.*

	R [$cmH_2O \cdot L/s$]	**E [cmH_2O/L]**
Measured	8.1	65.4
Target	≈9	≈50

8.3.2 Surgical Insufflation Side (Abdominal Component)

The abdominal component of the model simulates the abdominal cavity during insufflation and is connected to the surgical insufflator. Consequently, it should behave similarly to the insufflated abdomen, which expands and increases its volume alongside the increase of IAP. The abdominal compartment of the model should expand at high pressures and be able to sustain a pressure up to 20

hPa, which was the highest abdominal pressure applied in the animal experiments, without breaking. This way, the in vitro simulator can be used for the entire range of IAP that is used intra-operatively. Again, air-tightness was considered a necessary feature so that a stable insufflation pressure can be maintained. The desired volume range for the abdominal compartment was between 2-4 L so that it approaches the physiological values. Finally, the abdominal part should be significantly more compliant than the respiratory compartment to reflect the physiological relationship. Preferably, its mechanical properties should match the ones of the abdominal cavity of the pig. The required design features of the insufflation side of the model are listed in Table 12.

Table 12. *The individual design requirements for the abdominal part of the model.*

Abdominal Component Requirements
1. Expandable during insufflation
2. Able to sustain a pressure up to 20 hPa
3. Volume=2-4 L
4. Air-tight
5. Similar mechanical properties to the abdominal cavity of the pig

Despite the scarcity of information on abdominal simulators in the literature, it was found that the abdominal cavity is typically modelled by means of a latex weather balloon [94]. This way, its relatively high compliance and expandability is reflected by the flexible rubber material. The abdominal component in this study was selected to be represented by a commercially available latex bellow, which is depicted in Figure 25.

The compliance of the bellow corresponded to the compliance of the abdomen, while the resistance element was represented by the tube connecting the bellow to the surgical insufflator. The selection of a rubber bellow reflects the passive nature of the abdomen, as it stretches and increases its volume in response to the increase in the pressure of gas in its interior. The volume of the abdominal bellow was measured at ≈3 L at 5 hPa, corresponding closely to the physiological value. Moreover, the selected bellow displayed a very good ability of maintain a stable pressure of air in its interior, which suggested that it was air-tight.

Figure 25. *The latex bellow used as the abdominal component in the model.*

Finally, the mechanical properties of the latex bellow were measured by applying FOT and estimating the mechanical impedance, as described in 7.3. The resulting resistance and reactance curves are demonstrated in Figure 26. The target for the mechanical properties of the abdominal bellow was to approach those of the abdomen of the animal at the lowest insufflation pressure of 5 hPa (Table 4). The bellow properties are summarized and compared to the target values in Table 13. Of note, the coherence was above 95% at the entire frequency spectrum. It was observed that the estimations regarding the resistance of the abdominal bellow were in good accordance with the physiological results. With respect to the compliance, the results were within the range of the values that were obtained for the abdomen of the pig, despite the deviation that was observed. Therefore, it was concluded that the bellow displayed a satisfactory behavior and could be used as the abdominal compartment of the in vitro model.

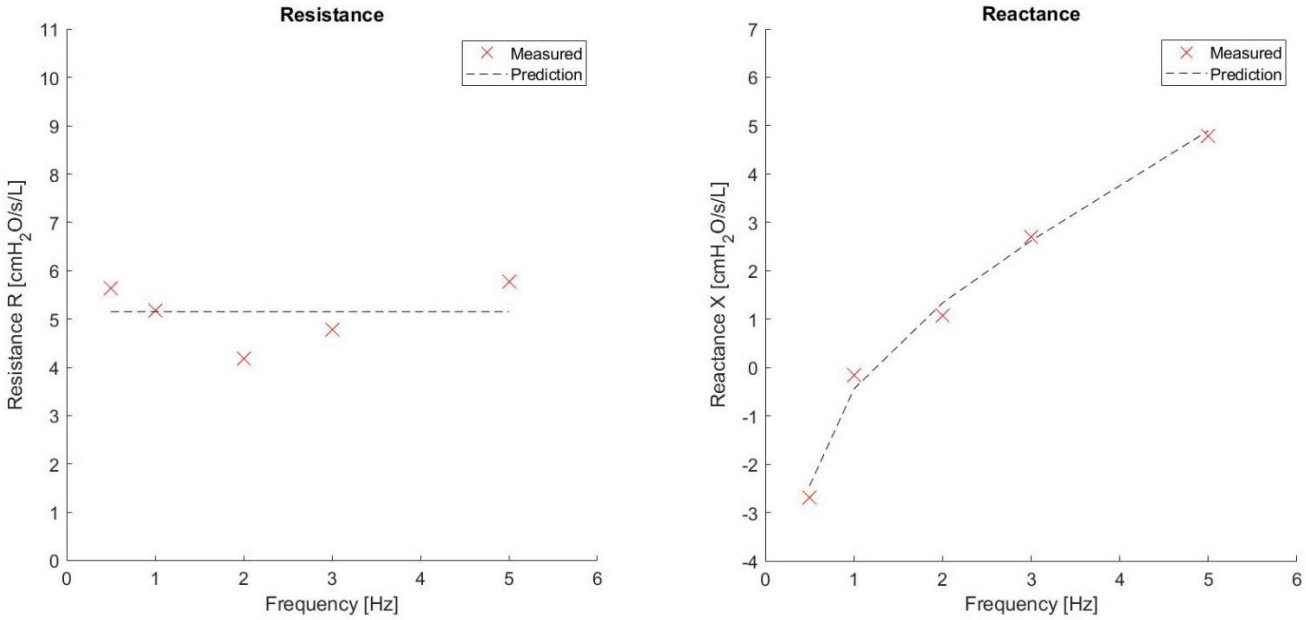

Figure 26. *The resistance and reactance curve estimated for the latex abdominal bellow with the use of the mathematical model described in 7.3*

Table 13. *The measured vs targeted mechanical properties for the abdominal component of the model.*

	R [$cmH_2O \cdot L/s$]	**C [L/ cmH_2O]**
Measured	5.2	0.107
Target	≈6	≈0.46

8.4 Design of the Model

After the individual components were determined, a 3D design of the prototype was created, so that the device can be visualized before being manufactured. The purpose of creating the design of the device was to visualize the relative position and movement between the functional elements as well as to conceptualize the frame of the model and document any additional materials necessary for its manufacturing, such as screws and nuts. Consequently, the 3D visualization of the simulator gave a complete overview of every design aspect and allowed to check its feasibility and dimensions before building it. The 3D design of the mechanical in vitro model, which was created in Autodesk Inventor, is demonstrated in Figure 27.

First of all, Figure 27 shows that the respiratory (red) bellow of the model is placed on top of the abdominal (black) rubber one. On top of the abdominal bellow and exteriorly, a plastic covering is placed. This plastic cap provides the interaction between the respiratory and abdominal compartment. The cap encompasses a plastic ring that is placed in the interior of the abdominal latex bellow, so that it maintains its shape and integrity during insufflation and interaction with the respiratory compartment. The expansion and contraction of both the respiratory and abdominal component occurs in one axis, perpendicularly to the base of the model.

Each of the functional components of the device is attached to a circular part, the bellow connector, as depicted in Figure 27. These bellow connectors have sockets to which the air-conducting tubes from the ventilator and the insufflator can be connected, ensuring the required compatibility. In addition, they have been specifically designed to match the dimensions of the bellows, allow a tight fit and secure that the configuration minimizes air leakage. Air from the ventilator and the insufflator is delivered to the bellows via tubes, which are plugged into the sockets of the bellow connectors.

The frame of the model was designed in a way that it offers stability during its operation. Three 20x20 mm aluminum extrusion profiles have been implemented to the configuration. Each extrusion profile is mounted at the bellow connectors via custom connecting parts, the frame connectors, specifically designed for this purpose. The frame connectors are mounted to the bellow connectors using screws, while also allowing the insertion and mounting of the extrusion profiles using sliding nuts and screws. The configuration comprised of the bellow connector, the extrusion profile and the frame connector can be visualized more clearly in Figure 28. This assembly composes the frame of the model and allows fixing of the functional components at the desired place. An additional advantage of the selected frame configuration is that the distance between the respiratory and abdominal compartment can easily be adjusted by loosening the screws of the bellow connectors and sliding them along the extrusion profiles.

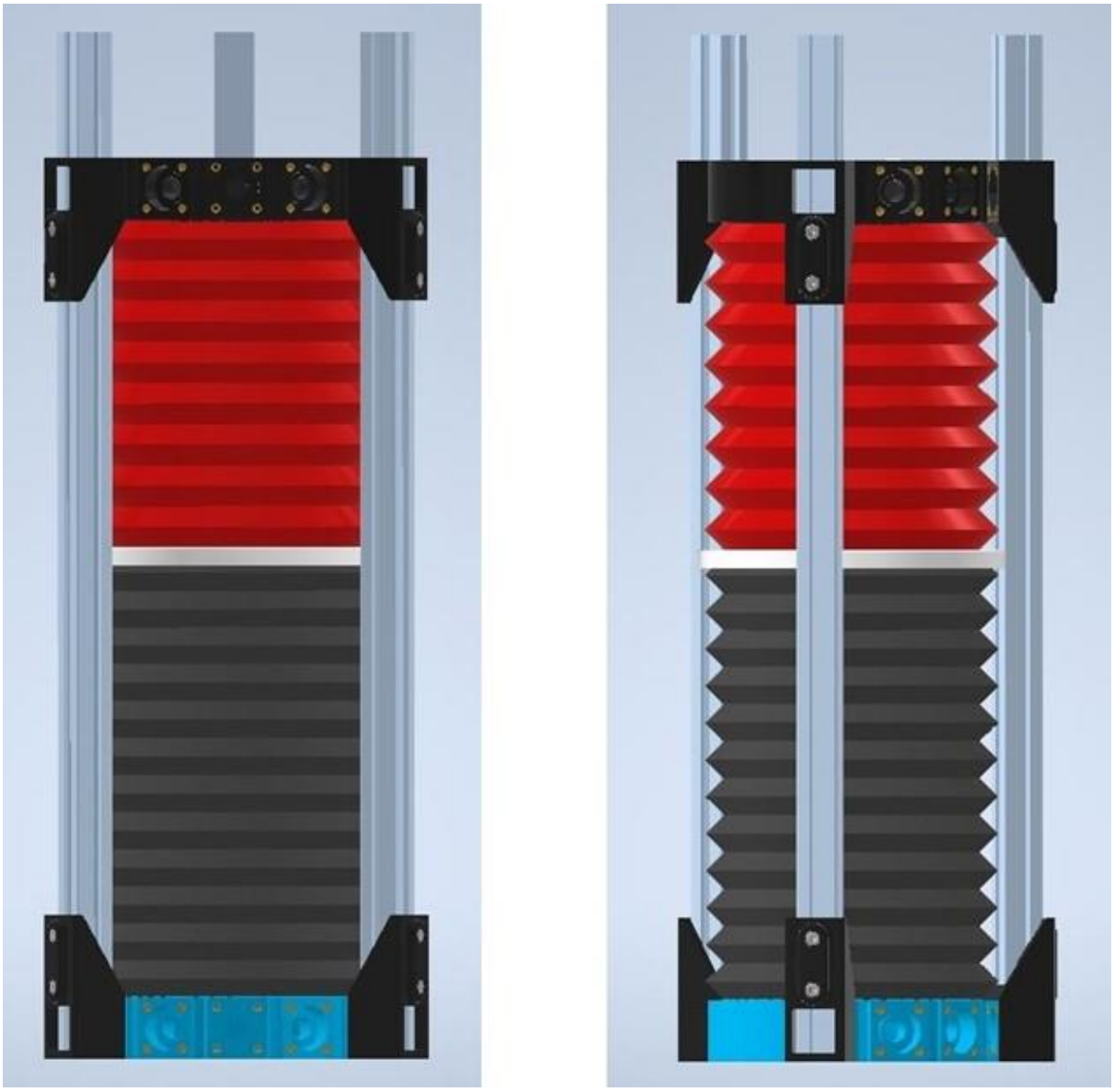

Figure 27. *The 3D design of the model, created in Autodesk Inventor.*

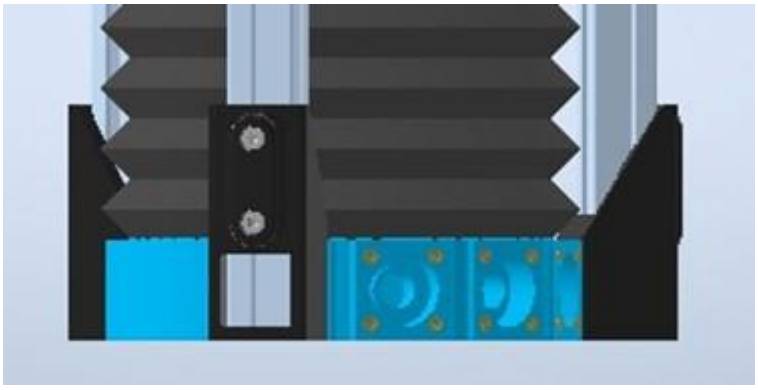

Figure 28. *The configuration between the frame connector (black), the extrusion profile and the bellow connector (blue). The frame connector is initially mounted to the bellow connector. The extrusion profile is inserted and mounted to the frame connector, fixing the system in place.*

8.5 Manufacturing of the Model

Manufacturing of the physical model was the last step in the development phase of the study. For the frame, the three 20x20 mm aluminum profiles of 1m in length were commercially available. The two bellow connectors were 3D printed using the Ultimaker S5 of Erasmus MC (Figure 29), with tough PLA (polylactic acid). The six frame connectors that were implemented in the model were 3D printed as well at Erasmus MC, using the same 3D printer, material, and printing conditions as the bellow connectors. PLA was selected because of its high strength and hardness, as it was necessary for both parts to provide stability to the mechanical model.

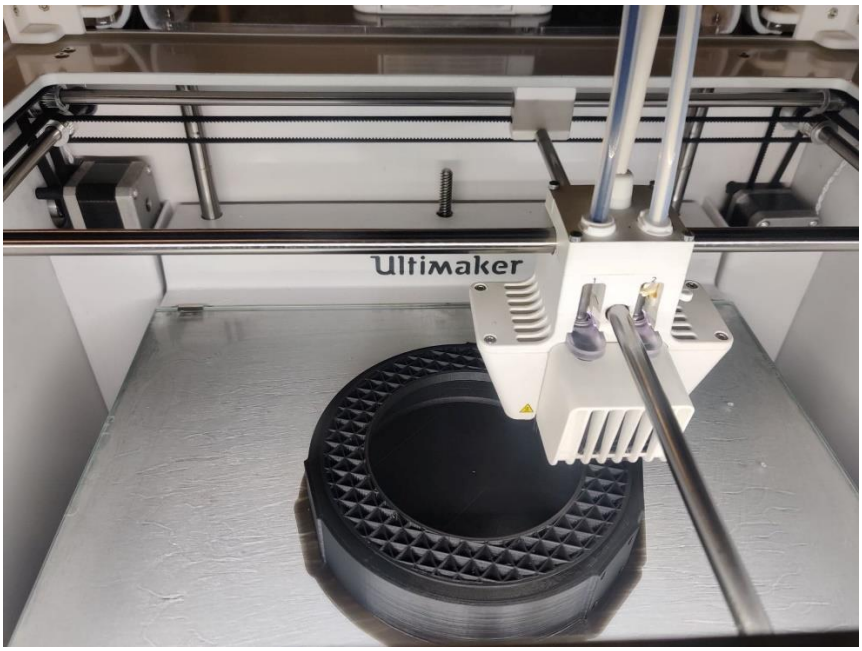

Figure 29. *The respiratory bellow connector was 3D printed at Erasmus MC.*

Assembling of the simulator began by mounting three frame connectors at each bellow connector. Four M3x8 stainless steel screws were used for the mounting of each frame connector. Each of the screws was fixed in a M2.5x3.5 metallic insert, that had been previously soldered in the screw sockets of the bellow connector, to ensure a tighter grip and prevent degradation and wear of the plastic during inserting and removing the screws. The 3D printed bellow connector and the mounted frame connectors are depicted in Figure 30. Of note, each bellow connector has three sockets, each one of which can be connected to an air-conducting tube. The sockets that are not being used can be covered by sealing caps, which were 3D printed at Erasmus MC with TPU 95A, to allow for an air-tight configuration.

The next step was to attach the respiratory and abdominal bellows to their respective connectors. The abdominal compartment was placed appropriately to serve as the base of the device and the extrusion profiles were inserted in the frame connectors. Two M4 aluminum sliding nuts were inserted between the dent surface of each extrusion profile and the respective frame connector. The sliding nuts acted as the inserts for the M4x10 screws that were fastened to secure the frame connector- extrusion profile assembly in place, as shown in Figure 28.

Finally, the respiratory component was inserted on top, sliding along the aluminum profiles towards the abdominal component, until the desired distance between the two parts was reached.

Then, the M4 screws were fastened to fixate it in place. The developed physical model is depicted in Figure 31.

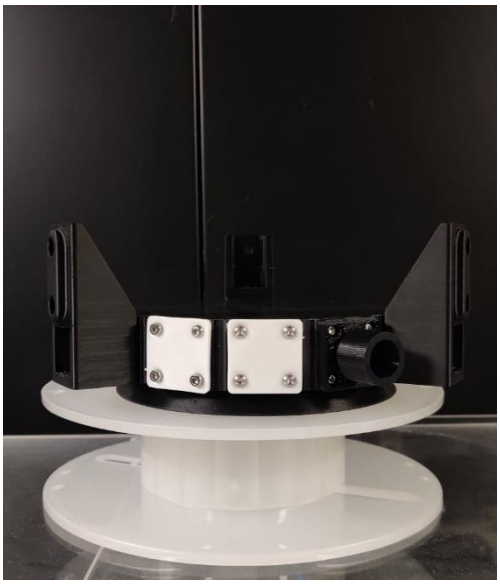

Figure 30. *The 3D printed respiratory bellow connector with the 3 mounted frame connectors. The tube socket that are not in used are sealed with the seal connectors, 3D printed with white TPU 95A.*

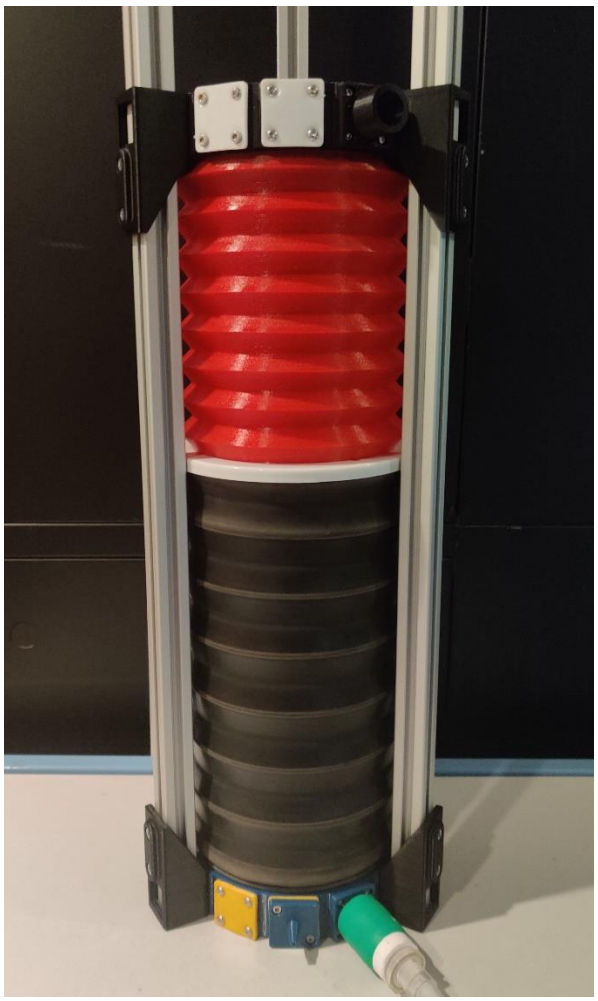

Figure 31. *The physical respiratory-abdominal model developed in the context of this thesis.*

VALIDATION

The developed physical model was validated by connecting it to the novel surgical insufflator and the mechanical ventilator and examining the mechanical behavior of the respiratory as well as the abdominal component at different insufflation pressures. The results were compared to the results acquired from the animal experiments, since the in vivo experimental conditions were recreated for the in vitro validation. Thus, the ability of the model to reproduce the mechanical interaction between the respiratory system and the insufflated abdomen was assessed. The procedure and the steps that were followed for validating the model as well as the obtained results are described below.

9. Validation Methodology

9.1 Goal

The goal of the validation was to evaluate the ability of the developed mechanical model to simulate the interaction between the respiratory system and the abdominal cavity during insufflation. More specifically, to examine whether the mechanical behavior of the compartments of the model is similar to the behavior observed in the animal experiments, as the insufflation pressure rises. A comparison between the results from the model and the results from the animal trial determined whether the developed device was an adequate representation of the interaction of the physiological systems.

9.2 Validation setup

The experimental setup used in the animal trials was reproduced for the testing of the model in order to form a consistent basis for the comparison between the two settings and acquire reliable results. The novel surgical insufflator was connected to the abdominal component of the model, while the same mechanical ventilator, Fabian HFO (Acutronic Medical Systems AG, Hirzel, Switzerland), was used for ventilating the respiratory bellow. The validation setup is depicted in Figure 32.

A pneumotachometer was attached to the output of the insufflator to measure the pressure and flow of the air that was administered to the abdominal part of the model. The air was delivered to the abdominal bellow with the use of a tube of 65cm in length and 1cm in diameter. Similarly, a pneumotachometer was placed at the output of the mechanical ventilator, to measure the pressure and flow of air in the respiratory compartment. The pneumotachometer was connected to the respiratory bellow with a 16.5 cm long tube of 1cm in diameter, which represented the ETT that was utilized for the ventilation of the animal.

Before the measurements, the pressure and flow sensor of each pneumotachometer were calibrated. Pressure calibration was accomplished by comparing the output of the pneumotachometer to a commercially available pressure sensor, while flow calibration was done with the use of a 100ml

calibration syringe. A closer look into the sensors that were implemented in the setup is shown in Figure 33.

Data acquisition and storage was accomplished with an interface that had previously been developed in LabVIEW and used for the animal trial. The interface allowed control of the insufflator by setting the desired insufflation pressure, while it also enabled the application of FOT. Moreover, it allowed storage of the measured data from the pneumotachometers directly to a laptop.

Finally, an additional pressure sensor was attached to the abdominal compartment of the model (Figure 34), to verify that the insufflation pressure in the interior of the abdominal bellow was consistent with the pressure level that was set on the insufflator. Likewise, the pressure, flow and volume measurements by the sensors that were integrated in the mechanical ventilator were checked to confirm that they are in consistency with the measurements of the respiratory pneumotachometer.

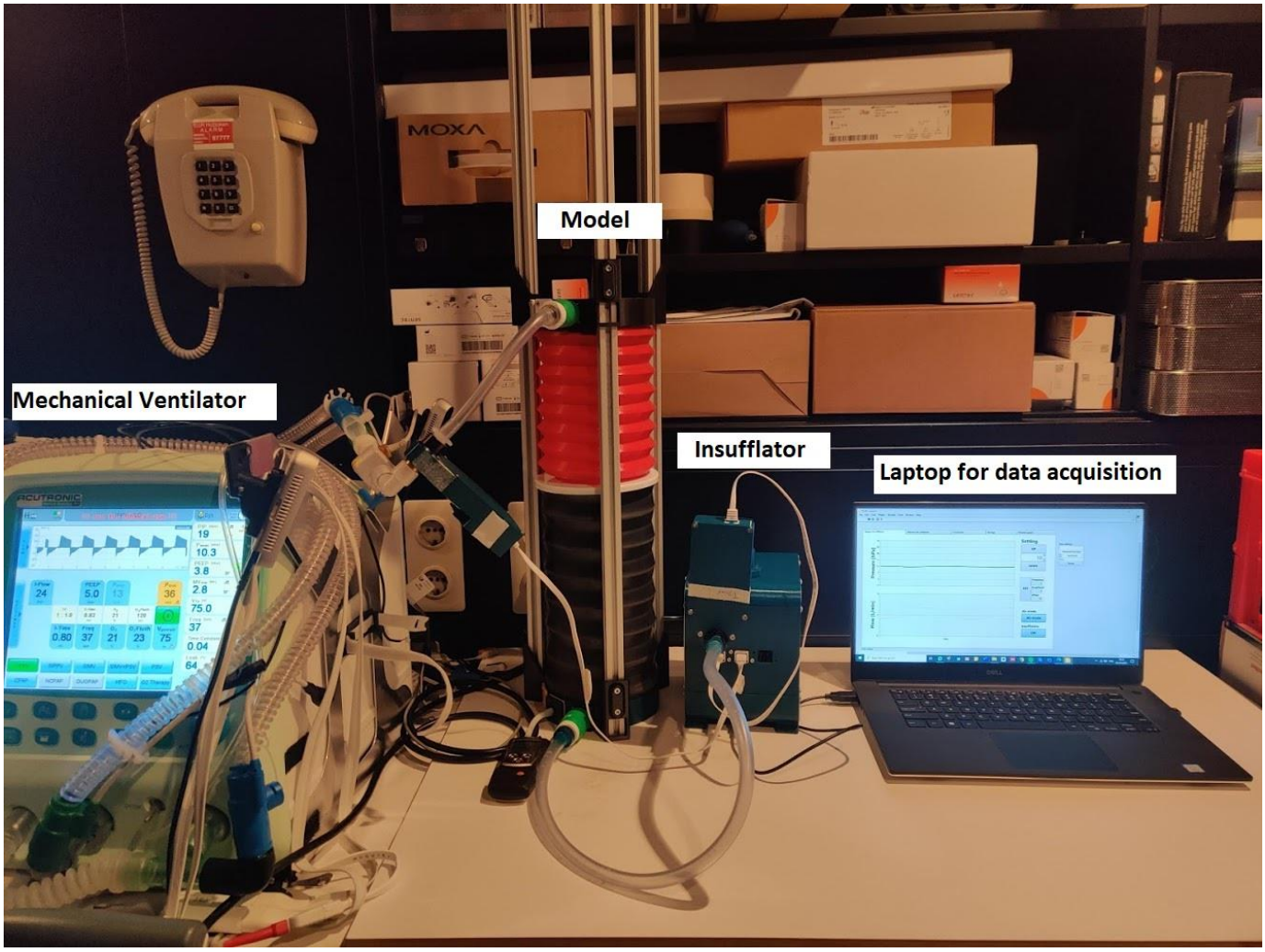

Figure 32. *The setup used for the validation of the developed model.*

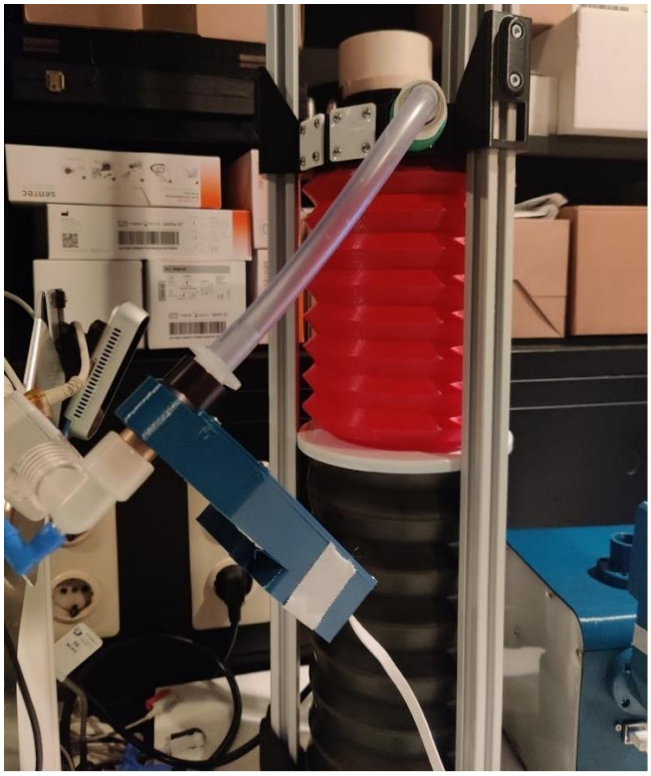

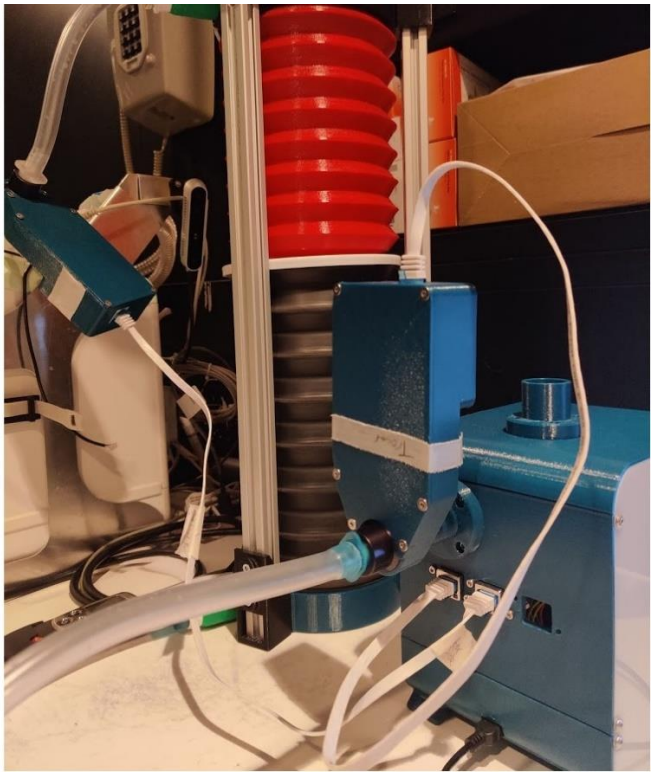

Figure 33. *Measurements were made by two pneumotachometers: one placed between the output of the ventilator and the respiratory bellow (left) and another one placed between the insufflator and the abdominal component of the model (right).*

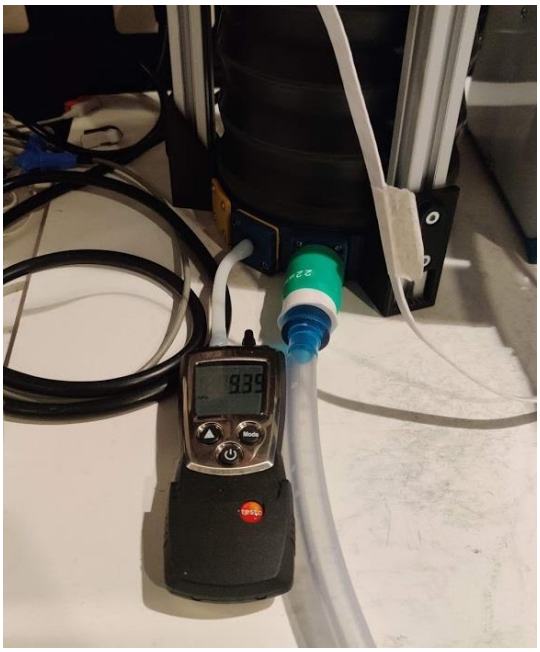

Figure 34. *An additional pressure sensor was utilized to verify that the pressure set by the insufflator could be maintained within the abdominal bellow of the model.*

9.3 Validation Protocol

Insufflation of the abdominal side of the model was performed by the surgical insufflator with atmospheric air through the tube that was described in 9.2. First, the insufflation pressure was set at its lowest value, 5 hPa, until the abdominal bellow expanded to the corresponding volume. Then, the respiratory bellow was connected to the mechanical ventilator and was fixed in place, so that when expanded to its maximum volume at end-inspiration, it made contact with the plastic covering of the abdominal bellow. This was the starting point of the validation procedure, since at the minimum insufflation pressure the abdomen was at its minimum volume and had minimum interaction with the respiratory side.

The insufflation pressure was then increased from 5 up to 20 hPa in a sequential manner, according to the steps that were followed in the animal experiment and described in 7.1. The pressure values that were used were: 5, 8, 10, 12, 14, 16, 18, and 20 hPa. At each insufflation pressure, at least 10 breaths from the ventilator were measured and stored. Then, FOT was applied by the surgical insufflator before shifting to the following IAP level. Measurement and storage of the ventilation data was done to investigate the effect of the insufflation on the respiratory side of the model, while the FOT was performed to examine the mechanical behavior of the abdominal component at every IAP.

The ventilation parameters that were set during the animal trial were selected for the validation as well, such as PEEP=5 hPa and V_t≈150 ml. These parameters were monitored and maintained constant for the entire course of the validation process. Similarly, the FOT was performed at the same frequency range. The excitation pressure signal was produced by the insufflator at 0.5, 1, 2, 3, 5, 10 and 15 Hz. The validation protocol is summed up in Table 14.

Table 14. *The experimental protocol applied during the in vitro validation of the model.*

Validation Protocol	
Insufflation Pressure	5, 8, 10, 12, 14, 16, 18, 20 hPa
Respiratory Measurement	10 breaths at each insufflation pressure
Abdominal Measurement	FOT at each insufflation pressure
Ventilation parameters	V_t≈150 ml, PEEP=5 hPa
FOT frequency range	0.5, 1, 2, 3, 5, 10, 15 Hz

The obtained measurements were stored and analyzed separately for the ventilation and insufflation side of the model. The respiratory analysis was performed in 10 breaths at each IAP level, which were isolated from the entire data set. This enabled a consistent comparison with the data acquired from the in vivo trial. The validation analysis for the ventilation side of the model was accomplished according to the procedure that is reported in 7.2. Besides the mechanical properties of the respiratory component (R_{aw} and E_{RS}), the obtained results included the tidal volume V_t, the volume measured at the abdominal side at end-inspiration (V_{ab}) and the time difference between their occurrence. Finally, PIP and ΔP were examined as well in relation to the increasing IAP. These results were subsequently compared to the corresponding in vivo outcomes to assess the capability of the model to adequately reproduce the mechanical interaction of the two systems.

The abdominal validation analysis was performed on the isolated FOT signal at each insufflation pressure according to 7.3. The mechanical impedance was estimated at each frequency level, while the 10 and 15 Hz frequencies were, again, disregarded due to the increasing effect of the inertial

term. The mechanical parameters of the abdominal bellow were calculated at every examined insufflation pressure and were compared to the values acquired from the animal. Table 15 summarizes the investigated parameters for the validation of the physical model.

Table 15. *The investigated parameters of the model validation.*

Mechanical Ventilation Side	Surgical Insufflation Side
Mechanical Properties (R, E)	Mechanical Properties (R,E)
Tidal Volume (V_t)	
Abdominal Volume (V_{ab})	
Time Difference between V_t and V_{ab}	
Peak Inspiratory Pressure (PIP)	
Driving Pressure (ΔP)	

9.4 Validation Results

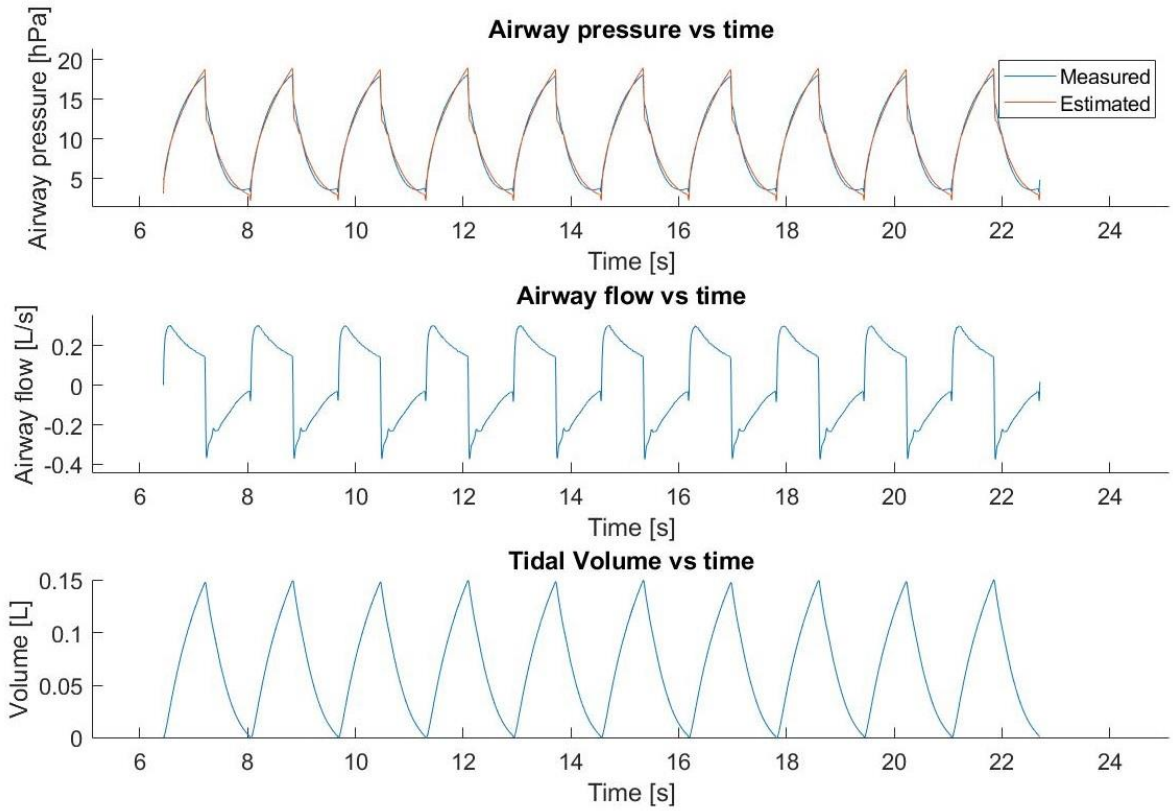

Figure 35. *The time signals of the airway pressure, flow and tidal volume for the respiratory compartment of the in vitro model, at the maximum insufflation pressure of 20 hPa.*

Figure 35 shows the time signals of the airway pressure, flow and tidal volume (P_{aw}, $\dot{V}_{aw}$ and V_t), measured in the respiratory compartment of the in vitro model at an insufflation pressure of 20 hPa. This graph was obtained at every investigated IAP, to verify that the waveforms for the in vitro simulator are similar to the respective waveforms for the animal. The airway pressure signal estimated by the mathematical model is superimposed onto the measured airway pressure, so that the 'goodness of fit' and, by extension, the accuracy of the mathematical model can be visualized. The respective time signals obtained from the animal trial at the insufflation pressure of 20 hPa are depicted in Figure 14.

The mechanical properties of the respiratory component of the model are displayed in Table 16 as the mean ± standard deviation of R_{aw}, E_{RS} and MSE, alongside the corresponding parameters for the in vivo trial. The dependence of these parameters on the increasing IAP is shown in the graphs of Figure 36.

Table 16. *The resistance, elastance and mean squared error (mean ± SD) of the respiratory bellow of the model (top) and the respiratory system of the animal (bottom) at every examined IAP.*

Model Results			
IAP [hPa]	**R_{aw} [$cmH_2O \cdot s/L$]**	**E_{RS} [cmH_2O/L]**	**MSE [hPa^2]**
5	8.9 ± 0.1	71.0 ± 0.2	14.1 ± 0.5
8	10.5 ± 0.1	77.9 ± 0.2	25.5 ± 0.3
10	10.5 ± 0.1	81.2 ± 0.2	26.8 ± 0.5
12	11.0 ± 0.1	85.2 ± 0.1	27.0 ± 0.3
14	11.2 ± 0.1	88.3 ± 0.1	28.5 ± 0.5
16	11.3 ± 0.1	91.1 ± 0.1	29.1 ± 0.6
18	11.3 ± 0.1	93.3 ± 0.2	29.5 ± 0.8
20	11.3 ± 0.1	94.9 ± 0.1	29.9 ± 0.5
In vivo Results			
IAP [hPa]	**R_{aw} [$cmH_2O \cdot s/L$]**	**E_{RS} [cmH_2O/L]**	**MSE [hPa^2]**
5	9.0 ± 0.1	48.0 ± 0.1	6.8 ± 0.5
8	9.6 ± 0.2	52.5 ± 0.3	7.0 ± 0.4
10	10.1 ± 0.1	57.3 ± 0.2	7.4 ± 0.5
12	10.6 ± 0.2	63.1 ± 0.4	8.8 ± 0.5
14	10.9 ± 0.2	71.2 ± 0.5	10.7 ± 0.1
16	11.1 ± 0.2	79.7 ± 0.8	14.2 ± 2.1
18	11.2 ± 0.1	89.0 ± 0.3	22.8 ± 1.2
20	11.1 ± 0.2	97.8 ± 1.2	26.3 ± 5.6

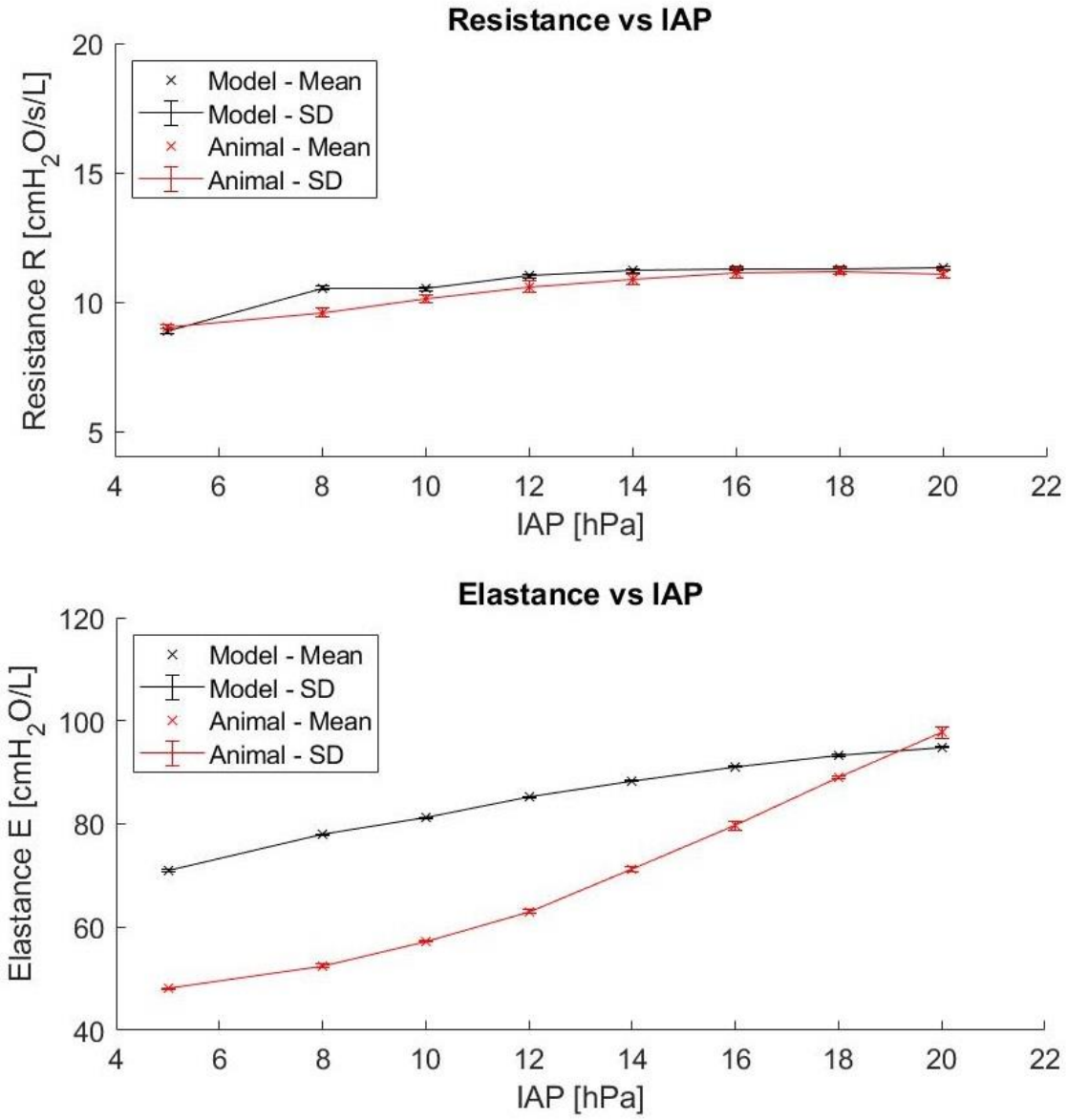

Figure 36. *Graphical representation of R (top) and E (bottom) for the respiratory component of the model and the respiratory system of the animal, as a function of the IAP.*

Table 16 and Figure 36 show that the airway resistance of the model displayed a slight increase alongside the rise in IAP, similarly to R_{aw} estimated the in vivo trial. Starting at 8.9 $cmH_2O{\cdot}s/L$ for IAP=5 hPa, the simulated R_{aw} rose to 10.5$cmH_2O{\cdot}s/L$ for IAP=8 hPa and then only a slight increase was observed, at it reached 11.3 $cmH_2O{\cdot}s/L$ for the maximum IAP of 20 hPa. Regarding the elastance E_{RS}, a dependence on the IAP was observed, as it gradually increased from 71 cmH_2O/L at 5 hPa to 94.9 cmH_2O/L at 20 hPa. A continuous increase was also observed in E_{RS} of the animal, which ranged from 48 cmH_2O/L to 97.8 cmH_2O/L respectively. As for the MSE of the mathematical algorithm for the in vitro model, Table 16 shows that it exhibited an increase from 14.1 hPa^2 at 5 hPa to 25.5 hPa^2 at 8 hPa. From that point on, a slight increase was noted with each rise in IAP until the maximum insufflation pressure, without exceeding 30 hPa^2. On the other hand, the in vivo MSE began at 6.8 hPa^2 for IAP=5 hPa and gradually rose alongside IAP, obtaining its highest value of 26.3 hPa^2 at 20 hPa. An additional visualization of the mechanical properties is demonstrated in Figure 36, which depicts the compliance

as a function of IAP. The compliance of the respiratory system is a widely used measure of the elastic properties of the lung parenchyma.

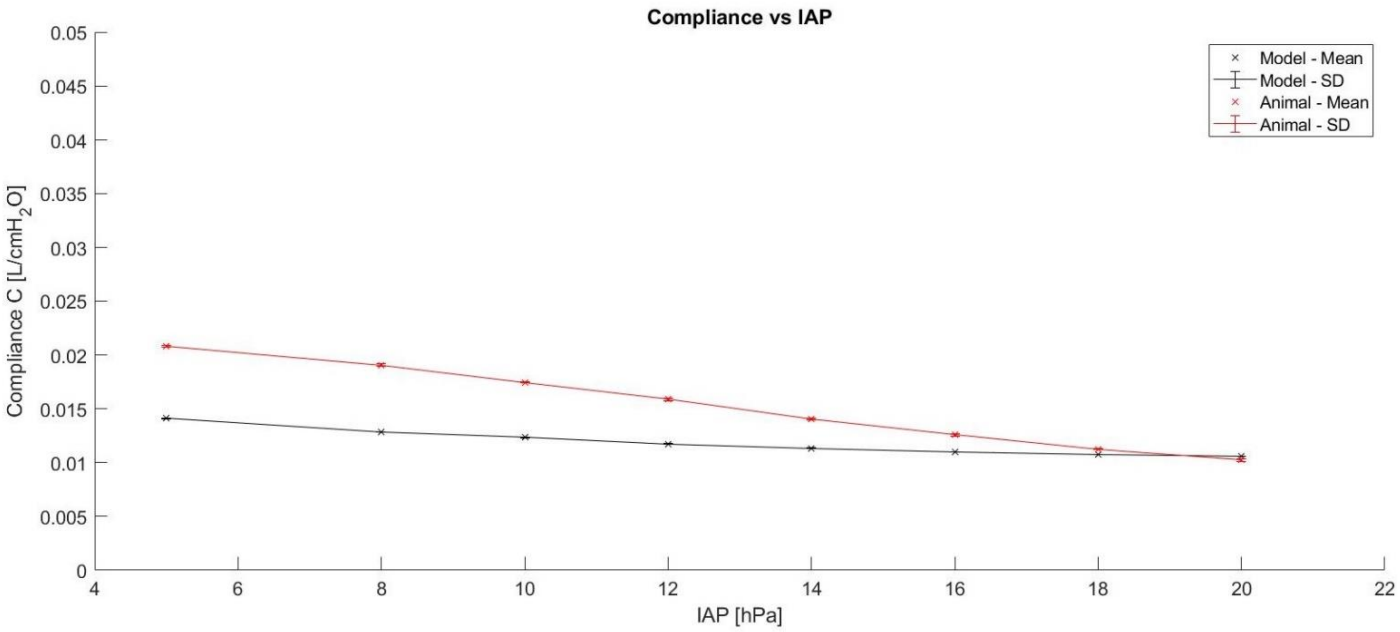

Figure 37. *Graph the compliance C of the respiratory component of the model and the respiratory system of the animal as a function of the IAP.*

The graph of Figure 37 shows the effect of IAP on the elastic properties only, excluding the airway resistance, so that a better comparison between the behavior of the in vitro model and the physiological system can be made. The compliance C_{RS}, calculated as the inverse of E_{RS}, showed a constant decrease from 0.014 L/cmH_2O (IAP=5 hPa) to 0.011 L/cmH_2O (IAP=20 hPa) for the in vitro model, and from 0.021 L/cmH_2O (IAP=5 hPa) to 0.01 L/cmH_2O (IAP=20 hPa) for the respiratory system of the animal.

The mechanical properties of the abdominal component of the simulator are presented in Table 17 and Figure 38. The parameters of the mathematical model (R, I, C and error) for the in vitro model alongside the corresponding parameters of the animal are contained in Table 17. Figure 38 shows the relationship between the mechanical parameters of interest (R_{tr} and C_{ab}) and IAP for the in vitro model and compares it to the relationship observed in the in vivo trial. It should be noted, that the highest IAP level at which the parameters of the abdominal side of the device were estimated was 18 hPa instead of 20 hPa. This was due to a malfunction in the surgical insufflator, which crushed during the application of FOT at IAP=20 hPa.

Table 17. *The resistance, elastance, inertia and the corresponding error in their estimation by the utilized mathematical model for the abdominal bellow of the in vitro model and abdomen of the animal at every examined IAP.*

Model Results				
IAP [hPa]	**R_{tr} [$cmH_2O \cdot L/s$]**	**I [$cmH_2O \cdot s^2/L$]**	**C_{ab} [L/ cmH_2O]**	**Error [$cmH_2O \cdot s/L$]**
5	4.9	0.17	0.089	1.9
8	5.0	0.16	0.060	2.3
10	5.0	0.15	0.057	1.9
12	5.1	0.15	0.054	1.7
14	5.0	0.16	0.051	1.8
16	4.8	0.16	0.050	1.6
18	4.9	0.16	0.050	1.3
In vivo Results				
IAP [hPa]	**R_{tr} [$cmH_2O \cdot L/s$]**	**I [$cmH_2O \cdot s^2/L$]**	**C_{ab} [L/ cmH_2O]**	**Error [$cmH_2O \cdot s/L$]**
5	5.3	0.20	0.465	2.7
8	5.6	0.22	0.122	2.9
10	5.9	0.22	0.085	2.1
12	6.0	0.21	0.069	1.8
14	6.1	0.21	0.049	1.7
16	6.1	0.21	0.035	1.9
18	6.0	0.21	0.028	2.4

The trocar resistance in the model was maintained virtually stable around 5 $cmH_2O \cdot L/s$, independently of the insufflation pressure, ranging between 4.8 $cmH_2O \cdot L/s$ (IAP=16 hPa) and 5.1 $cmH_2O \cdot L/s$ (IAP=12 hPa). In the animal trial, R_{tr} was kept generally stable around 6 $cmH_2O \cdot L/s$ for pressures higher than 10 hPa, after increasing from 5.3 $cmH_2O \cdot L/s$ and 5.6 $cmH_2O \cdot L/s$ at 5 and 8 hPa respectively.

With regards to the compliance, the abdominal component of the model started at a value of 0.089 L/cmH_2O at 5 hPa and displayed a gradual decrease as the insufflation pressure rose. This decrease was more profound at the lowest levels of insufflation pressure, as Figure 38 demonstrates. After reaching a value of 0.057 L/cmH_2O at 10 hPa, further increase in the IAP led to a less notable decrease in C_{ab}, which obtained its minimum value of 0.05 L/cmH_2O at 16 and 18 hPa. On the other hand, the abdomen of the animal was characterized by a C_{ab} of 0.465 L/cmH_2O at 5 hPa, which showed a consistent drop alongside the rise in IAP, reaching 0.049 L/cmH_2O at 14 hPa before eventually ending up at 0.028 L/cmH_2O at the highest level of insufflation pressure.

The inertial component I, which was considered insignificant in affecting the abdominal mechanical properties both in vitro and in vivo, was kept virtually constant between 0.15-0.17 $cmH2O \cdot s^2/L$ for the model and 0.20-0.22 $cmH2O \cdot s^2/L$ for the animal. Finally, the error, which was obtained as an indication of the reliability of the estimation algorithm, did not exceed 2.3 $cmH_2O \cdot s/L$ (IAP=8 hPa) for the simulator and 2.9 $cmH_2O \cdot s/L$ (IAP=8 hPa) for the in vivo system.

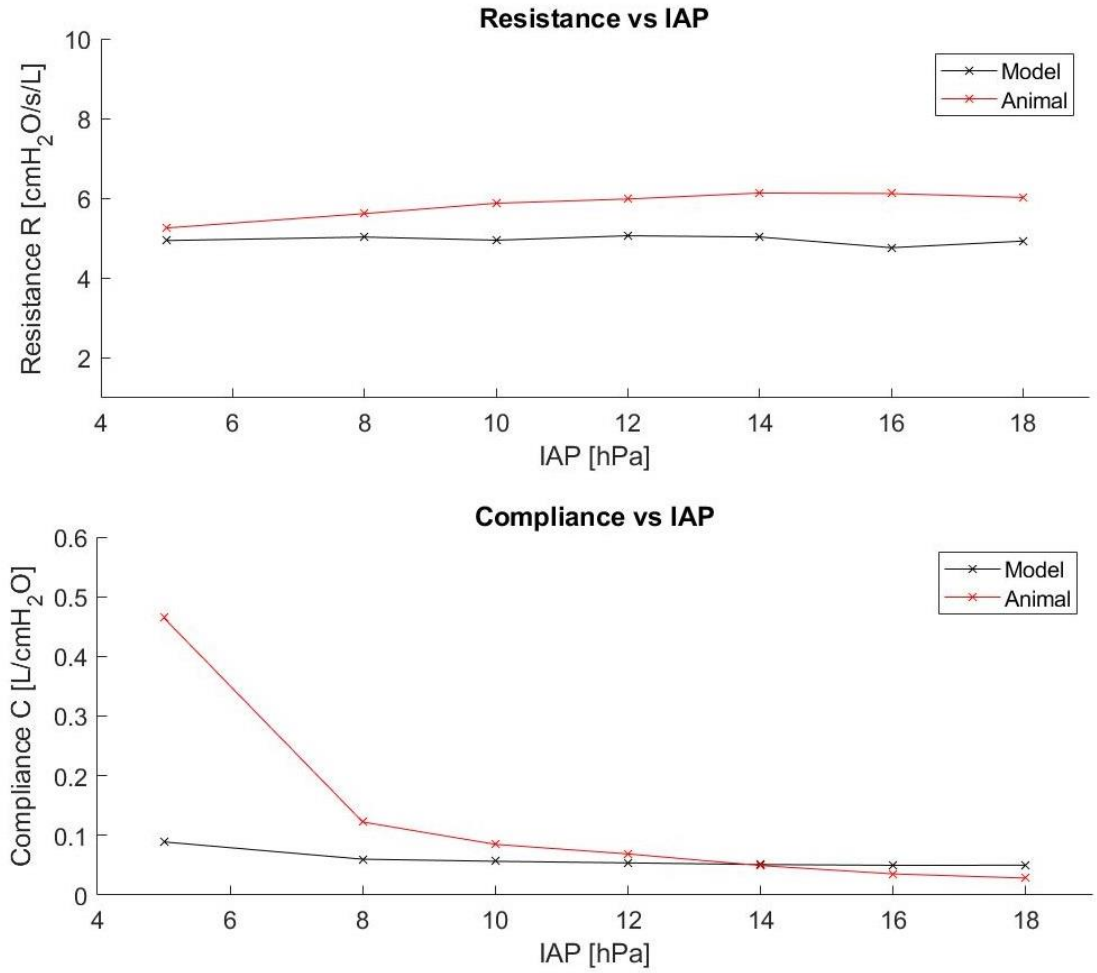

Figure 38. *Graphical representation of R (top) and C (bottom) for the abdominal component of the model and the abdomen of the animal, as a function of the IAP.*

Table 18 depicts the tidal volume, V_t, and the corresponding volume measured in the abdominal component of the model, V_{ab}, as a response to the tidal volume. Moreover, the time difference Δt between the occurrence of the two measurements was recorded and included in the table as well. The relationship between V_t and V_{ab} with IAP is depicted in the graphs of Figure 39, while Figure 40 demonstrates the effect of the increasing insufflation pressure on Δt.

According to Table 18 and Figure 39, V_t remained unaffected by the rise in IAP in both the in vitro and in vivo trial, as it maintained the value that was set in the mechanical ventilator. The delivered tidal volume by the mechanical ventilator remained nearly constant at ≈0.15 L for the model and ≈0.16 L during the in vivo experiment, corresponding to its initially set value. With respect to V_{ab}, it leaped from 0.031 L at 5 hPa to 0.073 L at 8 hPa for the in vitro model, and was then maintained nearly stable until 20 hPa, fluctuating between 0.06 L and 0.073 L. In the animal experiment, V_{ab} exhibited a rise from 0.04 L at 5 hPa to 0.053 L at 8 hPa, before stabilizing alongside the increase of IAP, ranging between 0.066 L and 0.083 L. Of note, standard deviation for both V_t and V_{ab} at every IAP remained significantly low, as it did not exceed 0.001 L.

Table 18. *The tidal and corresponding abdominal volume, and the time difference between their occurrence (mean ± SD), measured for the model (top) and during the animal experiment (bottom) at every examined IAP.*

Model Results			
IAP [hPa]	**V_t [L]**	**V_{ab} [L]**	**Δt [s]**
5	0.149 ± 0.001	0.031 ± 0.001	0.17 ± 0.01
8	0.147 ± 0.001	0.072 ± 0.001	0.12 ± 0.00
10	0.148 ± 0.001	0.067 ± 0.001	0.11 ± 0.00
12	0.148 ± 0.001	0.073 ± 0.001	0.10 ± 0.01
14	0.150 ± 0.001	0.072 ± 0.001	0.10 ± 0.00
16	0.149 ± 0.001	0.067 ± 0.001	0.09 ± 0.01
18	0.149 ± 0.001	0.064 ± 0.001	0.09 ± 0.01
20	0.149 ± 0.001	0.060 ± 0.001	0.09 ± 0.00

In vivo Results			
IAP [hPa]	**V_t [L]**	**V_{ab} [L]**	**Δt [s]**
5	0.160 ± 0.003	0.040 ± 0.001	0.62 ± 0.01
8	0.158 ± 0.003	0.053 ± 0.001	0.46 ± 0.02
10	0.161 ± 0.004	0.072 ± 0.001	0.36 ± 0.01
12	0.161 ± 0.004	0.078 ± 0.002	0.27 ± 0.01
14	0.163 ± 0.004	0.083 ± 0.002	0.21 ± 0.01
16	0.161 ± 0.002	0.073 ± 0.001	0.17 ± 0.00
18	0.164 ± 0.003	0.075 ± 0.001	0.14 ± 0.01
20	0.163 ± 0.003	0.066 ± 0.001	0.12 ± 0.01

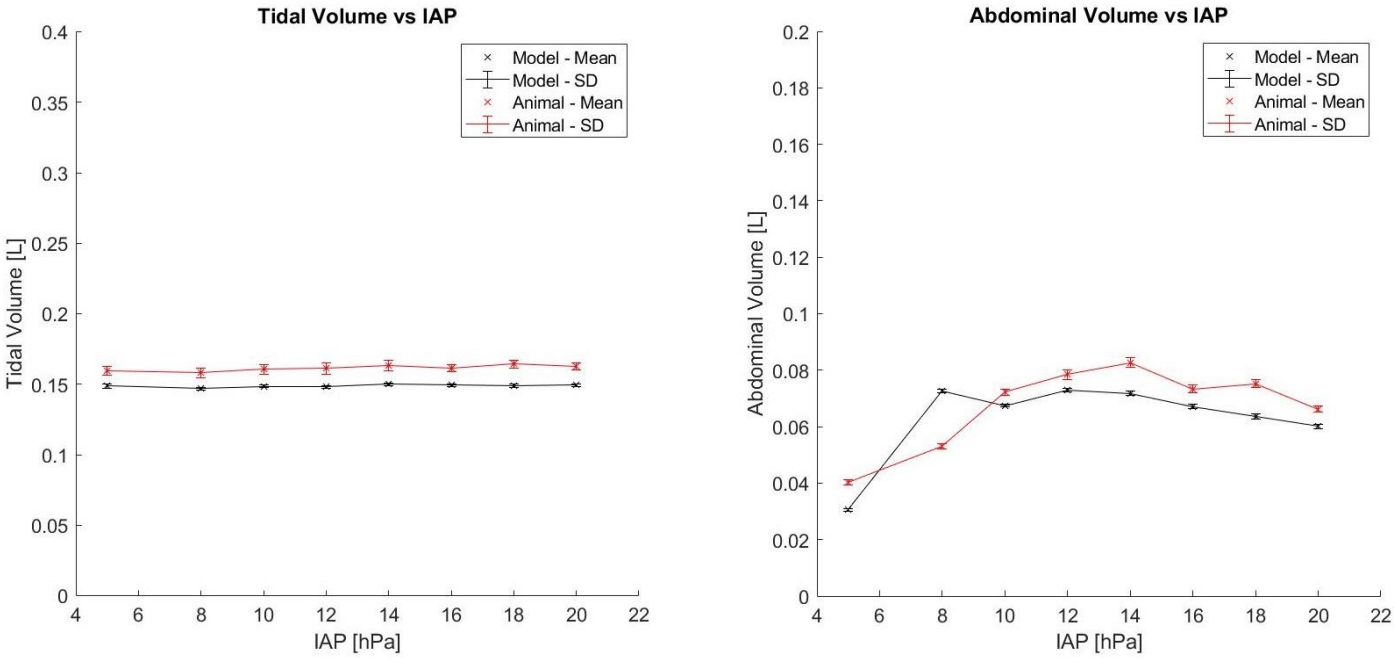

Figure 39. *Graphs of V_t and V_{ab} for the in vitro model and the animal used in the clinical trial as a function of the IAP.*

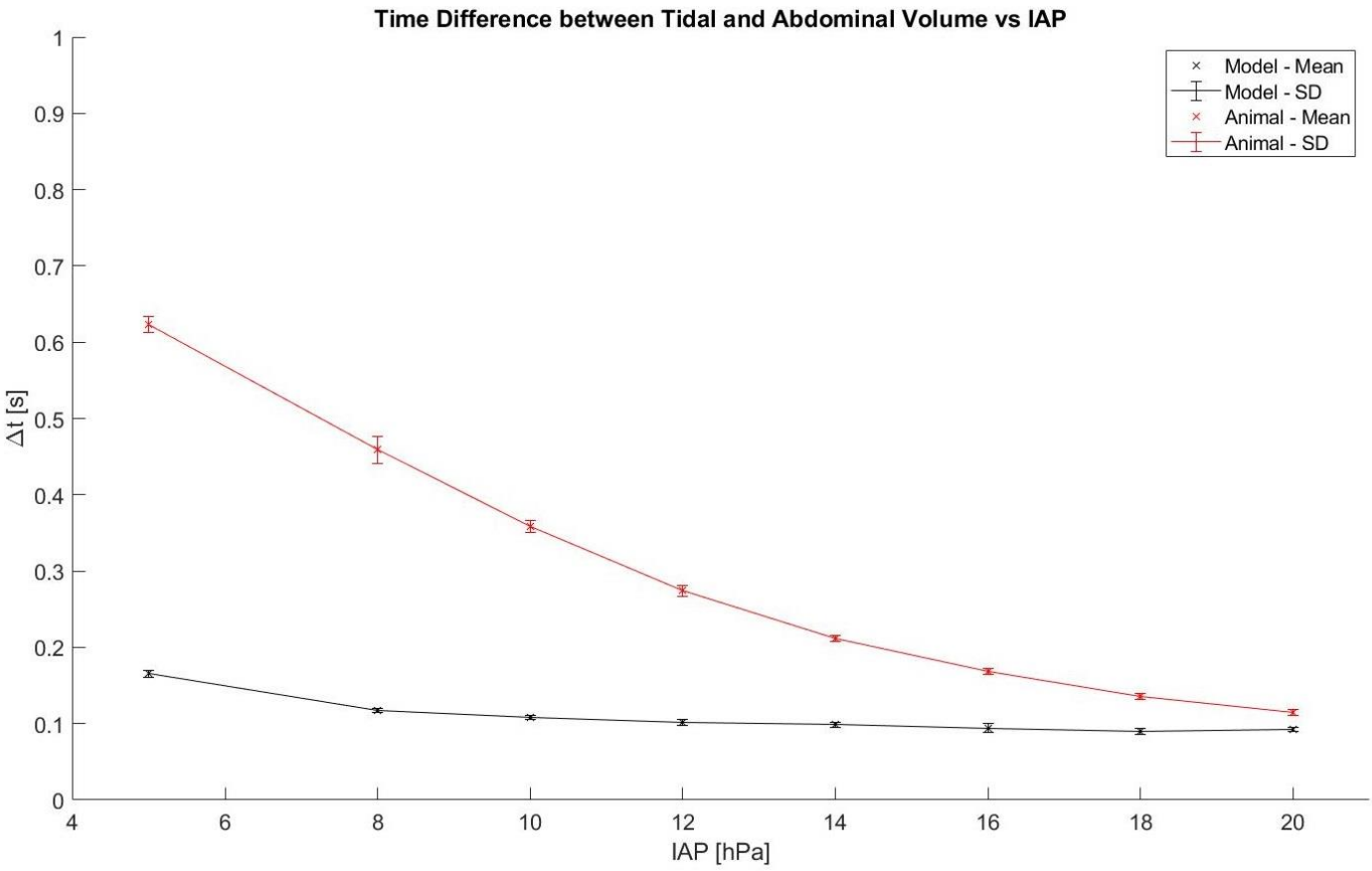

Figure 40. *Graph of the effect of IAP on the time difference Δt between the occurrence of V_t and V_{ab} for the model and the animal used in the clinical trial.*

Figure 40 demonstrates the effect of the increase in IAP on the time difference between the occurrence V_t and V_{ab}. The graph shows that there was a decrease in Δt for the model as IAP increased. More specifically, Δt dropped to almost half from 0.17 s at 5 hPa to 0.01 s at 20 hPa. As for the in vivo results, a sharp drop in Δt is demonstrated, as it displayed a nearly 5-fold decrease, falling from 0.62 s at 5 hPa to 0.12 s at 20 hPa of insufflation pressure. Again, the standard deviation was maintained at remarkably low levels.

Finally, the results for the difference between the peak inspiratory pressure (PIP) and PEEP as well as the driving pressure ΔP at each IAP are summarized in Table 19, while the graphs of Figure 41 and Figure 42 offer a graphical display of the effect of the increasing IAP on PIP-PEEP and ΔP respectively.

Table 19 and Figure 41 show that there was a dependence of PIP on the rise of IAP for the in vitro model. More specifically, as the insufflation rose from 5 up to 20 hPa, the PIP-PEEP difference increased continuously, starting at 9.8 hPa. This increase was more profound and steep up to IAP=14 hPa, for which PIP-PEEP reached 12.3 hPa. From that point on, although the difference continued to rise, it did not exceed the value of 13 hPa, stopping at 13 hPa at IAP=20 hPa. A similar dependence of PIP on IAP was also demonstrated by the in vivo results. There, the PIP-PEEP started at lower values (8.7 hPa at IAP=5hPa), but increased sharply, reaching its maximum value of 16.1 hPa at IAP=20 hPa.

With regards to ΔP, an increasing trend alongside the rise in the insufflation pressure was observed in both the model and the respiratory system of the animal, as Table 19 and Figure 42 confirm. ΔP displayed a gradual increase in the in vitro model, starting at 10.6 hPa at 5 hPa of insufflation pressure. Again, the observed increase was more notable until IAP=14 hPa, for which the calculated driving pressure was 13.2 hPa. Then, the increase continued at a lower rate and ΔP reached its maximum value of 14.2 hPa at the maximum insufflation pressure of 20 hPa. The effect of IAP on the driving pressure was similar in the in vivo results, where a significant and continuous increase was observed from ΔP=7.7 hPa at IAP=5 hPa to ΔP=15.9 hPa at IAP=20 hPa. Once more, the values of the standard deviations were significantly smaller than the calculated mean values of the investigated parameters.

Table 19. *The difference between the peak inspiratory pressure and PEEP, and the driving pressure (mean ± SD), calculated for the respiratory side of the model (top) and respiratory system of the animal (bottom) at every examined IAP.*

Model Results		
IAP [hPa]	**PIP-PEEP [hPa]**	**ΔP [hPa]**
5	9.8 ± 0.1	10.6 ± 0.2
8	11.0 ± 0.1	11.4 ± 0.1
10	11.4 ± 0.1	12.1 ± 0.1
12	11.9 ± 0.1	12.6 ± 0.1
14	12.3 ± 0.1	13.2 ± 0.1
16	12.6 ± 0.1	13.6 ± 0.1
18	12.9 ± 0.1	13.9 ± 0.2
20	13.0 ± 0.1	14.2 ± 0.1
In vivo Results		
IAP [hPa]	**PIP-PEEP [hPa]**	**ΔP [hPa]**
5	8.7 ± 0.1	7.7 ± 0.2
8	9.3 ± 0.1	8.3 ± 0.2
10	9.9 ± 0.2	9.2 ± 0.2
12	10.7 ± 0.3	10.2 ± 0.2
14	12.1 ± 0.1	11.6 ± 0.2
16	13.5 ± 0.2	12.9 ± 0.3
18	14.7 ± 0.1	14.6 ± 0.2
20	16.1 ± 0.1	15.9 ± 0.4

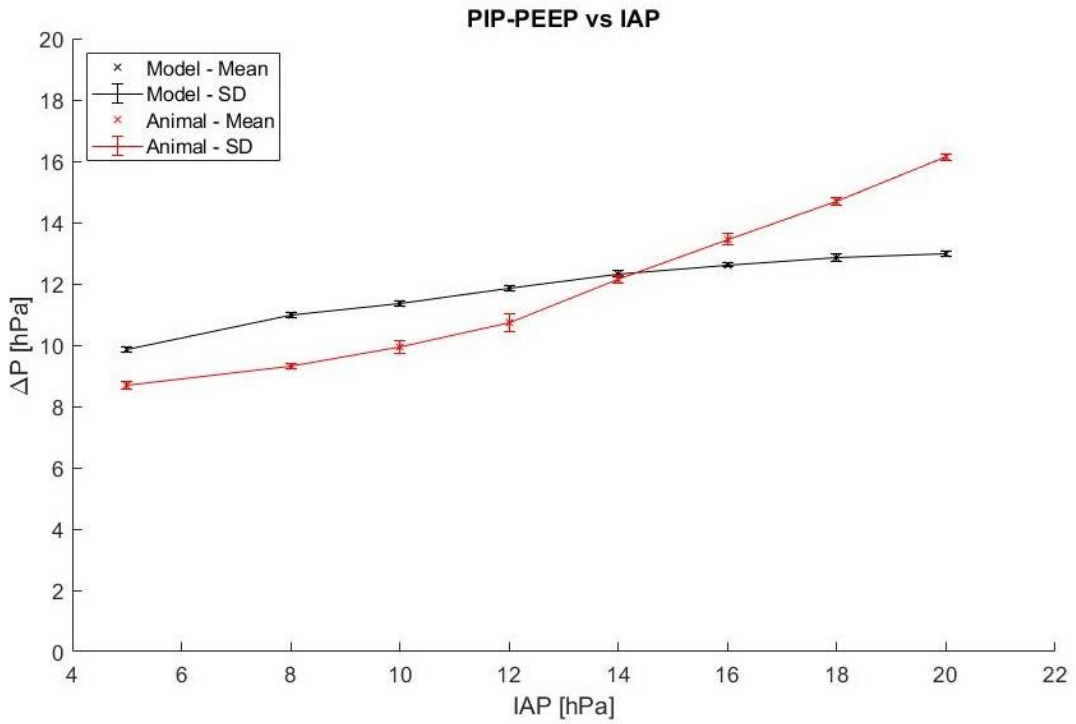

Figure 41. *Graph of PIP-PEEP for the in vitro model and the animal used in the clinical trial as a function of the IAP.*

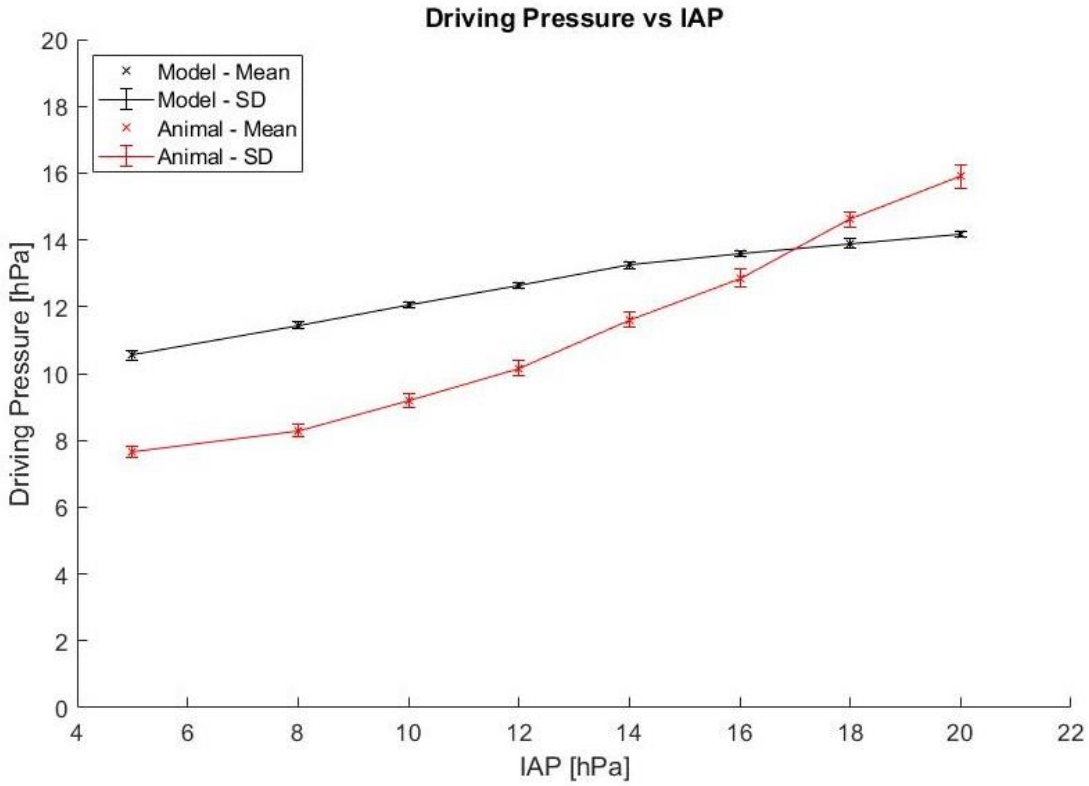

Figure 42. *Graph of the driving pressure ΔP for the respiratory side of the in vitro model (top) and the respiratory system of the animal used in the clinical trial (bottom) as a function of the IAP.*

EVALUATION

10. Discussion

The goal of this study was to develop a physical in vitro model that simulates the interaction between the respiratory system and abdominal cavity during surgical insufflation, so that the performance of the novel surgical insufflator developed at Erasmus MC can be evaluated. The created device was validated with in vitro experiments, during which the mechanical properties and functional parameters of the model were recorded and compared to the corresponding parameters that were obtained from an animal experiment.

The ability of the mechanical model to recreate the effect of surgical insufflation on the respiratory system was assessed first. First of all, the obtained waveforms of the airway pressure, flow and tidal volume for the in vitro model came in good accordance with the corresponding signals for the animal, at every investigated insufflation pressure.

The results regarding the mechanical properties R_{aw} and E_{RS} showed that the increase in the insufflation pressure slightly affected the airway resistance, which remained essentially stable at high insufflation pressures, but greatly impacted the respiratory compliance. The compliance of the model displayed a continuous decrease alongside the rise in IAP and matched the trend observed in the animal experiments. It is well-documented in the literature, and also reported in the in vivo trials, that the rise in the abdominal pressure deteriorates the mechanical properties of the respiratory system by increasing its elastance and forcing it to a less compliant mechanical behavior [71–73,79,95]. Physiologically, this behavior is explained by the stiffening of the chest wall at higher pressures, which causes the overall compliance of the respiratory system to decrease as well, since $1/C_{RS}=1/C_{CW}+1/C_L$ and the compliance of the lungs remains unchanged [21]. Although slightly stiffer than the respiratory system, the ventilation side of the physical model sufficiently reflected this effect, as confirmed by the progressive decrease in its compliance, which was analogous to the decreasing trend of C_{RS} in the animal trial. In addition, the model is capable of adequately simulating the airway resistance as well, as its values during the in vitro trial closely matched the values observed in the animal experiment. These estimations, produced by the linear, single-compartment mathematical model of the respiratory system, are considered reliable, since the error was maintained at relatively stable and low levels at every examined IAP (below 30 hPa^2) and it did not exceed the maximum error observed in the animal experiments.

The abdominal mechanical properties in the model were represented by R_{tr} and C_{ab}. Again, the increase in IAP had a limited effect on R_{tr} of the model, as it was kept stable at the entire range of investigated pressures, and was a good approximation to the physiological resistance observed in the abdomen of the animal. With respect to the stiffness of the system, the compliance of the abdominal bellow approached the behavior of the physiological compliance to a certain extent. More specifically, the abdominal compliance was higher at the lowest pressures, displayed a notable decrease as pressure rose from 5 to 10 hPa, and from that point on the drop in the compliance was significantly less prominent. The observed trend in the behavior of the compliance of the model is considered sufficient for the proof-of-concept of the simulator.

However, it is clear that the abdominal bellow of the in vitro device was stiffer than the abdomen of the animal, and this difference in the initial stiffness appears to have an effect in the final results. It was shown that the abdomen of the animal was not only more compliant than the latex bellow of the model, but it also displayed a significantly higher capacity of variation in its compliance. Despite being more compliant at the lowest pressure, the abdominal wall of the animal eventually reached a compliance that was lower than that of the simulator at the pressure of 18 hPa. The abdominal compartment of the model reached its compliance capacity at 16 hPa, and further increase in the pressure did not result in additional extension of its volume. On the contrary, the abdominal wall of the animal showed a higher range of compliance, being more compliant at low pressures at stiffer at the highest IAP level. Although the mechanical behavior of the latex bellow of the model was relatable to the behavior of the abdomen in vivo, this difference in the overall compliance spectrum can be explained by the intrinsic mechanical properties of the materials of each system. The rubber material simulated better the abdominal mechanical properties at low insufflation pressures, while at higher IAP its ability to capture the variation in the compliance capacity of the abdomen was limited.

With respect to the tidal volume, it was maintained stable throughout the validation of the model and it was shown that it is not affected by the rise in the abdominal pressure. The model allowed the mechanical ventilator to deliver the set tidal volume at every pressure, regardless of the decrease in the compliance. Volume-controlled ventilation of the model was performed throughout the validation test. Tidal volume is one of the most important parameter of mechanical ventilation and should generally maintained constant, as abrupt fluctuations can severely affect the pulmonary function and increase the risk for the patient [96–98]. Abdominal insufflation normally leads to a drop in the tidal volume, because of the limited and anomalous movement of the diaphragm. PEEP applied by the ventilator in combination with VCV counterbalance this effect [72,76]. The beneficial outcome of PEEP and VCV was observed in the animal experiments as well, where the tidal volume was maintained at a constant level. The physical model showed a very good capability of reproducing this outcome and ensuring the delivery of the fixed tidal volume.

As the lungs of the patient expand and reach their maximum volume at end-inspiration, the surgical insufflator allows a certain amount of gas to flow outside of the abdominal cavity. This amount of gas, quantified by V_{ab}, is one of the features of the insufflator that enable better preservation of a stable pneumoperitoneum. Measurement of V_{ab} in the model was comparable and showed good accordance with the corresponding measurement in the animal trial. After a slight increase at the lowest levels of IAP, V_{ab} was constant for the rest of the investigated pressures. As IAP increases and the diaphragm moves cranially due to the abdominal expansion, the respiratory system comes in closer contact with the abdomen. Thus, at that point, changes in the lung volume and the resulting movements of the diaphragm affect the abdomen to a higher degree. This phenomenon was clearly reflected in the in vitro device. Since V_{ab} occurs as a response of the insufflator to the tidal volume, its stability for pressures above 8 hPa comes in good accordance with the measurements of the fixed tidal volume. The results of V_t and V_{ab}, highlight the ability of the model to capture this mechanical interaction both in terms of its behavior but also in terms of the absolute values of the measured quantities. The results obtained by the animal experiments are well-represented and reflected in the in vitro simulator.

The decrease in Δt between the occurrence of V_t and V_{ab} in both the in vivo and in vitro settings can be viewed as an indication of the increasing rigidity of the system. The shift in the diaphragm, as a result of the increased insufflation pressure, makes the abdomen more responsive to changes in the respiratory system. In addition, the increasing stiffness of the respiratory system alongside the rise in IAP makes the respiratory and abdominal system as well as their interaction more rigid, as reflected by the drop in Δt. The more notable drop in Δt in the in vivo trial was due to the higher initial compliance of the animal and its higher variation capacity. Both the abdominal and the respiratory side of

the model are less compliant than the respiratory system and abdomen of the animal. Also, as IAP increases, the change in the compliance of both sides of the model is less than the change observed in the in vivo system. The model has comparable rigidity at higher insufflation pressures to the in vivo system, but since the animal starts from a higher compliance, the change in its rigidity is considerably higher and reflected by the more noticeable change in Δt. Therefore, the trend in the rigidity (Δt) is analogous to the trends observed in the compliance of the individual compartments of the model and depends on the change in the compliance (ΔC) of each system.

An additional consequence of abdominal insufflation in combination with volume-controlled ventilation is the rise in PIP and ΔP. Maintenance of a stable V_t despite the decrease in C_{RC} was expected to exert an increasing effect on the measured ΔP and PEEP [72]. First of all, by definition, the compliance of a system indicates the amount of pressure that is required for a specific change in volume. Thus, the drop in C_{RS} means that a higher pressure is necessary to deliver the same V_t. This is reflected by the increase in PIP in the mechanical ventilator, as IAP increases. The ventilator is set to deliver a fixed amount of air to the system, and since the higher elastance acts as an opposing force, it increases the maximum pressure (PIP) that is required to overcome it and provide the set V_t. Similarly, ΔP is the overall pressure above PEEP applied by the ventilator to the respiratory system, to achieve the desired tidal volume. Again, the stiffening of the chest wall at higher IAP in combination with the stable V_t results in a systematic increase of ΔP alongside IAP.

These outcomes were confirmed by the results in the animal experiment and were clearly visible in the validation of the in vitro model. An increase in both PIP and ΔP was observed in the validation results, which comes in accordance with the expected theoretical outcome and indicates the ability of the model to capture this significant effect of the increase in the insufflation pressure. The initially lower compliance of the model compared to the respiratory system of the animal affected the results, as the rise in PIP and ΔP is not as steep as it was in the in vivo setting. This also explains the deviation in the absolute values of the measured quantities in the model. The relatively stiff respiratory bellow of the model requires higher PIP and ΔP even at the lowest insufflation pressures, without leaving much room for further increase as the IAP rises. Nevertheless, the increasing trend is clearly observed, as the result of the capability of the model to adequately simulate this interaction.

The validation results showed to be in good accordance with the outcomes of the in vivo clinical trial. Additionally, the results acquired for the model were consistent with each other, as the obtained functional parameters such as V_t, V_{ab}, Δt, PIP and ΔP displayed a behavior that was expected based on the estimated mechanical properties. This suggests that, despite its limitations, the developed model exhibits sufficient capability of representing the intra-operative interaction between the respiratory system and insufflated abdomen. Overall, the mechanical and functional parameters of the respiratory system are captured and reflected in the prototype of the in vitro model. This indicates that the assumptions made for the development of the model were reasonable and the design decisions contributed to creating an adequate representation of the physiological interaction.

Laparoscopic surgery is one of the most widely used types of minimally invasive surgery. Since its introduction in the early 1990s, the vast majority of abdominal and pelvic operations are performed laparoscopically, replacing the traditional open surgery. Throughout the entire procedure, the patient is under general anesthesia. Intra-operative mechanical ventilation is required to help the patient maintain sufficient lung function, because anesthesia greatly reduces, or even completely ceases the respiratory drive and the muscular component of breathing [19,22]. VCV is widely used in clinical practice because it is considered a safe and effective approach for anesthetized patients [41,43]. With respect to laparoscopy, VCV is the preferred ventilation mode because it ensures the delivery of a fixed tidal volume to the patient [42] despite the changes in the compliance of the chest wall and lungs, that occur due to the increase in IAP. Therefore, validating the model by investigating the effect of IAP on the

respiratory mechanical properties and pressures is meaningful for this particular ventilation mode, which aims at ensuring sufficient pulmonary gas exchange.

On the contrary, pressure-controlled ventilation (PCV) aims at maintaining a fixed inspiration pressure. In this case, the rise in IAP would result in a gradual decrease in V_t, while P_{aw} would remain constant alongside the increasing stiffness of the respiratory system. VCV is generally preferred over PCV, because a reduction in V_t can jeopardize the patient [96–98]. Overall, the impact of the increasing insufflation pressure on respiratory mechanics during VCV is a widely encountered problem in the clinical setting. The developed in vitro model contributes in mitigating the side effects associated with abdominal insufflation by offering knowledge on the respiratory-abdominal interaction. This, in turn, is the first step for improving the post-operative outcome of such a widely applied procedure, which affects a large number of patients.

11. Recommendations

The in vitro model showed promising results in terms of simulating the respiratory-abdominal interaction during insufflation and allowed broader understanding of the insufflator's performance as well as the mechanical behavior of the individual systems. However, the results suggest that there is still room for improvement in the performance of the model. There are certain points of attention for further research that can potentially make the model more versatile and expand its applications.

The proposed modifications can be the first step towards adapting the model for simulating the respiratory-abdominal interaction in humans. The current device has been specifically developed for the pig. However, these improvements offer flexibility and by modifying the dimensions and mechanical properties of the individual model components, simulation of the effect of IAP in humans can be accomplished.

11.1 Compliance of the Individual Components

The functional components of the model, both in the respiratory and the abdominal side, displayed a lower compliance than the respective physiological structures. Although this difference in compliance did not lead to large deviations in the behavior of the model compared to the animal in terms of the observed pattern in the measured parameters, it led to slight differences in terms of the absolute values.

The manufacturing of the custom 3D printed respiratory bellow of the desired compliance was hindered by the quality of the print. Although TPU 95A is one of the most flexible and widely available materials for additive manufacturing, printing a structure with such a high height-to-thickness ratio proved challenging and often compromised the air-tightness of the bellow. Careful selection of the printing settings enabled the manufacturing of the bellow that was eventually implemented in the model, which exhibited air-tightness and an adequate compliance, despite being slightly stiffer than the desired level. Therefore, manufacturing of a respiratory bellow with the use of a more sophisticated 3D printer and with an even more flexible material, such as silicone, is worth investigating. Such a printer and material combination could allow for creating bellows with greater height, thus more compliant, while not causing inconsistencies and punctures on the surface, which lead to air leakage.

Besides, such a solution could be implemented for the manufacturing of the insufflation bellow as well, in order to decrease its compliance.

11.2 Addition of Physical Interaction

Interaction between the ventilation and insufflation side was achieved by adjusting the position and distance between the individual compartments, so that they come in contact. This approach was sufficient for proving the feasibility of the in vitro model and establishing the proof-of-concept for the device.

A more sophisticated assembly, which is a closer match to the physiological anatomy and physiology, is suggested for future investigation. The addition of a component to act as the physical interaction between the two compartments of the model, could benefit the system by offering a better representation of the physiological conditions. The function of this component would correspond to the function of the diaphragm. Therefore, its main role would be to act as the connective link between the individual compartments of the device. The compliance of the additional part, which could be implemented in the form of an elastic membrane or a spring between the two sides, should be close to the compliance of the diaphragm. In combination with the more near-physiologic compliances of the rest of the model parts, it is assumed to benefit the performance of the simulator. More specifically, the simulator is expected to produce an improved behavior that better mimics the mechanical interaction observed in the in vivo system.

Such an addition is believed to improve the ability of the model to capture the relationship and interplay between the two sides to a greater extent. If accomplished, it would pave the way for further additions and modifications. For instance, the effect of cardiac oscillations and the interplay between the cardiovascular and respiratory system during insufflation are of particular interest.

11.3 Bicompartment Mathematical Model

The rationale for selecting the linear, single-compartment mathematical model that was utilized in this thesis was based on its capability of accurately capturing the healthy respiratory mechanics and the non-linear relationship between pressure and volume. Indeed, this was confirmed by the results in both the animal experiment and the validation of the physical model. Nevertheless, the utilized mathematical model assumes that the mechanical properties of the respiratory system (R_{aw}, E_{RS}) remain unchanged within each breath and only captures the breath-to-breath variations. Although this assumption is rational, based on the pulmonary function of a healthy subject in the absent of respiratory diseases, the effect of insufflation on within-breath variations of the mechanical properties could be worth-investigating.

The use of the bicompartment model has been suggested by several authors as means for providing an even more accurate representation of the respiratory function [84,88,99]. More specifically, the implementation of the series or the viscoelastic mathematical model could be useful in the context of the in vitro simulator. These mathematical models, allow the estimation of changes in the mechanical properties during the inhalation and exhalation phases, separately. Additionally, the viscoelastic model takes into consideration the stress adaptation of the lung component.

The implementation of such a model is towards the direction of making the overall configuration a closer approximation of the physiological conditions by analyzing the function of each lung individually. This is expected to contribute to a better simulation, and enable the investigation of the impact of insufflation on the mechanical properties during inhalation and exhalation. Finally, it will

enable exploring the respiratory effect of the pneumoperitoneum in patients with an underlying respiratory disease.

12. Conclusions

This thesis indicated that it is feasible to simulate the interaction between the respiratory system and the abdomen during surgical insufflation with an in vitro model. The developed model can adequately mimic the experimental data from the performed clinical trials and can be used for the evaluation of the performance and safety of a surgical insufflator.

The mechanical model was manufactured following the defined design requirements, which were formulated based on a preliminary analysis that was done on previously performed in vivo trials. The in vitro simulator was used in a series of trials to assess the effect of the insufflation pressure on the respiratory functions, and especially on the functional pressures and volumes. The abdominal and respiratory mechanical behavior observed in the in vivo experiments were reflected in the developed model. Despite some deviations in the simulated mechanical properties, the prototype gave satisfactory results in terms of the expected theoretical interaction between the respiratory system and the abdomen as a function of the insufflation pressure. Therefore, it is considered as a good proof-of-concept, while additional modifications to optimize its function are worth investigating.

Although it was initially created for the novel surgical insufflator developed at Erasmus MC, the in vitro model can be utilized for the evaluation of the performance and safety of every insufflator. It offers a broader understanding of the functional attributes of the insufflator as well as knowledge on the interplay between two dynamic physiological systems during laparoscopy.

The device can be used complementary to animal experiments as it offers flexibility and repeatability, allowing more tests to be performed and intraoperative situations to be investigated. The in vitro simulator is subject to certain additions and improvements that are expected to optimize its function and give insights to more relevant mechanical processes during insufflation. This way, a broader and more objective evaluation of the insufflator can be achieved. Such improvements can contribute to an increase in the reliability and the number of tests that the model is able to undertake, further reducing the reliance on animal experiments.

REFERENCES

1. Ott DE. Abdominal compliance and laparoscopy: A review. *J Soc Laparoendosc Surg*. 2019;23(1). doi:10.4293/JSLS.2018.00080

2. Diagnostic Laparoscopy. http://www.laparoscopicexperts.com/diagnostic-laparoscopy/. Accessed January 27, 2021.

3. Bucur P, Hofmann M, Menhadji A, et al. Comparison of Pneumoperitoneum Stability Between a Valveless Trocar System and Conventional Insufflation: A Prospective Randomized Trial. *Urology*. 2016;94:274-280. doi:10.1016/j.urology.2016.04.022

4. Herati AS, Atalla MA, Rais-Bahrami S, Andonian S, Vira MA, Kavoussi LR. A new valve-less trocar for urologic laparoscopy: Initial evaluation. *J Endourol*. 2009;23(9):1535-1539. doi:10.1089/end.2009.0376

5. Nepple KG, Kallogjeri D, Bhayani SB. Benchtop evaluation of pressure barrier insufflator and standard insufflator systems. *Surg Endosc*. 2013;27(1):333-338. doi:10.1007/s00464-012-2434-x

6. Annino F, Topazio L, Autieri D, Verdacchi T, De Angelis M, Asimakopoulos AD. Robotic partial nephrectomy performed with Airseal versus a standard CO2 pressure pneumoperitoneum insufflator: a prospective comparative study. *Surg Endosc*. 2017;31(4):1583-1590. doi:10.1007/s00464-016-5144-y

7. Luketina RR, Knauer M, Köhler G, et al. Comparison of a standard CO2 pressure pneumoperitoneum insufflator versus AirSeal™: Study protocol of a randomized controlled trial. *Trials*. 2014;15(1):239. doi:10.1186/1745-6215-15-239

8. Nguyen NT, Wolfe BM. The physiologic effects of pneumoperitoneum in the morbidly obese. *Ann Surg*. 2005;241(2):219-226. doi:10.1097/01.sla.0000151791.93571.70

9. Nyerges. Pain Mechanisms in Laparoscopic Surgery. *Semin Laparosc Surg*. 1994;1(4):215-218. doi:10.1053/SLAS00100215

10. Vlot J, Wijnen R, Stolker RJ, Bax K. Optimizing working space in porcine laparoscopy: CT measurement of the effects of intra-abdominal pressure. *Surg Endosc*. 2013;27(5):1668-1673. doi:10.1007/s00464-012-2654-0

11. Bagnoli P, Vismara R, Fiore GB, Costantino ML. A mechanical model lung for hydraulic testing of total liquid ventilation circuits. *Int J Artif Organs*. 2005;28(12):1232-1241. doi:10.1177/039139880502801207

12. Chase JG, Yuta T, Mulligan KJ, Shaw GM, Horn B. A novel mechanical lung model of pulmonary diseases to assist with teaching and training. *BMC Pulm Med*. 2006;6(1):21. doi:10.1186/1471-2466-6-21

13. Mešić S, Babuška R, Hoogsteden HC, Verbraak AFM. Computer-controlled mechanical

simulation of the artificially ventilated human respiratory system. *IEEE Trans Biomed Eng*. 2003;50(6):731-743. doi:10.1109/TBME.2003.812166

14. Verbraak AFM, Beneken JEW, Bogaard JM, Versprille A. Computer-controlled mechanical lung model for application in pulmonary function studies. *Med Biol Eng Comput*. 1995;33(6):776-783. doi:10.1007/BF02523009

15. Verbraak AFM, Rijnbeek PR, Beneken JEW, Bogaard JM, Versprille A. A new approach to mechanical simulation of lung behaviour: Pressure-controlled and time-related piston movement. *Med Biol Eng Comput*. 2001;39(1):82-89. doi:10.1007/BF02345270

16. Cappa P, Sciuto SA, Silvestri S. A novel preterm respiratory mechanics active simulator to test the performances of neonatal pulmonary ventilators. *Rev Sci Instrum*. 2002;73(6):2411. doi:10.1063/1.1480453

17. Ngo C, Schlözer R, Vollmer T, Winter S, Misgeld B, Leonhardt S. A simulative model approach of cardiopulmonary interaction. In: *IFMBE Proceedings*. Vol 51. Springer Verlag; 2015:1679-1682. doi:10.1007/978-3-319-19387-8_408

18. Meka V V., van Oostrom JH. Bellows-less lung system for the human patient simulator. *Med Biol Eng Comput*. 2004;42(3):413-418. doi:10.1007/BF02344718

19. Silva PL, Pelosi P, Rocco PRM. Optimal mechanical ventilation strategies to minimize ventilator-induced lung injury in non-injured and injured lungs. *Expert Rev Respir Med*. 2016;10(12):1243-1245. doi:10.1080/17476348.2016.1251842

20. Hess DR, Medoff BD, Fessler MB. Pulmonary mechanics and graphics during positive pressure ventilation. *Int Anesthesiol Clin*. 1999;37(3):15-34. doi:10.1097/00004311-199903730-00005

21. Hess DR. Respiratory mechanics in mechanically ventilated patients. *Respir Care*. 2014;59(11):1773-1794. doi:10.4187/respcare.03410

22. Ball L, Costantino F, Fiorito M, Amodio S, Pelosi P. Respiratory mechanics during general anaesthesia. *Ann Transl Med*. 2018;6(19):379-379. doi:10.21037/atm.2018.09.50

23. Marieb EN, Hoehn K. The Respiratory System. In: *Human Anatomy & Physiology*. Vol 61. 9th ed. Pearson; 1999:801-848. doi:10.2307/4450703

24. Hoffman M. Lungs (Human Anatomy): Picture, Function, Definition, Conditions. https://www.webmd.com/lung/picture-of-the-lungs. Accessed February 4, 2021.

25. Mead J. *Mechanical Properties of Lungs*.; 1961.

26. Respiratory system | the lung association. https://www.lung.ca/lung-health/lung-info/respiratory-system. Accessed February 4, 2021.

27. Charalampidis C, Youroukou A, Lazaridis G, et al. Pleura space anatomy. *J Thorac Dis*. 2015;7(Suppl 1):S27-32. doi:10.3978/j.issn.2072-1439.2015.01.48

28. Mechanics of Ventilation | SEER Training. https://training.seer.cancer.gov/anatomy/respiratory/mechanics.html. Accessed February 4, 2021.

29. Levine IN. Thermodynamics. In: *Physical Chemistry*. 6th ed. McGraw-Hill; 2009:10-17.

http://mkimia.fst.unair.ac.id/wp-content/uploads/2018/04/Ira-Levine-Physical-Chemistry-6th-edition-McGraw-Hill-Science_Engineering_Math-2008.pdf. Accessed February 4, 2021.

30. Severgnini P, Selmo G, Lanza C, et al. Protective mechanical ventilation during general anesthesia for open abdominal surgery improves postoperative pulmonary function. *Anesthesiology*. 2013;118(6):1307-1321. doi:10.1097/ALN.0b013e31829102de

31. Hedenstierna G, Edmark L. The effects of anesthesia and muscle paralysis on the respiratory system. *Intensive Care Med*. 2005;31(10):1327-1335. doi:10.1007/s00134-005-2761-7

32. Hans GA, Sottiaux TM, Lamy ML, Joris JL. Ventilatory management during routine general anaesthesia. *Eur J Anaesthesiol*. 2009;26(1):1-8. doi:10.1097/EJA.0b000e000000f1fb

33. Potchileev I, Doroshenko M, Mohammed AN. *Positive Pressure Ventilation*. StatPearls Publishing; 2020. http://www.ncbi.nlm.nih.gov/pubmed/32809751. Accessed February 5, 2021.

34. Jackson C. Mechanical Ventilation: Background, Classifications of Positive-Pressure Ventilators, Indications for Mechanical Ventilation. https://emedicine.medscape.com/article/304068-overview#a1. Published September 15, 2020. Accessed February 5, 2021.

35. Corrado A, Gorini M. Negative-pressure ventilation: Is there still a role? *Eur Respir J*. 2002;20(1):187-197. doi:10.1183/09031936.02.00302602

36. Slutsky A. History of Mechanical Ventilation: From Vesalius to Ventilator-induced Lung Injury. *Am J Respir Crit Care Med*. 2015;191(10):1106-1115. doi:10.1164/rccm.201503-0421PP

37. Bajwa SJS, Kulshrestha A. Anaesthesia for laparoscopic surgery: General vs regional anaesthesia. *J Minim Access Surg*. 2016;12(1):4-9. doi:10.4103/0972-9941.169952

38. Belani K. Pelvic laparoscopy - Clinical Pain Advisor. https://www.clinicalpainadvisor.com/home/decision-support-in-medicine/anesthesiology/pelvic-laparoscopy/. Accessed February 5, 2021.

39. Isamade E, Agbo D, Sagay A, Musa J, Egbodo C, Agbo D. Non-intubated Ambulatory Anaesthesia for Diagnostic gynaecological laparoscopy. *J West African Coll Surg*. 2013;3(1):14-24. http://www.ncbi.nlm.nih.gov/pubmed/25453009. Accessed February 5, 2021.

40. Ventilator-Associated Pneumonia | Saint Luke's Health System. https://www.saintlukeskc.org/health-library/ventilator-associated-pneumonia. Accessed February 5, 2021.

41. Patel B. Overview of Mechanical Ventilation - Critical Care Medicine - MSD Manual Professional Edition. https://www.msdmanuals.com/professional/critical-care-medicine/respiratory-failure-and-mechanical-ventilation/overview-of-mechanical-ventilation. Published March 2020. Accessed February 8, 2021.

42. Gertler R. Mechanical ventilation during anesthesia in adults - UpToDate. Wolters Kluwer. https://www.uptodate.com/contents/mechanical-ventilation-during-anesthesia-in-adults/print. Published January 27, 2021. Accessed February 8, 2021.

43. Bauman KA, Hyzy RC. *Volume-Controlled Mechanical Ventilation*. Vol 1. Oxford University Press; 2016. doi:10.1093/med/9780199600830.003.0095

44. Gertler R, Joshi GP. Modern understanding of intraoperative mechanical ventilation in normal and diseased lungs. *Adv Anesth*. 2010;28(1):15-33. doi:10.1016/j.aan.2010.07.002

45. Ball L, Dameri M, Pelosi P. Modes of mechanical ventilation for the operating room. *Best Pract Res Clin Anaesthesiol*. 2015;29(3):285-299. doi:10.1016/j.bpa.2015.08.003

46. Sembroski E, Sanghavi D, Bhardwaj A. *Inverse Ratio Ventilation*. StatPearls Publishing; 2020. http://www.ncbi.nlm.nih.gov/pubmed/30571016. Accessed February 13, 2021.

47. Acosta P, Santisbon E, Varon J. "The Use of Positive End-Expiratory Pressure in Mechanical Ventilation." *Crit Care Clin*. 2007;23(2):251-261. doi:10.1016/j.ccc.2006.12.012

48. Silva PL, Rocco PRM. The basics of respiratory mechanics: ventilator-derived parameters. *Ann Transl Med*. 2018;6(19):376-376. doi:10.21037/atm.2018.06.06

49. Rossi A, Polese G, Brandi G, Conti G. Intrinsic positive end-expiratory pressure (PEEPi). *Intensive Care Med*. 1995;21(6):522-536. doi:10.1007/BF01706208

50. Caramez MP, Borges JB, Tucci MR, et al. Paradoxical responses to positive end-expiratory pressure in patients with airway obstruction during controlled ventilation*. *Crit Care Med*. 2005;33(7):1519-1528. doi:10.1097/01.CCM.0000168044.98844.30

51. Manzano F, Fernández-Mondéjar E, Colmenero M, et al. Positive-end expiratory pressure reduces incidence of ventilator-associated pneumonia in nonhypoxemic patients. *Crit Care Med*. 2008;36(8):2225-2231. doi:10.1097/CCM.0b013e31817b8a92

52. Jackson C. What is positive end-expiratory pressure (PEEP) therapy and how is it used with mechanical ventilation? https://www.medscape.com/answers/304068-104783/what-is-positive-end-expiratory-pressure-peep-therapy-and-how-is-it-used-with-mechanical-ventilation. Accessed February 13, 2021.

53. Sivieri EM, Dysart K, Abbasi S. Evaluation of Pulmonary Function in the Neonate. In: *Fetal and Neonatal Physiology*. Elsevier; 2017:754-765.e3. doi:10.1016/b978-0-323-35214-7.00074-3

54. Turner MJ, MacLeod IM, Rothberg AD. Effects of temperature and composition on the viscosity of respiratory gases. *J Appl Physiol*. 1989;67(1):472-477. doi:10.1152/jappl.1989.67.1.472

55. Sanborn WG, Tyco B/. *Applied Respiratory Physiology: Use of Ventilator Waveforms and Mechanics in the Management of Critically Ill Patients*. Vol 50.

56. Mendelson Y. Biomedical Sensors. In: *Introduction to Biomedical Engineering*. Elsevier Inc.; 2011:609-666. doi:10.1016/B978-0-12-374979-6.00010-1

57. Lucangelo U, Bernabè F, Blanch L. Lung mechanics at the bedside: make it simple. *Curr Opin Crit Care*. 2007;13(1):64-72. doi:10.1097/MCC.0b013e32801162df

58. Benditt JO. Esophageal and Gastric Pressure Measurements. *Respir Care*. 2005;50(1).

59. Mauri T, Yoshida T, Bellani G, et al. Esophageal and transpulmonary pressure in the clinical setting: meaning, usefulness and perspectives. *Intensive Care Med*. 2016;42(9):1360-1373. doi:10.1007/s00134-016-4400-x

60. MILIC-EMILI J, MEAD J, TURNER JM. TOPOGRAPHY OF ESOPHAGEAL PRESSURE AS A FUNCTION OF POSTURE IN MAN. *J Appl Physiol*. 1964;19:212-216. doi:10.1152/jappl.1964.19.2.212

61. MEAD J, McILROY MB, SELVERSTONE NJ, KRIETE BC. Measurement of intraesophageal pressure. *J Appl Physiol*. 1955;7(5):491-495. doi:10.1152/jappl.1955.7.5.491

62. Esophageal Catheter-Balloon used in Adults | Download Scientific Diagram. https://www.researchgate.net/figure/Esophageal-Catheter-Balloon-used-in-Adults_fig1_26431889. Accessed February 16, 2021.

63. Williams EC, Motta-Ribeiro GC, Melo MFV. Driving Pressure and Transpulmonary Pressure: How Do We Guide Safe Mechanical Ventilation? *Anesthesiology*. 2019;131(1):155-163. doi:10.1097/ALN.0000000000002731

64. Amato MBP, Meade MO, Slutsky AS, et al. Driving Pressure and Survival in the Acute Respiratory Distress Syndrome. *N Engl J Med*. 2015;372(8):747-755. doi:10.1056/nejmsa1410639

65. Gattinoni L, Pesenti A, Avalli L, Rossi F, Bombino M. Pressure-volume curve of total respiratory system in acute respiratory failure. Computed tomographic scan study. *Am Rev Respir Dis*. 1987;136(3):730-736. doi:10.1164/ajrccm/136.3.730

66. Neto AS, Hemmes SNT, Barbas CSV, et al. Association between driving pressure and development of postoperative pulmonary complications in patients undergoing mechanical ventilation for general anaesthesia: A meta-analysis of individual patient data. *Lancet Respir Med*. 2016;4(4):272-280. doi:10.1016/S2213-2600(16)00057-6

67. Ladha K, Melo MFV, McLean DJ, et al. Intraoperative protective mechanical ventilation and risk of postoperative respiratory complications: Hospital based registry study. *BMJ*. 2015;351. doi:10.1136/bmj.h3646

68. Protti A, Andreis DT, Monti M, et al. Lung stress and strain during mechanical ventilation: Any difference between statics and dynamics? *Crit Care Med*. 2013;41(4):1046-1055. doi:10.1097/CCM.0b013e31827417a6

69. Loring SH, Topulos GP, Hubmayr RD. Transpulmonary pressure: The importance of precise definitions and limiting assumptions. *Am J Respir Crit Care Med*. 2016;194(12):1452-1457. doi:10.1164/rccm.201512-2448CP

70. Mead J, Takishima T, Leith D. Stress distribution in lungs: a model of pulmonary elasticity. *J Appl Physiol*. 1970;28(5):596-608. doi:10.1152/jappl.1970.28.5.596

71. Chiumello D, Carlesso E, Cadringher P, et al. Lung stress and strain during mechanical ventilation for acute respiratory distress syndrome. *Am J Respir Crit Care Med*. 2008;178(4):346-355. doi:10.1164/rccm.200710-1589OC

72. Sharma KC, Brandstetter RD, Brensilver JM, Jung LD. Cardiopulmonary physiology and pathophysiology as a consequence of laparoscopic surgery. *Chest*. 1996;110(3):810-815. doi:10.1378/chest.110.3.810

73. Mazzinari G, Diaz-Cambronero O, Alonso-Iñigo JM, et al. Intraabdominal pressure targeted positive end-expiratory pressure during laparoscopic surgery: An open-label, nonrandomized, crossover, clinical trial. *Anesthesiology*. 2020;132(4):667-677. doi:10.1097/ALN.0000000000003146

74. Andersson LE, Bååth M, Thörne A, Aspelin P, Odeberg-Wernerman S. Effect of carbon dioxide pneumoperitoneum on development of atelectasis during anesthesia, examined by spiral

computed tomography. *Anesthesiology*. 2005;102(2):293-299. doi:10.1097/00000542-200502000-00009

75. Gurusamy KS, Vaughan J, Davidson BR. Low pressure versus standard pressure pneumoperitoneum in laparoscopic cholecystectomy. *Cochrane Database Syst Rev*. 2014;2014(3). doi:10.1002/14651858.CD006930.pub3

76. Simonneau G, Vivien A, Sartene R, et al. Diaphragm dysfunction induced by upper abdominal surgery. Role of postoperative pain. *Am Rev Respir Dis*. 1983;128(5):899-903. doi:10.1097/00132586-198512000-00026

77. Pelosi P, Quintel M, Malbrain MLNG. Effect of intra-abdominal pressure on respiratory mechanics. In: *Acta Clinica Belgica*. Vol 62. Acta Clinica Belgica; 2007:78-88. doi:10.1179/acb.2007.62.s1.011

78. Valenza F, Chevallard G, Fossali T, Salice V, Pizzocri M, Gattinoni L. Management of mechanical ventilation during laparoscopic surgery. *Best Pract Res Clin Anaesthesiol*. 2010;24(2):227-241. doi:10.1016/j.bpa.2010.02.002

79. Puri GD, Singh H. Ventilatory effects of laparoscopy under general anaesthesia. *Br J Anaesth*. 1992;68(2):211-213. doi:10.1093/bja/68.2.211

80. Malbrain MLNG, Roberts DJ, De Laet I, et al. The role of abdominal compliance, the neglected parameter in critically ill patients - A consensus review of 16. Part 1: Definitions and pathophysiology. *Anaesthesiol Intensive Ther*. 2014;46(5):392-405. doi:10.5603/AIT.2014.0062

81. Navajas D, Farré R. Oscillatory Mechanics. In: *Mechanics of Breathing*. Springer Milan; 2002:146-156. doi:10.1007/978-88-470-2916-3_12

82. Kaczka DW, Dellacá RL. Oscillation mechanics of the respiratory system: Applications to lung disease. *Crit Rev Biomed Eng*. 2011;39(4):337-359. doi:10.1615/CritRevBiomedEng.v39.i4.60

83. Dellaca' RL. Measurement of Respiratory System Impedances. In: *Mechanics of Breathing*. Springer Milan; 2002:157-171. doi:10.1007/978-88-470-2916-3_13

84. Lauzon A, T Bates JH, T Bates JF. *Estimation of Time-Varying Respiratory Mechanical Parameters by Recursive Least Squares*. Vol 71.; 1991.

85. Shukla SK, Talpin JP. *Synthesis of Embedded Software: Frameworks and Methodologies for Correctness by Construction*. Springer US; 2010. doi:10.1007/978-1-4419-6400-7

86. Barnas GM, Yoshino K, Stamenovic D, Kikuchi Y, Loring SH, Mead J. Chest wall impedance partitioned into rib cage and diaphragm-abdominal pathways. *J Appl Physiol*. 1989;66(1):350-359. doi:10.1152/jappl.1989.66.1.350

87. Carvalho AR, Zin WA. Respiratory system dynamical mechanical properties: Modeling in time and frequency domain. *Biophys Rev*. 2011;3(2):71-84. doi:10.1007/s12551-011-0048-5

88. Lorino AM, Lorino H, Harf A. A synthesis of the Otis, Mead, and Mount mechanical respiratory models. *Respir Physiol*. 1994;97(2):123-133. doi:10.1016/0034-5687(94)90020-5

89. Paštěka R, Forjan M. Actively breathing mechanical lung simulator development and preliminary measurements. In: *IFMBE Proceedings*. Vol 65. Springer Verlag; 2017:751-754. doi:10.1007/978-981-10-5122-7_188

90. Baldoli I, Cuttano A, Scaramuzzo RT, et al. A novel simulator for mechanical ventilation in newborns: MEchatronic REspiratory System SImulator for Neonatal Applications. *Proc Inst Mech Eng Part H J Eng Med*. 2015;229(8):581-591. doi:10.1177/0954411915593572

91. Rosenbaum A, Kirby C, Breen PH. New metabolic lung simulator: Development, description, and validation. *J Clin Monit Comput*. 2007;21(2):71-82. doi:10.1007/s10877-006-9058-4

92. Coropechi IC, Indre AI, Moa F, Vasile A. Mechanical test lung simulation device. In: *2020 8th E-Health and Bioengineering Conference, EHB 2020*. Institute of Electrical and Electronics Engineers Inc.; 2020. doi:10.1109/EHB50910.2020.9280171

93. Regli A, Hockings LE, Musk GC, et al. Commonly applied positive end-expiratory pressures do not prevent functional residual capacity decline in the setting of intra-abdominal hypertension: A pig model. *Crit Care*. 2010;14(4):R128. doi:10.1186/cc9095

94. Huntington CR, Prince J, Hazelbaker K, et al. Safety first: significant risk of air embolism in laparoscopic gasketless insufflation systems. *Surg Endosc*. 2019;33(12):3964-3969. doi:10.1007/s00464-019-06683-4

95. BARDOCZKY GI, ENGELMAN E, LEVARLET M, SIMON P. Ventilatory effects of pneumoperitoneum monitored with continuous spirometry. *Anaesthesia*. 1993;48(4):309-311. doi:10.1111/j.1365-2044.1993.tb06949.x

96. Futier E, Constantin J-M, Paugam-Burtz C, et al. A Trial of Intraoperative Low-Tidal-Volume Ventilation in Abdominal Surgery. *N Engl J Med*. 2013;369(5):428-437. doi:10.1056/NEJMoa1301082

97. Lellouche F, Dionne S, Simard S, Bussières J, Dagenais F. High tidal volumes in mechanically ventilated patients increase organ dysfunction after cardiac surgery. *Anesthesiology*. 2012;116(5):1072-1082. doi:10.1097/ALN.0b013e3182522df5

98. Gajic O, Frutos-Vivar F, Esteban A, Hubmayr RD, Anzueto A. Ventilator settings as a risk factor for acute respiratory distress syndrome in mechanically ventilated patients. *Intensive Care Med*. 2005;31(7):922-926. doi:10.1007/s00134-005-2625-1

99. Carvalho AR, Zin WA. Respiratory system dynamical mechanical properties: Modeling in time and frequency domain. *Biophys Rev*. 2011;3(2):71-84. doi:10.1007/s12551-011-0048-5

APPENDICES

Appendix A

A.1 Respiratory Analysis – MATLAB Code

```
clc; clear all; close all;
```

Selection of the data file

```
[file,path] = uigetfile; %Data Selection
addpath(path);
load(file);
```

Generation of the time vector

```
dt=1/fsample;
mintidaltime = 1.8;
t = linspace(0,length(flowAirway)*dt,length(flowAirway));

IAP = Trial_p_mean;
```

Data Viewer

```
figure(1) %Visualization of the data
pa=subplot(3,2,1);
plot(t,pressureAirway)
title('Airway pressure vs time')
xlabel('Time [s]')
ylabel('Pressure [hPa]')
set(gca,'FontSize',13)

pt=subplot(3,2,2);
plot(t,pressureTrocar)
title('Trocar pressure vs time')
xlabel('Time [s]')
ylabel('Pressure [hPa]')
set(gca,'FontSize',13)

fa=subplot(3,2,3);
plot(t,flowAirway)
title('Airway flow vs time')
xlabel('Time [s]')
ylabel('Flow [L/s]')
```

```
set(gca,'FontSize',13)

ft=subplot(3,2,4);
plot(t,flowTrocar)
title('Trocar flow vs time')
xlabel('Time [s]')
ylabel('Flow [L/s]')
set(gca,'FontSize',13)

pe=subplot(3,2,5);
plot(t,pressureEsophagus)
title('Esophageal pressure vs time')
xlabel('Time [s]')
ylabel('Pressure [hPa]')
set(gca,'FontSize',13)

linkaxes([pa,pt,pe,fa,ft],'x')
```

Selection of the data section

```
if IAP==5
    [x5,y5]=ginput(2);

    check=isfile('sections.mat');
       if check==1
           save('sections','x5','-append')
       else
           save('sections','x5');
       end

else if IAP==8
        [x8,y8]=ginput(2);

        check=isfile('sections.mat');
            if check==1
                save('sections','x8','-append')
            else
                save('sections','x8');
            end


    else if IAP==10
            [x10,y10]=ginput(2);

            check=isfile('sections.mat');
                if check==1
                    save('sections','x10','-append')
                else
                    save('sections','x10');
                end

        else if IAP==12
                [x12,y12]=ginput(2);

                check=isfile('sections.mat');
                    if check==1
                        save('sections','x12','-append')
```

```
                    else
                        save('sections','x12');
                    end

            else if IAP==14
                    [x14,y14]=ginput(2);

                    check=isfile('sections.mat');
                        if check==1
                            save('sections','x14','-append')
                        else
                            save('sections','x14');
                        end

                else if IAP==16
                        [x16,y16]=ginput(2);

                        check=isfile('sections.mat');
                            if check==1
                                save('sections','x16','-append')
                            else
                                save('sections','x16');
                            end

                    else if IAP==18
                            [x18,y18]=ginput(2);

                            check=isfile('sections.mat');
                                if check==1
                                    save('sections','x18','-append')
                                else
                                    save('sections','x18');
                                end

                        else if IAP==20
                                [x20,y20]=ginput(2);

                                check=isfile('sections.mat');
                                    if check==1
                                        save('sections','x20','-append')
                                    else
                                        save('sections','x20');
                                    end
                            end
                        end
                    end
                end
            end
        end
    end
end
```

Loading of the selected section

```
load('sections.mat')

if IAP==5
```

```
    section_all=(round((x5(1)/dt)):round((x5(2)/dt)));
else if IAP==8
        section_all=(round((x8(1)/dt)):round((x8(2)/dt)));
    else if IAP==10
            section_all=(round((x10(1)/dt)):round((x10(2)/dt)));
        else if IAP==12
                section_all=(round((x12(1)/dt)):round((x12(2)/dt)));
            else if IAP==14
                    section_all=(round((x14(1)/dt)):round((x14(2)/dt)));
                else if IAP==16
                        section_all=(round((x16(1)/dt)):round...
                            ((x16(2)/dt)));
                    else if IAP==18
                            section_all=(round((x18(1)/dt)):round...
                                ((x18(2)/dt)));
                        else if IAP==20
                                section_all=(round((x20(1)/dt)):round...
                                    ((x20(2)/dt)));
                            end
                        end
                    end
                end
            end
        end
    end
end

[Breath_start,locset_all] = findpeaks(-cumsum(flowAirway(section_all)),...
    'MinPeakDistance'...
                        ,mintidaltime/dt);

prompt = 'Enter the number of breaths:  ';
b = input(prompt);

locset=locset_all(end-b:end);

section=section_all(locset(1)):1:section_all(locset(end));
```

Plotting of flow at the airway and the trocar

```
figure(2)
fa = subplot(2,1,1);
plot(t(section),flowAirway(section))
title('Airway flow vs Time')
ylabel('Airway flow [L/s]')
xlabel('Time [s]')
title('Airway flow vs Time')
set(gca,'FontSize',13)


ft = subplot(2,1,2);
plot(t(section),flowTrocar(section))
title('Trocar flow vs Time')
ylabel('Trocar flow [L/s]')
xlabel('Time [s]')
title('Trocar flow vs Time')
set(gca,'FontSize',13)
```

```
linkaxes([fa,ft],'x')
```

Flow Integration and volume drift correction

```
volumeAirway_drift=cumsum((flowAirway(section))*dt); %Numeric integration
                                                     %to calculate volume

volumeAirway=detrend(volumeAirway_drift); %Performs a linear fit to volume
                                          %and then removes the trend
drift=volumeAirway_drift-volumeAirway;    %Yields the computed trend line

volumeAirway=volumeAirway+abs(0-volumeAirway(1)); %Resulting volume starts
                                                  %at 0


volumeTrocar_drift=cumsum((flowTrocar(section))*dt);

volumeTrocar=detrend(volumeTrocar_drift);
drift=volumeTrocar_drift-volumeTrocar;

volumeTrocar=volumeTrocar-abs(0-volumeTrocar(1));


figure (3)
va = subplot(2,1,1);
plot(t(section),volumeAirway);hold on
ylabel('Airway Volume [L]')
xlabel('Time [s]')
title('Airway Volume vs Time')
set(gca,'FontSize',13)

vt = subplot(2,1,2);
plot(t(section),volumeTrocar);hold on
ylabel('Trocar Volume [L]')
xlabel('Time [s]')
title('Trocar Volume vs Time')
set(gca,'FontSize',13)

linkaxes([va,vt],'x')


[pksAirway,locsAirway]=findpeaks(volumeAirway,...
    'MinPeakDistance',mintidaltime/dt);
[pksTrocar,locsTrocar]=findpeaks(-volumeTrocar,...
    'MinPeakDistance',mintidaltime/dt);

timesAirway=section(locsAirway)*dt;
timesTrocar=section(locsTrocar)*dt;

va = subplot(2,1,1);
plot (timesAirway,pksAirway,'or');hold on

vt = subplot(2,1,2);
plot (timesTrocar,-pksTrocar,'or');
```

Estimation of the pressure peaks, transpulmonary pressure and P_{peak}-PEEP

```
[pawpks,locspawpks]=findpeaks(pressureAirway(section),...
    'MinPeakDistance',mintidaltime/dt);
timespawpks=section(locspawpks)*dt;

[pespks,locspespks]=findpeaks(pressureEsophagus(section),...
    'MinPeakDistance',mintidaltime/dt);

timespespks=section(locspespks)*dt;

figure(4)
paw=subplot(2,1,1);
plot(t(section),pressureAirway(section));
hold on
plot(timespawpks,pawpks,'or');
ylabel('Airway Pressure [hPa]')
xlabel('Time [s]')
title('Airway Pressure vs Time')
set(gca,'FontSize',13)

pes=subplot(2,1,2);
plot(t(section),pressureEsophagus(section));
hold on
plot(timespespks,pespks,'or');
ylabel('Esophageal Pressure [hPa]')
xlabel('Time [s]')
title('Esophageal Pressure vs Time')
set(gca,'FontSize',13)

TranspulmonaryP=pawpks-pespks;

DeltaP=pawpks-Trial_p_mean;
```

Calculation of Δt, tidal time and storage of the IAP value

```
Vtidal = pksAirway; % Tidal volume
Vab = -pksTrocar ;  % Abdominal volume

delta_t = timesTrocar'-timesAirway'; % Time difference

tTidal=zeros((length(locset)-1),1); % Time needed for each breath
for i=1:length(locset)-1
    tTidal(i,1)=section_all(locset(i+1))*dt-section_all(locset(i))*dt;
end
tTidal;

iap=zeros(length(locset)-1,1);
iap(:,1)=Trial_p_mean; % IAP

experiment=zeros(length(locset)-1,1);
experiment(:,1)=Experiment_number; % Experiment number



breathCount=zeros(length(locset)-1,1); % Breath count
```

```
for i=1:length(locset)-1
    breathCount(i,1)=i;
end
breathCount;
```

Plotting of the time signals of pressure, flow and volume

```
figure(5)
ax1 = subplot(3,1,1);
plot(t(section),pressureAirway(section));hold on
title('Airway pressure vs time')
ylabel('Airway pressure [hPa]')
xlabel('Time [s]')
set(gca,'FontSize',13)

ax2 = subplot(3,1,2);
plot(t(section),flowAirway(section));
title('Airway flow vs time')
ylabel('Airway flow [L/s]')
xlabel('Time [s]')
set(gca,'FontSize',13)

ax3 = subplot(3,1,3);
plot(t(section),volumeAirway); % Numeric integration
title('Tidal volume vs time')
ylabel('Volume [L]')
xlabel('Time [s]')
set(gca,'FontSize',13);hold on
```

Estimation of the predicted pressure(Y_est), resistance, elastance and mean square error

The for loop calculates the Y_est and A_est for each breath. The if condition was added to make sure that there are no overlapping samples when shifting to the next breath.

```
Y=zeros(length(section),1);
A_est=zeros((length(locset)-1),3);
Y_est=zeros(length(section),1);
Err=zeros((length(locset)-1),1);

for i=1:length(locset)-1

    if i==1                              %section of the first breath
        s = locset(i): 1 :locset(i+1);   %is from locset(1) up to locset(2)
        section_breath=section(1,i:length(s));

        y = pressureAirway(section_breath);  % Y, pressure as output
        X = [ones(length(t(section_breath)),1)... % Ones to estimate P0
        (flowAirway(section_breath))...           % Flow
        cumsum((flowAirway(section_breath))*dt)]; % Volume

        P       = inv(X'*X);
```

```
        a_est   = P * X' * y; % Linear algebra for LSQ approach
        y_est   = X * a_est;  % Estimated P from model

        A_est(i,:)=a_est; % A_est gives [PO Resistance Elastance].
                          % Each row  corresponds to the values
                          % for one breath

        Y(1:length(section_breath))=y;
        Y_est(1:length(section_breath))=y_est;

        err = sum((y-y_est).^2)/length(section_breath); %mean squared error
        Err(i)=err;

     else
        s_old=locset(1):1:locset(i);  %section of each following breath (i)
        s=(locset(i)+1): 1 :locset(i+1); % is from locset(i)+1 up to
                                         %locset(i+1)

        section_breath=section(1,(length(s_old)+1):length(s_old)+length(s));


        y = pressureAirway(section_breath);
        X = [ones(length(t(section_breath)),1)...
        (flowAirway(section_breath))...
        cumsum((flowAirway(section_breath))*dt)];


        P       = inv(X'*X);
        a_est   = P * X' * y;
        y_est   = X * a_est;

        A_est(i,:)=a_est;

        Y((length(s_old)+1):length(s_old)+length(s))=y;
        Y_est((length(s_old)+1):length(s_old)+length(s))=y_est;

        err     = sum((y-y_est).^2)/length(section_breath);
        Err(i)=err;

    end
end



        R       = A_est(:,2) ;                          % Resistance
        E       = A_est(:,3)  ;                         % Elastance
        Err     = Err;                                  %MSE
```

Visualization of the predicted pressure

```
figure(5)
ax1 = subplot(3,1,1);
plot(t(section),Y_est);hold on
legend('Measured','Estimated')
linkaxes([ax1,ax2,ax3],'x')
hold off
```

Storage of the results to a separate file

```
nameV=['ResultsVolume' num2str(IAP) '_Exp' num2str(Experiment_number)];
V.(nameV) = [experiment,iap,breathCount,Vtidal,tTidal,delta_t,Vab,...
    pawpks,pespks,DeltaP,TranspulmonaryP];

check=isfile('ResultsAnimal_Vent.mat');
if check==1
save('Results', '-struct', 'V','-append');
else
save('Results', '-struct', 'V');
end

nameP=['ResultsParameters' num2str(IAP) '_Exp' num2str(Experiment_number)];
Par.(nameP)  =[experiment,iap,breathCount,R,E,Err];
save('Results', '-struct', 'Par','-append');
```

Published with MATLAB® R2019b

A.2 Abdominal Analysis – MATLAB Code

```
close all; clear all; clc;

load('Impedance_FOT_20190907000005-T2_20,0hPa_UP.mat')  %Load the data file

freqstim=[0.5 1 2 3 5];
omegastim=2*pi*freqstim;
C_exp=C_exp(1:5);     % remove the 10hz and 15hz frequencies
Z_exp=Z_exp(1:5);     % remove the 10hz and 15hz frequencies

figure(1)
ax1=subplot(1,2,1);
plot(freqstim,real(Z_exp),'xr','MarkerSize',14)
xlim([0 6])
ylim([0 11])
title('Resistance')
xlabel('Frequency [Hz]')
ylabel('Resistance R [cmH_{2}O/s/L]')
set(gca,'FontSize',13)
set(gca,'box','off')
axis square
hold on;

ax2=subplot(1,2,2);
plot(freqstim,imag(Z_exp),'xr','MarkerSize',14)
xlim([0 6])
ylim([-4 7])
title('Reactance')
xlabel('Frequency [Hz]')
ylabel('Reactance X [cmH_{2}O/s/L]')
```

```
set(gca,'FontSize',13)
set(gca,'box','off')
axis square
hold on;

par0=[4.8 0.25 0.015 ];
```

Calling of the RIC model and least-squares method functions to estimate the resistance, inertance and compliance

```
Z_err           = @(par_Z)Z_RIC_err(par_Z,omegastim,transpose(Z_exp))
[par_z err_Z]   = fminsearch(Z_err,par0) %Finds the parameters that
                                        %minimize Zerr

Z_est=feval(@Z_RIC,par_z,omegastim);    %Returns the impedance estimation
                                        %for which the error is minimized

figure(1)
ax1=subplot(1,2,1);
plot(freqstim,real(Z_est),'--k')
legend('Measured','Prediction')

ax2;subplot(1,2,2)
plot(freqstim,imag(Z_est),'--k')
legend('Measured','Prediction')

RIC=par_z;
error=err_Z;

nameV=['RIC' num2str(20)];
V.(nameV) = [par_z];

check=isfile('ResultsAnimal_Insuf.mat');
if check==1
save('Results', '-struct', 'V','-append');
else
save('Results', '-struct', 'V');
end

nameP=['error' num2str(20)];
Par.(nameP) = [err_Z];

save('Results', '-struct', 'Par','-append');
```

Published with MATLAB® R2019b

A.2.1 Function of the RIC model

RIC model

```
function eval = Z_RIC(par,omega)

R = par(1); % Resistance
I = par(2); % Inductance
C = par(3); % Compliance

eval = R + (1i.*omega.*I) + (1./(1i.*omega.*C));
```

Published with MATLAB® R2019b

A.2.2 Function of the least-squares method (Z_err)

RIC model – Z_err

Par, omega and z should be a row vector

```
function eval = Z_RIC_err(par,omega,Z)

R = par(1); % Resistance
I = par(2); % Inductance
C = par(3); % Compliance

Z_err = Z - (R + (1i.*omega.*I) + (1./(1i.*omega.*C))); %Zerr=Zexp-Zest

eval = sum(sqrt(conj(Z_err).*Z_err)); %modulus of Zerr (complex number)
```

Published with MATLAB® R2019b

Appendix B

B.1 Paper

Development of an In Vitro Model for the Evaluation of a Surgical Insufflator

Author: Stergios Georgantas
Delft University of Technology, Department of Biomedical Engineering
Erasmus MC - Sophia Children's Hospital, Department of Pediatric Surgery

Abstract: Abdominal gas insufflation creates the necessary space for manipulation of the surgical instruments in laparoscopic surgery. However, it is known to disrupt the normal respiratory mechanics. A novel surgical insufflator, capable of performing individualized pressure adjustments, has been recently developed at Erasmus MC - Sophia Children's Hospital. The performance of this insufflator was evaluated in animal experiments. However, animal trials display certain disadvantages, such as limited repetitiveness, protocols that had to respect physiological limitations and ethical considerations. A mechanical in vitro model was developed for the assessment of surgical insufflators. The design requirements were based on a preliminary analysis, performed on data from animal experiments. Validation of the model was performed by implementing the model in the same setting as used in the animal experiments and by comparing the mechanical behavior of the model to the behavior obtained by the preliminary analysis. The developed model displayed a satisfactory capability of representing the respiratory-abdominal interaction and was a good proof-of-concept. Further improvements are recommended to increase performance and applicability.

Keywords: Laparoscopic surgery, abdominal insufflation, surgical insufflator, respiratory system, in vitro model, mechanical properties

1. Introduction

The first step in laparoscopic surgery is the creation of the pneumoperitoneum with pressurized insufflation of carbon dioxide gas. During abdominal insufflation, the intra-abdominal pressure (IAP) increases, distending the abdomen and increasing the intra-abdominal volume (IAV), creating the internal workspace to perform that is necessary to perform surgery. Maintaining a stable insufflation pressure is one of the greatest challenges in laparoscopy, as gas inevitably escapes through the trocar, which opens to accommodate the surgical instruments, or during surgical suctioning[1,2]. Conventional surgical insufflators respond to leakage and pressure loss by adjusting the pressure of the delivered gas[3]. However, such insufflation systems usually have a delay in their response[4,5]. Abrupt loss in the insufflation pressure leads to a reduction in the established abdominal workspace, prolonging the surgical time and increasing the risk of complications for the patient[1,2].

The stretching capacity of the abdomen is patient-dependent, which means that there is no universal pressure that can be utilized for the establishment of an optimal pneumoperitoneum for every patient [6]. The insufflation pressure is seldom adjusted by the surgeon, and is set without any quantitative assessment or feedback. To resolve these challenges faced by the conventional devices, a novel surgical insufflator has been developed at the department of Pediatric Surgery of Erasmus MC - Sophia Children's Hospital. This new device is enhanced with respect to conventional devices with the ability to maintain a stable pneumoperitoneum at an optimal, individualized pressure.

Recently, the performance of the novel insufflator has been assessed with animal experiments. Nevertheless, experimenting on animals is a difficult, time-consuming and expensive procedure due to the strict legislation and protocols, as well as the ethical considerations that need to be

addressed. The performance and effect of the insufflator on the respiratory function could be investigated with an in vitro simulator. Such models allow for a significantly faster and inexpensive testing procedure, higher flexibility and increased repeatability when compared to animal models[7].

Despite the variety of existing simulators for the respiratory system [8–14], there is currently no report in the literature of an in vitro model that combines and simulates the interaction between the respiratory system and the insufflated abdomen. The goal of this thesis is to develop an in vitro model that simulates the interaction between the respiratory system and the abdominal cavity during surgical insufflation. The model is intended for providing an evaluation platform for the performance of the newly developed surgical insufflator and obtaining broader knowledge of the effect of abdominal insufflation onto the respiratory mechanics. Additionally, it could be used for head-to-head comparison between different insufflators.

1.1 Respiratory Mechanics

Respiratory mechanics can be investigated by the measurement of pressure and flow as a means to express and assess the respiratory function. The airway pressure (P_{aw}), inspiratory flow ($\dot{V}_I$) and tidal volume (V_t) are the fundamental respiratory measurements during mechanical ventilation. P_{aw} and $\dot{V}_I$ are measured in the proximal airway of the patient, while V_t is calculated by integrating $\dot{V}_I$.

The airway pressure can be predicted mathematically by the equation of motion of the respiratory system, which relates it to $\dot{V}_I$ and V_t [15]:

$$P_{vent} + P_{mus} = E_{RS} \cdot V_t(t) + R_{aw} \cdot \dot{V}_I(t) + PEEP + PEEP_i + I \cdot \ddot{V}_I(t) \quad (1)$$

P_{vent} is the airway pressure that is applied by the mechanical ventilator, P_{mus} is the pressure created by the action of the inspiratory muscles of the patient, E_{RS} is the elastance of the respiratory system, V_t is the tidal volume, R_{aw} is the airway resistance, $PEEP$ is the extrinsic positive end-expiratory pressure applied by the ventilator, $PEEP_i$ is the intrinsic PEEP. The term indicating the inertia, I, due to acceleration of the air column, is assumed to be insignificant during normal quiet breathing and is, therefore, usually neglected [16]. In addition, since the breathing activity of the patient is completely suppressed during anesthesia, P_{mus} is disregarded as well.

The term $E_{RS} \cdot V_t(t)$ represents the pressure required to overcome the elastic forces of the respiratory system[15]. Since the elastance is defined as the inverse of the compliance, the term can be alternatively written as $V_t(t)/C_{RS}$, where C_{RS} is the compliance of the respiratory system. The term $R_{aw} \cdot \dot{V}_I(t)$ denotes the pressure that is required to overcome the frictional forces during the flow of gas across the airway [15].

E_{RS} (or C_{RS}) and R_{aw} are known as the dynamic properties of the respiratory system and can be estimated with a multiple linear regression analysis, such as linear least-squares fitting (LSF), to fit the equation of motion to the measured variables of P_{aw}, $\dot{V}_I$ and V_t [15,16]. This method assumes a linear single-compartment mathematical model, which does not take into account any changes in C_{RS} and R_{aw} within each breath. The LSF approach allows superimposing the pressure waveform predicted by the mathematical model onto the measured P_{aw}, enabling the assessment of the 'goodness of fit'[15].

1.2 Respiratory-Abdominal Interaction

During laparoscopy, the pressurized pneumoperitoneum exerts a direct mechanical effect on the respiratory system. Additionally, CO_2 absorption causes changes in the physiology of the patient; however, this effect is beyond the scope of this study. As the thoracic and abdominal compartment are linked by the diaphragm, the mechanical properties of the respiratory system and the overall respiratory function are dependent on the IAP level.

The rise in IAP obstructs the movement of the diaphragm during breathing and forces it to shift cranially [17,18]. The restricted movement of the diaphragm may decrease the tidal volume and functional residual capacity (FRC) [19,20]. In addition, the chest wall becomes stiffer at higher insufflation pressures [16,17]. As a result, the compliance of the respiratory system decreases due to a drop in the chest wall compliance (C_{CW}), while lung compliance (C_L) remains constant. Application of a PEEP by the mechanical ventilator ameliorates this effect by opposing the collapse of the alveoli and the reduction in V_t, while maintaining lung volume after expiration [17,21].

To counteract the reduction in Vt, volume-controlled ventilation (VCV) is often applied to maintain an adequate Vt and pulmonary gas exchange. Despite the beneficial effect of PEEP, the decrease in C_{RS} inevitably results in a rise in the peak inspiratory pressure (PIP) as well as the driving pressure (ΔP) [17]. The latter is applied to the entire respiratory system of the patient to achieve ventilation and represents the global strain in the lungs. Spikes in PIP and ΔP are related to the occurrence of major post-operative complications, such as edema and acute respiratory distress syndrome (ARDS) [22,23]. Consequently, this rise in the intrathoracic pressure eventually leads to an increase in the work of breathing [17,24].

1.3 Abdominal Mechanical Properties

During insufflation, the mechanical properties of the elastic boundaries of the abdominal cavity, such as the abdominal wall and diaphragm, determine the limits of abdominal distention[6]. Estimation of the abdominal mechanical behavior is of particular importance, as it is patient-dependent and defines the IAV-IAP relationship during surgical insufflation. The abdominal mechanical properties are expressed as the abdominal compliance (C_{ab}). This represents a measure of the ease of abdominal distention, and depends on the elasticity of the abdominal wall as well as the diaphragm [6,25]. By definition, the abdominal compliance is the ratio of the change in the IAV over the change in IAP and is expressed in L/cmH_2O:

$$C_{ab} = \frac{\Delta(IAV)}{\Delta(IAP)} \quad (2)$$

A minimally invasive approach for estimating C_{ab} is the application of the Forced Oscillation Technique (FOT), which has been extensively used for the assessment of the mechanical behavior of the respiratory system [26,27]. FOT involves the application of an oscillating low-amplitude external pressure signal in a sequential oscillation frequency range, and the measurement of the generated flow [26]. The mechanical properties of the abdominal wall are derived from the relationship between the externally applied oscillatory pressure (input) and the resulting oscillatory flow (output).

The complex ratio between the stimulating pressure (P) and the generated oscillatory flow ($\dot{V}$) as a function of the oscillatory frequency (ω) defines the mechanical impedance (Z)[27] :

$$Z = \frac{P(\omega)}{\dot{V}(\omega)} \quad (3)$$

$Z(\omega)$ arises from the resistive, inertial and elastic contributions of the abdomen and can be expressed by separating its resistive (R) and reactive (X) components [27]:

$$Z(\omega) = R(\omega) + jX(\omega) \quad (4)$$

The resistance R is related to energy dissipation, while the reactance X is associated with energy storage.

Once $Z(\omega)$ is estimated, the acquired impedance data are fitted onto mathematical models that define the relationship between parameters of known physiological meaning and the impedance[28]. With this method the mechanical properties specific to the abdomen can be quantified by identifying the parameters of the model. A commonly utilized model is the RIC model, which represents the abdomen as a combination of resistance R, inertance I and compliance C in series [26]. Thus, the RIC model expresses Z as[27] :

$$Z(\omega) = R + j\omega I + \frac{1}{j\omega C} \quad (5)$$

Estimation of the RIC model parameters is achieved with the use of a multivariable regression analysis tool such as the Least-Squares Method. This results in the quantification of the abdominal mechanical properties, as a value for C_{ab} is obtained.

2. Methods

For the development of the model, a preliminary analysis was first conducted, to examine the respiratory and abdominal mechanical properties as a function of IAP during insufflation. The design requirements were then formulated and the design of the model was created. Finally, the model was manufactured and assembled. Validation of its function was performed by comparing the results from the preliminary analysis to the results obtained from the model.

2.1 Preliminary Analysis

2.1.1. Experimental Setup

The preliminary analysis was performed on data obtained from animal experiments that were

conducted at Erasmus MC in August 2019. A 20kg piglet underwent intra-abdominal insufflation at a range of IAP values, followed by the application of FOT, while its respiratory function was assessed.

Volume-controlled mechanical ventilation was applied, with $V_t \approx 160$ ml, using the neonatal intensive care ventilator Fabian HFO (Acutronic Medical Systems AG, Hirzel, Switzerland). The PEEP level and the respiratory rate were adapted to manage the O_2 and CO_2 levels during the experiment. Abdominal insufflation was performed at 5, 8, 10, 12, 14, 16, 18 and 20 hPa using the novel surgical insufflator. At each IAP level, P_{aw} and $\dot{V}_I$ were continuously measured at the endotracheal tube. Likewise, the pressure and flow of the insufflation gas (P_{tr} and $\dot{V}_{tr}$) were measured at the trocar.

Finally, before increasing the IAP, FOT was performed in the abdomen of the animal to estimate the abdominal mechanical properties at each IAP. An external pressure signal was applied by the insufflator to the abdominal wall at 0.5, 1, 2, 3, 5, 10, and 15 Hz. Once the FOT measurement was obtained, the IAP changed to the following value and the described process was repeated.

2.1.2 Respiratory Analysis

The respiratory analysis was performed in MATLAB. The recorded P_{aw} and $\dot{V}_I$ at every examined IAP were utilized for assessing the respiratory function.

First, a specific segment of the entire experimental data set was isolated, during which tidal volumes and pressures of mechanical ventilation were stable. This was done to ensure that the obtained pressures and flows were solely due to ventilation, so that the results truly reflect the respiratory mechanical properties. Once the data segment was selected, 10 full breaths were isolated and analyzed. This number was considered acceptable for providing the analysis algorithm with sufficient information in order to give reliable results, and ensured that the same of number of breaths were analyzed at every examined IAP. Breaths were selected with an algorithm, which detected the local minima in the V_t waveform, each one indicating the start of a breath.

Once breath selection was completed, it was observed that the V_t signal displayed a systematic decrease over time. This phenomenon, called sensor drift error, is an invariably encountered problem when integrating a flow signal. It occurs due to asymmetries in the flow sensor or differences in the temperature and humidity levels in the inspired and expired air[29]. The linear trend in the signal was removed by subtracting the mean from the tidal volume data, forcing the mean of the waveform to zero.

Subsequently, a linear, single-compartment mathematical model was fitted to the measured respiratory parameters (P_{aw}, $\dot{V}_{aw}$ and V_t) with the Recursive Least-Squares (RLS) algorithm. The analysis began by considering the linear model:

$$Y = XA + N \tag{6}$$

where Y was the vector of the predicted pressure by the model ($\hat{P}_{aw}$), X was the matrix of the independent parameters (P_{aw}, $\dot{V}_{aw}$ and V_t), A was the vector of parameters to be estimated (R, E) and N was the error between predicted and the modelled pressure.

The RLS algorithm calculated the parameters (A) by minimizing the sum of the squared residuals between the prediction of the pressure by the model and the actual measured P_{aw}. The least squares estimate was given by:

$$\hat{A} = [X^T X]^{-1} X^T Y \tag{7}$$

The predicted pressure $\hat{P}_{aw}$, R and E were calculated by the model and stored for each of the 10 analyzed breaths. The mean squared error (MSE) between the estimated and measured pressure was computed as shown in Equation 8 and stored for each breath as well, giving an indication on the accuracy of the model:

$$MSE = \frac{1}{n}\sum_{i=1}^{n}\left(P_{aw\,i} - \hat{P}_{aw\,i}\right)^2 \tag{8}$$

The analysis procedure was repeated for every examined IAP. The results from each IAP were subsequently processed, such that the mean and standard deviation of R, E and MSE were computed for the 10 breaths at every IAP. Besides the mechanical parameters, the effect of IAP on V_t, V_{tr} (volume of gas in the trocar), PIP and ΔP were investigated as well.

2.1.3 Abdominal Analysis

The first step of the abdominal analysis was to manually isolate the segment of data that corresponded to the application of the FOT. This was done to ensure that the abdominal analysis focused on the FOT without any other interferences, so that the results truly reflect the abdominal mechanical behavior of the animal.

After the segment isolation, the mechanical impedance (Z) of the abdomen was calculated as a function of frequency. Since Z(ω) is defined as the ratio between the imposed insufflation pressure and the resulting trocar flow, its computation was achieved by estimating the transfer function between the two time signals in MATLAB.

Although the frequency spectrum for the FOT in the animal experiment ranged up to 15 Hz, the frequencies considered for the abdominal analysis of this study were 0.5, 1, 2, 3, and 5 Hz. The decision to exclude the frequencies 10 and 15 Hz from the analysis is explained by expressing the reactance as:

$$X(\omega) = \omega I - \frac{1}{\omega C} \qquad (9)$$

where the compliance C represents the elastic properties of the abdomen. Barnas et al.[30] specified that, for the abdominal wall, the inertial term ωI has a negligible and irrelevant contribution to the overall reactance for up to 5 Hz. Therefore, it was decided that the abdominal analysis should be extended up to 5 Hz in order for the acquired results to truly reflect the compliance of the abdomen.

Z(ω) was then calculated as the transfer function between the pressure and flow signals in the trocar, at each frequency of every examined IAP.The obtained resistance and reactance were then fitted to the RIC mathematical model, which was described in the introduction, so that C_{ab} could be estimated:

$$Z_{est}(\omega) = R + j\omega I + \frac{1}{j\omega C} \qquad (10)$$

where Z_{est} was the predicted impedance by the model. The fitting of the measured impedance was done in MATLAB using the multivariable nonlinear algorithm of the Least-Squares Method. The function of the algorithm was to yield Z_{est} by minimizing the deviation between the predicted and measured impedance, thus minimizing the error for each k measurement:

$$\text{err} = \sum_{k=1}^{K}(|\mathrm{Z_{est}}(\omega_\mathrm{k}) - \mathrm{Z}(\omega_\mathrm{k})|) \qquad (11)$$

The initial values of R, I and C were obtained using a minimization algorithm in MATLAB, that finds the minimum of an unconstrained multivariable function. The least-squares algorithm was fitted with the calculated impedance for each IAP, predicted Z_{est} and returned the parameters R, I and C.

2.2 Design and Manufacturing

Table 20. *Design requirements of the model.*

Design Requirements	
1.	In vitro
2.	Distinct respiratory component
3.	Compatibility with the mechanical ventilator
4.	Distinct abdominal component
5.	Compatibility with the surgical insufflator
6.	Respiratory and abdominal component are in contact
7.	R and E estimation during respiratory-abdominal interaction

The development phase began with specifying the design requirements, which are presented in Table 1. This was accomplished by breaking down the problem statement and translating it into the necessary features of the device.

The respiratory component of the model was decided to be composed of a compliant bellow. The bellow was 3D printed using the Ultimaker S5 (Ultimaker B.V., The Netherlands) at Erasmus MC. The selected printing material was thermopliastic polyurethane (TPU 95A), one of the most compliant materials that can be used in 3D printing. Its selection was driven by the need for flexibility, so that alternate expansion and contraction of the bellow can take place when connected to the mechanical ventilator.

With regards to the abdominal component, data from the literature suggested that the abdomen is typically simulated by a rubber material [31,32], so that it is capable of expanding and increasing its volume alongside the increase of IAP. Thus, a commercially available latex bellow was selected for the simulation of the abdomen.

After the individual parts were determined, the 3D design of the prototype was created, as depicted in Figure 1, so that the device can be visualized before being manufactured. Figure 1 shows that the respiratory (red) bellow of the model is placed on top of the abdominal (black) rubber one. On top of the abdominal bellow and exteriorly, a plastic covering provides the respiratory-abdominal interaction. Each of the bellows is attached to a circular bellow connector, which allows connection with the mechanical ventilator and the insufflator. Stability of the configuration was ensured by three 20x20 mm aluminum extrusion profiles, which were attached to the bellow connectors via additional custom connecting parts, the frame connectors.

Figure 43. *3D design of the in vitro model.*

The bellow connectors and frame connectors were 3D printed at Erasmus MC as well, with the Ultimaker S5. Tough PLA, which offers high strength and hardness, was used as the printing material. This was desired as, it was necessary for both parts to provide stability to the physical model. The extrusion profiles, the utilized screws and nuts as well as the abdominal bellow were commercially available.

2.3 Validation

The ability of the model to simulate the interaction between the respiratory and abdominal side during insufflation was evaluated. A comparison between the results from the model and the results from the animal trial determined whether the developed device was an adequate representation of the interaction of the physiological systems.

The experimental setup used in the animal trials was reproduced for testing of the model. The novel surgical insufflator was connected to the abdominal component of the model, while the same mechanical ventilator, was used for ventilating the respiratory bellow. The validation setup is depicted in Figure 2. The pressure and flow of air were measured at both the ventilation and insufflation side of the model with the use of 2 pneumotachometers, each placed at the respective side. Before the measurements, the pressure and flow sensor of each pneumotachometer was calibrated.

Pressure calibration was accomplished by comparing the output of the pneumotachometer to a commercially available pressure sensor, while flow calibration was done with the use of 100ml calibration syringe. Data acquisition and storage was accomplished with an interface that had previously been developed in LabVIEW for the animal trial.

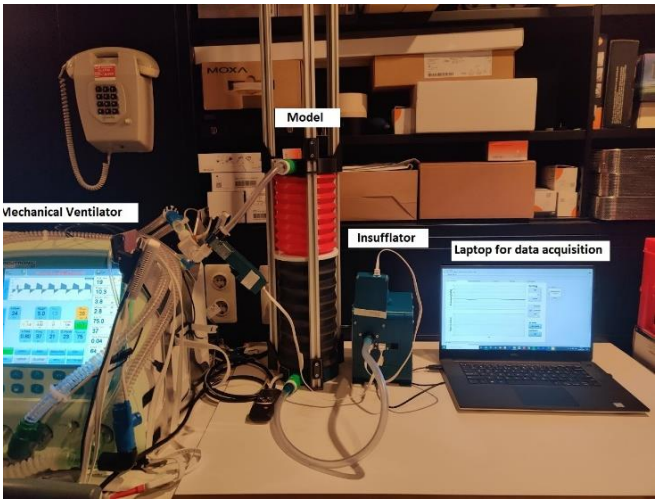

Figure 44. *The setup used for the validation of the model.*

3. Results

The mechanical properties of the respiratory and abdominal component of the model are shown in Figure 3, alongside the respective properties obtained from the preliminary analysis. In both the in vitro and in vivo model, R_{aw} showed a limited dependence on IAP. It displayed a slight rise from 8.8 $cmH_2O{\cdot}s/L$ for the model and 9.1 $cmH_2O{\cdot}s/L$ for the animal at 5 hPa to 11 and 10.6 $cmH_2O{\cdot}s/L$, respectively, at 12 hPa, before stabilizing at higher pressures. Similarly, the trocar resistance (R_{trocar}) displayed a constant behavior around 5 $cmH_2O{\cdot}s/L$ for the model, while

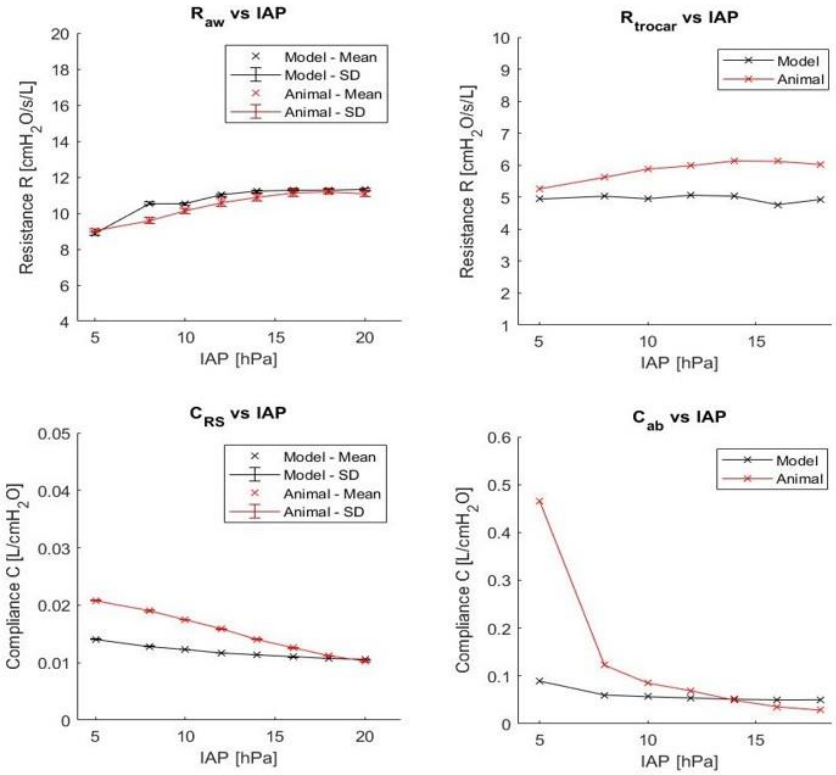

Figure 45. *Comparison between the resistance and compliance estimated for the respiratory (Raw, C_{RS}) and abdominal component (Rtrocar, Cab) of the model with the corresponding parameters of the preliminary analysis*

in the animal it increased from 5.3 $cmH_2O \cdot s/L$ at 5hPa to 6 $cmH_2O \cdot s/L$ at 12 hPa, and was maintained there until the IAP reached18 hPa.

With regards to C_{RS}, it displayed a gradual drop alongside the increase in IAP for both the model and the animal. Starting at 0.014 L/cmH_2O at 5 hPa it exhibited a progressive decrease until 0.011 L/cmH_2O at 20 hPa. Accordingly, C_{RS} in the animal decreased systematically from 0.021 to 0.01 L/cmH_2O.

Finally, a decreasing trend was observed in C_{ab} as well, both in vivo and in vitro. For the model, C_{ab} was 0.089 L/cmH_2O at 5 hPa and eventually dropped to the value of 0.05 L/cmH_2O at 18 hPa. In the animal, a significantly more prominent change in C_{ab} was observed, which began from 0.465 L/cmH_2O at 5 hPa and ended up at 0.028 L/cmH_2O at 18 hPa. In both cases, the most notable change in C_{ab} was observed from 5 to 8 hPa, as the model and animal C_{ab} reached 0.06 and 0.122 L/cmH_2O, respectively.

The results regarding V_t and V_{ab}, as well as the Δt between the two measurements are shown in Figure 4. In both cases, V_t was unaffected by pressure and was constant for the entire pressure range, at the value that was set at the mechanical ventilator (0.15L for the model and 0.16L for the animal). V_{ab} leaped from 0.031 L at 5 hPa to 0.073 L at 8 hPa for the model and remained nearly constant until 20 hPa, fluctuating between 0.06 L and 0.073 L. The behavior of V_{ab} for the animal was very similar, as it rose from 0.04 L at 5 hPa to 0.053 L at 8 hPa and was then stable between 0.066 L and 0.083 L.

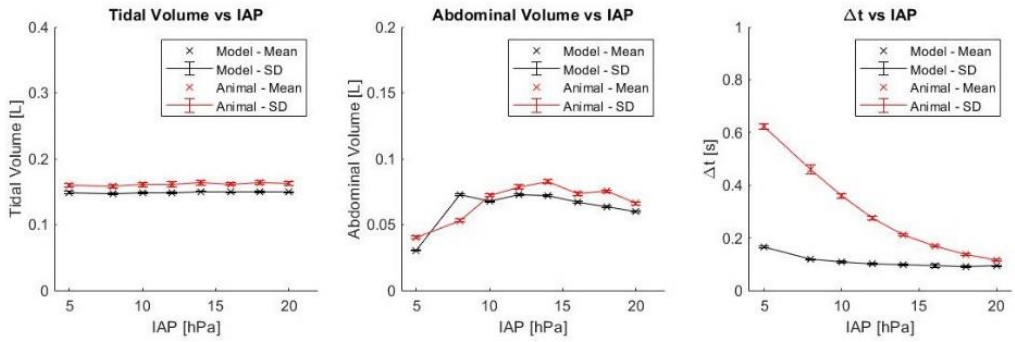

Figure 46. *Graphs of V_t, V_{ab} and Δt vs IAP for the in vitro model and the animal.*

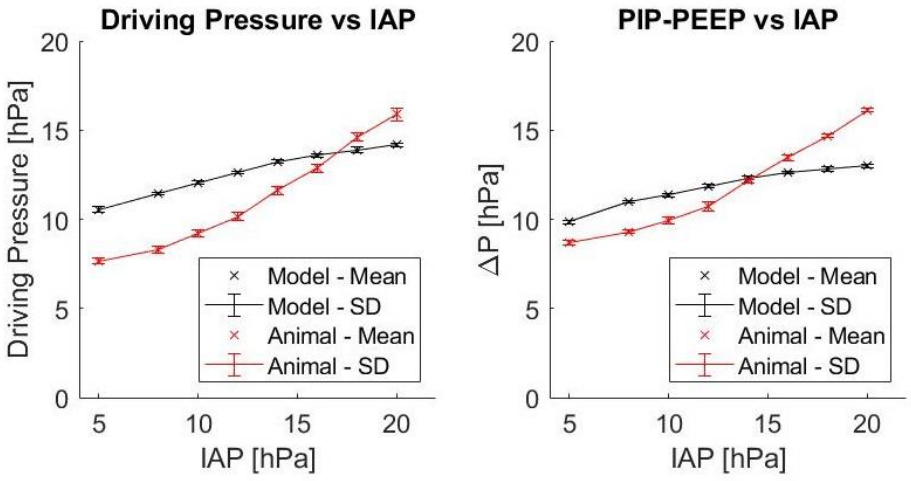

Figure 47. *The effect of IAP on ΔP(left) and PIP (right) for the model and the animal.*

Figure 4 shows the decrease in the time difference between the occurrence of V_t and V_{ab} for the model and the animal with an increase in IAP. For the model, Δt dropped to almost half from 0.17 s at 5 hPa to 0.01 s at 20 hPa. As for the animal, it displayed nearly a 5-fold decrease, falling from 0.62 s at 5 hPa to 0.12 s at 20 hPa.

The effect of IAP on ΔP and PIP is shown in Figure 5. ΔP exhibited a continuous increase alongside the increase in IAP. For the model, ΔP started at 10.6 hPa and reached a maximum value of 14.2 hPa at an IAP of 20 hPa, while for the animal ΔP began at 7.7 hPa and rose until 15.9 hPa at the maximum IAP. For the same insufflation pressures, PIP-PEEP increased from 9.8 to 13 hPa in the model, and from 8.7 to 16.1 hPa in the animal.

4. Discussion

The goal of this study was to develop a physical in vitro model that simulates the interaction between the respiratory system and abdominal cavity during surgical insufflation. The created device was validated with in vitro experiments, during which the mechanical properties and functional parameters of the model were recorded and compared to the corresponding parameters that were obtained from an animal experiment.

4.1 Mechanical Properties

The developed model adequately captured the dependence of the respiratory and abdominal mechanical properties on IAP. The simulated R_{aw}, which showed a slight increase at the lowest insufflation pressures, matched the trend and physiological values observed in the animal experiments. With respect to the abdominal compartment, the simulated R_{trocar} showed an independent behavior from IAP, as it was kept almost stable for the entire range of the investigated pressures, and was a good approximation to the measured R_{trocar} for the animal.

Although slightly stiffer than the in vivo respiratory system, the pulmonary compartment of the device sufficiently reflected the effect of IAP on C_{RS}, as confirmed by its gradually declining behavior. It is well-documented in the literature, and also reported in the in vivo trials, that the rise in IAP deteriorates the mechanical properties of the respiratory system by increasing its elastance and forcing it to a less compliant mechanical behavior[17,18,24,33,34]. Despite its initially higher stiffness, the ventilation side of the model became, indeed, even stiffer as the insufflation pressure increased, while the simulated C_{RS} also approached the in vivo levels for the highest pressures.

The total respiratory compliance C_{RS} is determined by the compliance of the chest wall (C_{CW}) and the lung tissue compliance (C_L). As the insufflation pressure increases, the chest wall becomes gradually stiffer, while C_L remains constant [16]. Therefore, it is the drop in C_{CW}, that results in the decrease of C_{RS} as the insufflation pressure increases.

With respect to C_{ab}, the compliance of the abdominal bellow approached the behavior of the measured compliance to a certain extent. Similarly

to the animal, the simulated C_{ab} displayed a notable decrease as pressure shifted from 5 to 8 hPa, and from that point on the drop in the compliance was significantly less prominent. However, the abdominal bellow was stiffer than the abdomen of the animal, and this difference in the initial stiffness appeared to have an effect in the final results, as evidenced by the fact that C_{ab} in the animal displayed a much more prominent drop when the pressure shifted from 5 to 8 hPa. The in vivo abdomen was not only more compliant than the latex bellow, but also displayed a significantly higher variation in its compliance. This differences can be explained by the intrinsic mechanical properties of the materials of each system. Rubber was adequate in capturing the change in C_{ab} at low pressures, but its ability to simulate the variation in the overall compliance capacity of the abdomen was limited.

4.2 Tidal and Abdominal Volume

V_t should generally be maintained constant, as abrupt fluctuations can severely affect the pulmonary function and increase the risk for the patient [35–37]. Abdominal insufflation normally leads to a drop in the tidal volume, because of the limited and anomalous movement of the diaphragm; thus, PEEP applied by the ventilator in combination with VCV counterbalance this effect [17,21]. The beneficial outcome of PEEP and VCV was noted in the animal experiments as well, where the tidal volume was maintained at constant levels. The physical model showed a very good capability of reproducing this outcome and ensuring the delivery of the fixed tidal volume.

As the lungs reach their maximum volume at end-inspiration, the surgical insufflator allows a certain amount of gas to flow outside of the abdominal cavity. This amount of gas, quantified by V_{ab} and is one of the features of the insufflator that enable better preservation of a stable pneumoperitoneum. Measurement of V_{ab} in the model was comparable and showed good accordance with the corresponding measurement in the animal trial. V_{ab} exhibited an increase at the lowest insufflation pressures, and was then nearly constant for the rest of the investigated pressures. As IAP increases and the diaphragm moves cranially due to the abdominal expansion, the respiratory system comes in closer contact with the abdomen. Thus, at that point, changes in the lung volume affect the abdomen to a higher degree. This phenomenon was clearly reflected in the in vitro device.

The decrease in Δt between the occurrence of V_t and V_{ab} in both the in vivo and in vitro settings can be viewed as an indication for the increasing rigidity of the system. The shift in the diaphragm in combination with the increasing stiffness of the respiratory system, makes the overall respiratory-abdominal interaction more rigid, as reflected by the drop in Δt. The more notable drop in Δt in the in vivo trial was due to the higher initial compliance of the animal and its higher variation capacity. The model has comparable rigidity at higher insufflation pressures to the in vivo system, but since the animal starts from a higher compliance, the change in its rigidity is considerably higher and reflected by the more noticeable change in Δt. Thus, the trend in the rigidity (Δt) is analogous to the trends observed in the compliance of the individual compartments of the model and depends on the change in the compliance (ΔC) of each system.

4.3 Respiratory Pressures

The maintenance of a stable V_t despite the decrease in C_{RS} was expected to exert an increasing effect on the measured ΔP and PIP [17]. As ΔP is the overall pressure above PEEP applied by the ventilator to the respiratory system, to achieve the desired V_t, the stiffening of the chest wall in combination with the stable V_t resulted in a systematic increase of ΔP alongside IAP.

Similarly, the drop in C_{RS} means that a higher pressure is necessary to deliver the same V_t. The ventilator is set to deliver a fixed amount of air to the system, and since the higher elastance acts as an opposing force, it increases maximum pressure (PIP) to overcome it and provide the set V_t.

These outcomes were confirmed by the results in the animal experiment and were clearly visible in the validation of the in vitro model. An increase in both PIP and ΔP was obtained in the validation results, which is in accordance with the expected theoretical outcome and indicates the ability of the model to capture this significant effect of the increase in the insufflation pressure. The initially lower compliance of the model compared to the respiratory system of the animal affected the

results, as the rise in PIP and ΔP is not as steep as it was in the in vivo setting. This also explains the deviation in the absolute values of the measured quantities in the model. The relatively stiff respiratory bellow of the model requires higher PIP and ΔP even at the lowest insufflation pressures, without leaving much room for further increase as the IAP rises. Nevertheless, the increasing trend is clearly observed, as the result of the capability of the model to adequately simulate this interaction.

4.4 Clinical Relevance

Laparoscopic surgery is one of the most widely used types of minimally invasive surgery. Since its introduction in the early 1990s, the vast majority of abdominal and pelvic operations are performed laparoscopically, replacing the traditional open surgery.

Throughout the entire procedure, the patient is under general anesthesia. Intra-operative mechanical ventilation is required to help the patient maintain sufficient lung function, because anesthesia greatly reduces, or even completely ceases the respiratory drive and the muscular component of breathing [38,39]. VCV is widely used in clinical practice because it is considered a safe and effective approach for anesthetized patients [40,41]. With respect to laparoscopy, VCV is the preferred ventilation mode because it ensures the delivery of a fixed tidal volume to the patient [42] despite the changes in the compliance of the chest wall and lungs, that occur due to the increase in IAP. Therefore, validating the model by investigating the effect of IAP on the respiratory mechanical properties and pressures is meaningful for this particular ventilation mode, which aims at ensuring sufficient pulmonary gas exchange.

On the contrary, pressure-controlled ventilation (PCV) aims at maintaining a fixed inspiration pressure. In this case, the rise in IAP would result in a gradual decrease in V_t, while P_{aw} would remain constant alongside the increasing stiffness of the respiratory system. VCV is generally preferred over PCV, because a reduction in V_t can jeopardize the patient [35–37].

Overall, the impact of the increasing insufflation pressure on respiratory mechanics during VCV is a widely encountered problem in the clinical setting. The developed in vitro model contributes in mitigating the side effects associated with abdominal insufflation by offering knowledge on the respiratory-abdominal interaction. This, in turn, is the first step for improving the post-operative outcome of such a widely applied procedure, which affects a large number of patients.

4.5 Future Recommendations

The functional components of the model, both in the respiratory and the abdominal compartment, displayed a slightly lower compliance than the respective physiological structures. Although this difference in compliance did not lead to a deviation in the patterns observed in the simulated parameters, it led to slight differences in terms of the absolute values. Manufacturing of a respiratory bellow with the use of a more sophisticated printer and with an even more flexible material, such as silicone, is worth investigating. Such a printer and material combination could allow for creating more compliant bellows and could be implemented for the manufacturing of the insufflation bellow as well in order to decrease its compliance.

Interaction between the ventilation and insufflation side was achieved by adjusting the position and distance between the individual compartments, so that they come in contact. Although, this approach was sufficient for ensuring the feasibility of the in vitro model, the addition of a component to act as the physical interaction between the two compartments of the model, could benefit the system by offering a better representation of the physiological conditions. The selection of such a part, which could be implemented in the form of a spring or an elastic membrane between the two bellows, would simulate the compliance of the diaphragm. Therefore, it can potentially improve the ability of the model to capture the interplay between the two systems to a greater extent. If accomplished, it would pave the way for further modifications such as the effect of cardiac oscillations.

Finally, the use of a bicompartment model, such as the series or the viscoelastic model could be useful for the in vitro simulation, instead of the linear single-compartment model that was preferred in this study. Bicompartment models have been suggested by several authors as a means for

providing an even more accurate representation of the respiratory function [29,43,44]. These models allow the estimation of the mechanical properties in the inhalation and exhalation phases, separately. The implementation of such a model is towards the direction of making the overall configuration a closer approximation of the physiological conditions by analyzing the function of each lung individually. This, in turn, will enable exploring the respiratory effect of the pneumoperitoneum in patients with an underlying respiratory diseases.

Overall the abovementioned modifications can be the first step towards adapting the model for simulating the respiratory-abdominal interaction in humans. The current device has been specifically developed for the pig. However, these improvements offer flexibility and by modifying the dimensions and mechanical properties of the individual model components, implementation of the device for simulating the effect of IAP in humans can be accomplished.

5. Conclusions

This thesis indicated that it is feasible to simulate the interaction between the respiratory system and the abdomen during surgical insufflation with an in vitro model. The developed model can adequately mimic the experimental data from the performed clinical trials and can be used for the evaluation of the performance and safety of the surgical insufflator. Despite some deviations in the simulated mechanical properties, the prototype gave satisfactory results in terms of the expected theoretical interaction between the respiratory system and the abdomen as a function of the insufflation pressure. Therefore, it is considered a good proof-of-concept.

The device offers a broader understanding of the functional attributes of the insufflator as well as knowledge on the interplay between two dynamic physiological systems during laparoscopy

Additional modifications to optimize the function of the model and offer insights to more relevant mechanical processes during insufflation are worth investigating. This could enable the estimation of the effect of insufflation pressure on the compliance of the rib cage and diaphragm individually. Such improvements can contribute to an increase in the reliability and the number of tests that the model is able to undertake, further reducing the reliance on animal experiments.

References

1. Bucur P, Hofmann M, Menhadji A, et al. Comparison of Pneumoperitoneum Stability Between a Valveless Trocar System and Conventional Insufflation: A Prospective Randomized Trial. *Urology*. 2016;94:274-280. doi:10.1016/j.urology.2016.04.022
2. Herati AS, Atalla MA, Rais-Bahrami S, Andonian S, Vira MA, Kavoussi LR. A new valve-less trocar for urologic laparoscopy: Initial evaluation. *J Endourol*. 2009;23(9):1535-1539. doi:10.1089/end.2009.0376
3. Nepple KG, Kallogjeri D, Bhayani SB. Benchtop evaluation of pressure barrier insufflator and standard insufflator systems. *Surg Endosc*. 2013;27(1):333-338. doi:10.1007/s00464-012-2434-x
4. Annino F, Topazio L, Autieri D, Verdacchi T, De Angelis M, Asimakopoulos AD. Robotic partial nephrectomy performed with Airseal versus a standard CO2 pressure pneumoperitoneum insufflator: a prospective comparative study. *Surg Endosc*. 2017;31(4):1583-1590. doi:10.1007/s00464-016-5144-y
5. Luketina RR, Knauer M, Köhler G, et al. Comparison of a standard CO2 pressure pneumoperitoneum insufflator versus AirSeal™: Study protocol of a randomized controlled trial. *Trials*. 2014;15(1):239. doi:10.1186/1745-6215-15-239
6. Ott DE. Abdominal compliance and laparoscopy: A review. *J Soc Laparoendosc Surg*. 2019;23(1). doi:10.4293/JSLS.2018.00080
7. Bagnoli P, Vismara R, Fiore GB, Costantino ML. A mechanical model lung for hydraulic testing of total liquid ventilation circuits. *Int J Artif Organs*. 2005;28(12):1232-1241. doi:10.1177/039139880502801207
8. Chase JG, Yuta T, Mulligan KJ, Shaw GM, Horn B. A novel mechanical lung model of pulmonary diseases to assist

with teaching and training. *BMC Pulm Med*. 2006;6(1):21. doi:10.1186/1471-2466-6-21

9. Mešić S, Babuška R, Hoogsteden HC, Verbraak AFM. Computer-controlled mechanical simulation of the artificially ventilated human respiratory system. *IEEE Trans Biomed Eng*. 2003;50(6):731-743. doi:10.1109/TBME.2003.812166
10. Verbraak AFM, Beneken JEW, Bogaard JM, Versprille A. Computer-controlled mechanical lung model for application in pulmonary function studies. *Med Biol Eng Comput*. 1995;33(6):776-783. doi:10.1007/BF02523009
11. Verbraak AFM, Rijnbeek PR, Beneken JEW, Bogaard JM, Versprille A. A new approach to mechanical simulation of lung behaviour: Pressure-controlled and time-related piston movement. *Med Biol Eng Comput*. 2001;39(1):82-89. doi:10.1007/BF02345270
12. Cappa P, Sciuto SA, Silvestri S. A novel preterm respiratory mechanics active simulator to test the performances of neonatal pulmonary ventilators. *Rev Sci Instrum*. 2002;73(6):2411. doi:10.1063/1.1480453
13. Ngo C, Schlözer R, Vollmer T, Winter S, Misgeld B, Leonhardt S. A simulative model approach of cardiopulmonary interaction. In: *IFMBE Proceedings*. Vol 51. Springer Verlag; 2015:1679-1682. doi:10.1007/978-3-319-19387-8_408
14. Meka V V., van Oostrom JH. Bellows-less lung system for the human patient simulator. *Med Biol Eng Comput*. 2004;42(3):413-418. doi:10.1007/BF02344718
15. Lucangelo U, Bernabè F, Blanch L. Lung mechanics at the bedside: make it simple. *Curr Opin Crit Care*. 2007;13(1):64-72. doi:10.1097/MCC.0b013e32801162df
16. Hess DR. Respiratory mechanics in mechanically ventilated patients. *Respir Care*. 2014;59(11):1773-1794. doi:10.4187/respcare.03410
17. Sharma KC, Brandstetter RD, Brensilver JM, Jung LD. Cardiopulmonary physiology and pathophysiology as a consequence of laparoscopic surgery. *Chest*. 1996;110(3):810-815. doi:10.1378/chest.110.3.810
18. Mazzinari G, Diaz-Cambronero O, Alonso-Iñigo JM, et al. Intraabdominal pressure targeted positive end-expiratory pressure during laparoscopic surgery: An open-label, nonrandomized, crossover, clinical trial. *Anesthesiology*. 2020;132(4):667-677. doi:10.1097/ALN.0000000000003146
19. Andersson LE, Bååth M, Thörne A, Aspelin P, Odeberg-Wernerman S. Effect of carbon dioxide pneumoperitoneum on development of atelectasis during anesthesia, examined by spiral computed tomography. *Anesthesiology*. 2005;102(2):293-299. doi:10.1097/00000542-200502000-00009
20. Gurusamy KS, Vaughan J, Davidson BR. Low pressure versus standard pressure pneumoperitoneum in laparoscopic cholecystectomy. *Cochrane Database Syst Rev*. 2014;2014(3). doi:10.1002/14651858.CD006930.pub3
21. Simonneau G, Vivien A, Sartene R, et al. Diaphragm dysfunction induced by upper abdominal surgery. Role of postoperative pain. *Am Rev Respir Dis*. 1983;128(5):899-903. doi:10.1097/00132586-198512000-00026
22. Neto AS, Hemmes SNT, Barbas CSV, et al. Association between driving pressure and development of postoperative pulmonary complications in patients undergoing mechanical ventilation for general anaesthesia: A meta-analysis of individual patient data. *Lancet Respir Med*. 2016;4(4):272-280. doi:10.1016/S2213-2600(16)00057-6
23. Ladha K, Melo MFV, McLean DJ, et al. Intraoperative protective mechanical ventilation and risk of postoperative respiratory complications: Hospital based registry study. *BMJ*. 2015;351. doi:10.1136/bmj.h3646
24. Puri GD, Singh H. Ventilatory effects of laparoscopy under general anaesthesia. *Br J Anaesth*. 1992;68(2):211-213.

doi:10.1093/bja/68.2.211

25. Malbrain MLNG, Roberts DJ, De Laet I, et al. The role of abdominal compliance, the neglected parameter in critically ill patients - A consensus review of 16. Part 1: Definitions and pathophysiology. *Anaesthesiol Intensive Ther*. 2014;46(5):392-405. doi:10.5603/AIT.2014.0062
26. Navajas D, Farré R. Oscillatory Mechanics. In: *Mechanics of Breathing*. Springer Milan; 2002:146-156. doi:10.1007/978-88-470-2916-3_12
27. Kaczka DW, Dellacá RL. Oscillation mechanics of the respiratory system: Applications to lung disease. *Crit Rev Biomed Eng*. 2011;39(4):337-359. doi:10.1615/CritRevBiomedEng.v39.i4.60
28. Dellaca' RL. Measurement of Respiratory System Impedances. In: *Mechanics of Breathing*. Springer Milan; 2002:157-171. doi:10.1007/978-88-470-2916-3_13
29. Lauzon A, T Bates JH, T Bates JF. *Estimation of Time-Varying Respiratory Mechanical Parameters by Recursive Least Squares*. Vol 71.; 1991.
30. Barnas GM, Yoshino K, Stamenovic D, Kikuchi Y, Loring SH, Mead J. Chest wall impedance partitioned into rib cage and diaphragm-abdominal pathways. *J Appl Physiol*. 1989;66(1):350-359. doi:10.1152/jappl.1989.66.1.350
31. Huntington CR, Prince J, Hazelbaker K, et al. Safety first: significant risk of air embolism in laparoscopic gasketless insufflation systems. *Surg Endosc*. 2019;33(12):3964-3969. doi:10.1007/s00464-019-06683-4
32. Condino S, Carbone M, Ferrari V, et al. How to build patient-specific synthetic abdominal anatomies. An innovative approach from physical toward hybrid surgical simulators. *Int J Med Robot Comput Assist Surg*. 2011;7(2):202-213. doi:10.1002/rcs.390
33. BARDOCZKY GI, ENGELMAN E, LEVARLET M, SIMON P. Ventilatory effects of pneumoperitoneum monitored with continuous spirometry. *Anaesthesia*. 1993;48(4):309-311. doi:10.1111/j.1365-2044.1993.tb06949.x
34. Chiumello D, Carlesso E, Cadringher P, et al. Lung stress and strain during mechanical ventilation for acute respiratory distress syndrome. *Am J Respir Crit Care Med*. 2008;178(4):346-355. doi:10.1164/rccm.200710-1589OC
35. Futier E, Constantin J-M, Paugam-Burtz C, et al. A Trial of Intraoperative Low-Tidal-Volume Ventilation in Abdominal Surgery. *N Engl J Med*. 2013;369(5):428-437. doi:10.1056/NEJMoa1301082
36. Lellouche F, Dionne S, Simard S, Bussières J, Dagenais F. High tidal volumes in mechanically ventilated patients increase organ dysfunction after cardiac surgery. *Anesthesiology*. 2012;116(5):1072-1082. doi:10.1097/ALN.0b013e3182522df5
37. Gajic O, Frutos-Vivar F, Esteban A, Hubmayr RD, Anzueto A. Ventilator settings as a risk factor for acute respiratory distress syndrome in mechanically ventilated patients. *Intensive Care Med*. 2005;31(7):922-926. doi:10.1007/s00134-005-2625-1
38. Silva PL, Pelosi P, Rocco PRM. Optimal mechanical ventilation strategies to minimize ventilator-induced lung injury in non-injured and injured lungs. *Expert Rev Respir Med*. 2016;10(12):1243-1245. doi:10.1080/17476348.2016.1251842
39. Ball L, Costantino F, Fiorito M, Amodio S, Pelosi P. Respiratory mechanics during general anaesthesia. *Ann Transl Med*. 2018;6(19):379-379. doi:10.21037/atm.2018.09.50
40. Patel B. Overview of Mechanical Ventilation - Critical Care Medicine - MSD Manual Professional Edition. https://www.msdmanuals.com/professional/critical-care-medicine/respiratory-failure-and-mechanical-ventilation/overview-of-mechanical-ventilation. Published March 2020. Accessed February 8, 2021.
41. Bauman KA, Hyzy RC. *Volume-Controlled Mechanical Ventilation*. Vol 1. Oxford University Press; 2016. doi:10.1093/med/9780199600830.003.

0095
42. Gertler R. Mechanical ventilation during anesthesia in adults - UpToDate. Wolters Kluwer. https://www.uptodate.com/contents/mechanical-ventilation-during-anesthesia-in-adults/print. Published January 27, 2021. Accessed February 8, 2021.
43. Carvalho AR, Zin WA. Respiratory system dynamical mechanical properties: Modeling in time and frequency domain. *Biophys Rev*. 2011;3(2):71-84. doi:10.1007/s12551-011-0048-5
44. Lorino AM, Lorino H, Harf A. A synthesis of the Otis, Mead, and Mount mechanical respiratory models. *Respir Physiol*. 1994;97(2):123-133. doi:10.1016/0034-5687(94)90020-5